Using an Accelerometer Sensor to Measure Human Hand Motion

by

Brian Barkley Graham

Submitted to the Department of Electrical Engineering and Computer Science
in Partial Fulfillment of the Requirements for the Degrees of
Bachelor of Science in Electrical Science and Engineering
and Master of Engineering in Electrical Engineering and Computer Science

at the

Massachusetts Institute of Technology

May 11, 2000

Signature of Author .....
Department of Electrical Engineering and Computer Science
May 11, 2000

Certified by .....
Charles G. Sodini
Professor of Electrical Engineering and Computer Science
Thesis Supervisor

Accepted by .....
Arthur C. Smith
Chairman, Department Committee on Graduate Students

Using an Accelerometer Sensor to Measure Human Hand Motion

By

Brian Barkley Graham

Submitted to the Department of Electrical Engineering and Computer Science

May 11, 2000

In partial fulfillment of the requirements for the Degrees of
Bachelor of Science in Electrical Science and Engineering
and Master of Engineering in Electrical Engineering and Computer Science

Abstract

Microfabricated accelerometer sensors have been developed to measure acceleration in a variety of applications, including automobile airbag crash sensors and seismic activity monitors. For this thesis a three-dimensional accelerometer sensor has been created for measuring involuntary human hand motion. The sensor uses three single-axis accelerometers fabricated at the MIT Microsystems Technology Laboratory (MTL). The size and mass of the sensor were limited to avoid altering hand motion being measured.

The MTL fabricated accelerometers have a proof mass restricted to motion along a single axis and constrained by angular springs. Acceleration of the sensor forces displacement of the proof mass, and the displacement is sensed using differential capacitors.

The accelerometer dies were packaged in leadless chip carriers (LCCs), and the LCCs were arranged in a three-axis configuration. A circuit was constructed to convert the differential capacitance signal into an analog signal and then into a digital signal before being read into a computer. The data acquisition program allows real-time analysis of the acceleration data, as well as storage of the data for more sophisticated subsequent analysis.

There are several sources of error in the accelerometer sensor system that limit the accuracy of measurement. Analog electrical noise limits the precision to $\pm$ 2.5 mg. There is a nonlinearity between the acceleration input and the analog voltage output of at least $\pm$ 7 mg. A third error source is cross-sensitivity, arising from movement in accelerometer proof masses from acceleration perpendicular to the intended axis of motion, and is 3.75% with this accelerometer sensor.

The three-dimensional accelerometer sensor has been demonstrated in the intended application of measuring human hand motion.

Thesis Supervisor: Charles G. Sodini
Title: Professor of Electrical Engineering

Acknowledgements

I would like to thank Professor Sodini for holding the class which initially introduced me to the MTL accelerometer sensor, and serving as my advisor throughout the project. I would also like to thank Professor Schmidt for more specific advice regarding the accelerometer dies and packaging issues. The project would have been impossible without the guidance of Jim MacArthur, who made frequent suggestions for solving the significant and frequency hurdles in the project. Chi-Fan Yung was extremely helpful with introducing me to the MTL accelerometers, their usage, and the acceleration testing equipment. Kei Ishihara initially led the fabrication project to create the accelerometers without which this project would be nonexistant. Joe Walsh was very helpful in teaching me how to use the gold wire bonding machine and helped me unclog several tips.

I would also like to thank my family, Betty, Michael, and Scott, and friends for supporting me throughout my time at MIT.

This project was supported by funding from the MIT Gordon Chair for the Technology Demonstration Systems Program.

Table of Contents

Index of Figures

Index of Tables

Chapter 1. Introduction

A. Overview

Sensors allow detection, analysis, and recording of physical phenomenon that are difficult to otherwise measure by converting the phenomenon into a more convenient signal. Sensors convert physical measurements such as displacement, velocity, acceleration, force, pressure, chemical concentration, or flow into electrical signals. The value of the original physical parameter can be back-calculated from the appropriate characteristics of the electrical signal (amplitude, frequency, pulse-width, etc.). Electrical outputs are very convenient because there are well known methods (and often commercially available off-the-shelf solutions) for filtering and acquiring electrical signals for real-time or subsequent analysis.

Sensor size is often important, and small sensors are desirable for many reasons including easier use, a higher sensor density, and lower material cost. A revolution in microfabricated sensors occurred with the application of semiconductor fabrication technology to sensor construction. By etching and depositing electrically conductive and nonconductive layers on silicon wafers, the sensor is created with the electrical sensing elements already built into the sensor. The products created using these techniques are called microelectromechanical systems, or MEMS. Other examples of MEMS are the application elements of inkjet printers[1].

The entire MEMS sensor is fabricated on a small section of a single silicon wafer or a stack of wafers bonded together. Reducing the area of the sensor layout both decreases the area of the sensor and increases the number of sensors produced on each wafer. The silicon dies are then packaged in chip carriers for use.

Many types of inertial sensors have been fabricated as MEMS. The original MEMS sensors were pressure sensors using piezoresistive sensing elements,[2] while current MEMS sensors include accelerometers (measuring either linear[3] or angular[4] acceleration), shear stress sensors,[5] chemical concentration sensors,[6] and gyroscopes.[7] This project uses single-axis MEMS linear accelerometer sensors fabricated at MIT to create a three-dimensional accelerometer sensor system suitable for measuring the acceleration of human hand motion.

B. Accelerometer Sensors

Accelerometer sensors measure the acceleration experienced by the sensor and anything to which the sensor is directly attached. Accelerometer sensors have many applications. The most common commercial application is impact sensors for triggering airbag deployment in

automobiles: when the acceleration exceeds 30 to 50 g's,[†] an accident is assumed and the airbags deploy.[8] Such sensors are designed to be rugged and reliable, and are made in high volume and at low cost by several chip manufacturers.[9] Airbag sensors don't need to be very accurate: with a threshold of 50 g's, an accuracy of 1 to 2 g is acceptable.

High precision accelerometer sensors have a variety of applications. They are used with gyroscopes (which can also be microfabricated using MEMS) in inertial guidance mechanisms: the displacement is calculated by twice integrating the acceleration signal, and the gyroscopes indicate the direction of displacement. Such components are used to make small inertial guidance units[10] in rockets and aircraft, which complement direct navigation using satellite global positioning.

When working with accelerometers in the earth's gravitational field, there is always the acceleration due to gravity. Thus the signal from an accelerometer sensor can be separated into two signals: the acceleration from gravity, and external acceleration. The acceleration from gravity allows measurement of the tilt of the sensor by identifying which direction is "down". By filtering out the external acceleration, the orientation of a three-axis sensor can be calculated from the accelerations on the three accelerometer axes. Orientation sensing can be very useful in navigation.

Ultra-high precision but low bandwidth accelerometer sensors have applications in seismology.[11] Two important seismology applications are detecting earthquakes and geophysical mapping (particularly for petroleum exploration). Geophysical accelerations are low frequency (<50 Hz) but require extremely high sensitivity-- errors less then 1 μg. An accelerometer[12] being developed at NASA's Jet Propulsion Laboratory (Pasadena, CA) for applications in seismology has a sensitivity of 1 ng/$Hz^{1/2}$ with a bandwidth of 0.05 to 50 Hz, for a total noise level of 7 ng.

Accelerometer sensors can also be used to indirectly infer the status of a machine. One proposed application of accelerometer sensors is detecting when a washing machine goes out of balance.[13] The range of acceleration is a few g's, and the precision required is mg's, with a bandwidth up to the frequency of rotation. By fixing a two-axis accelerometer (the axes perpendicular to the axis of rotation), an out-of-balance load is detected by excessive vibration. A more sophisticated analysis could determine in what way the rotor is off-balance and compensate appropriately. This application will be increasingly important as washing machine rotational speeds increase during the spin cycle to shed more water and reduce drying time, thereby decreasing the overall power consumption for washing clothes.

[†] One g is the acceleration due to gravity, 9.8 m/s^2

The goal of this thesis is to measure the three-dimensional acceleration of human hand motion with adequate accuracy and precision, the necessary bandwidth for normal human motion, and the amplitude range required for the highest normal accelerations. At the same time, the physical presence of the sensor should not alter the hand motion. The application of measuring something sensitive to external mass like the human hand[14] requires the accelerometer sensor to be extremely small and lightweight.

C. Hand Motion

The focus of this project is measuring involuntary hand motion in people who have a significant hand tremor.

Human hand motion can be broadly divided into two categories: voluntary and involuntary. Voluntary motion is intentional, such as throwing a baseball or changing the TV channel using a remote control. Involuntary motion is unintentional movement. One example of involuntary hand motion is the small vibrations in a person's hand when they are trying to keep their hand still, due to small imperfections in the human body's biomechanical feedback mechanisms. In healthy people this involuntary hand motion is small but measurable. Other examples of involuntary hand tremors are those arising from neurological diseases. A key symptom of Parkinson's disease is a significant resting hand tremor, which stops temporarily when the person consciously tries to keep their hand still. Essential tremor (called essential because it has no known external cause) is another common involuntary hand tremor,[15] which can change amplitude depending on the position of the hand.

A few different types of involuntary hand tremors and their characteristic frequency ranges are listed in Table 1-1. Noting that the frequency ranges differ depending on the tremor suggests clinical diagnosis of the unknown origin of a hand tremor may be aided by measuring the tremor frequency.

Table 1-1. Types of Involuntary Hand Tremors[14,16,17]

Tremor Type / Cause	Frequency	Notes
Normal Hand Tremor	9-25 Hz	Small amplitude [ref 14]
Essential Tremor	4-12 Hz	May worsen with position
Parkinson's Disease	3-8 Hz	Resting tremor
Cerebellar Lesions	1.5-4 Hz	

The highest amplitude of hand acceleration during movement is about ±5g. Higher accelerations (in the range of ±20 g) will arise from shocks, such as the impact of landing after a jump due to vibrations in the bones and tissue.[18] Similar amplitude shocks can occur if the

subject being studied accidentally bumps into a hard surface. Consequently, a robust device used for measuring human biomechanics must be able to withstand accelerations of ±20g or more.

The acceleration from hand vibration in normal people holding their hand as still as possible follows a Gaussian distribution, with a variance of about 15 mg.[19] In people with significant involuntary hand tremors, hand acceleration will be more on the order of ±1 g.[20]

D. Goals of the Project

The goal of this project is the development of a three-dimensional accelerometer sensor system for measuring involuntary hand motion. The system includes the physical sensor, the signal processing and data acquisition circuit, and the computer program to acquire and display the data. The project will showcase a specific accelerometer fabricated by the MIT Microsystems Technology Laboratory (MTL). The rest of the system will be built from commercially available components.

Based on the goal of measuring involuntary hand motion, target parameters for the accelerometer system can be specified and are listed in Table 1-2. To measure complex hand motion occurring in three dimensions, the sensor needs to measure acceleration along three mutually perpendicular axes to reconstruct the total acceleration of the system. The bandwidth of the sensor needs to be from a fairly low frequency of about 0.1 Hz to the highest frequency possible for hand motion, about 25 Hz. The highest acceleration amplitude for hand motion is about ±5 g, so this amplitude specifies the acceleration range required. Higher acceleration amplitudes are possible with shock, but measuring this type of acceleration isn't the goal of the project. However, the physical sensor should be able to withstand higher accelerations without being permanently damaged; a maximum of ±50 g's is reasonable. A resolution of 1 mg is appropriate for resolving very small involuntary accelerations in a normal human hand.

Table 1-2. Target Accelerometer System Parameters

Parameter	Target Value
Number of Axes	3
Frequency Range	0.1 to 25 Hz
Maximum Acceleration Amplitude	+/- 5 g
Maximum Acceleration w/o Damage	+/- 20 g
Acceleration Resolution	0.001 g

There are also physical requirements of the sensor associated with the goal of accurately measuring human hand motion. The human hand is fairly lightweight and consequently sensitive to external influences. Stiles and Randall[14] have analyzed the effect on the hand tremor power spectra of adding mass to the finger and the hand using one-dimensional accelerometer sensors.

For a small amount of added mass, their results indicate the peak frequency of finger tremor decreases 0.85 Hz for every gram of additional mass, and the peak frequency of hand tremor decreases by 0.018 Hz for every gram of additional mass. The amplitude of acceleration is also affected, but no solid data is presented.

The sensor also needs to be fairly small to avoid interfering with normal finger motion, such as affecting joint movement or touching an adjacent finger. Considering the mass of a typical finger ring and taking into account reasonable practical limitations for the minimum mass of the accelerometer sensor, a target mass of 5 grams maximum is reasonable. Similarly, the target maximum sensor volume is $(7\ mm)^3$. The physical target parameters are listed in Table 1-3.

Table 1-3. Target Physical Accelerometer Sensor Parameters

Parameter	Target Value
Mass	5 grams
Size	(7 mm)^3

The final system layout is diagrammed in Figure 1-1. The system consists of four sections connected with wire: the accelerometer sensor on the hand, the signal processing and data acquisition circuit (possibly on the upper arm), the digital circuit to convert the data for entry to the laptop, and the computer system. The wires connecting the accelerometer sensor to the signal processing circuit have their own physical requirements— they need to be very lightweight and flexible to avoid impeding hand movement, while resistant to fatigue after many cycles of flexing.

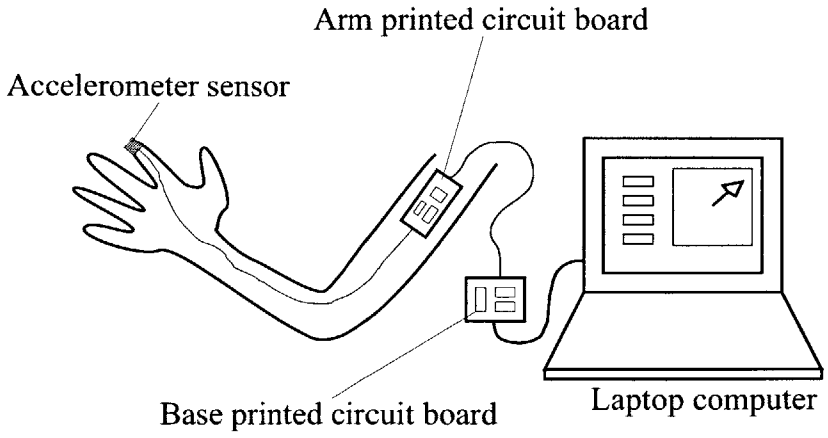

Figure 1-1. Diagram of the overall accelerometer system layout.

Chapter 2. Past Research and Applications with Hand Acceleration

A. Past Research with Involuntary Hand Motion

Involuntary hand tremor is a significant disability. In addition to preventing many normal activities using the hand such as writing, eating, and drinking, many people with serious involuntary hand tremor are socially embarrassed by their condition and sometimes become complete recluses.[21] Parkinson's disease affects at least 750,000 people in the United States.[22] Estimates for the frequency of essential tremor vary widely, ranging from 0.08 to 220 cases per 1000 people.[23] However, essential tremor is generally considered to be the most common neurological movement disorder. Overall, there are over one million people in the US affected by involuntary hand tremor. The tremor severity varies from an infrequent, small amplitude tremor confined to a single part of the body such as one finger, to continuous, large amplitude, bilateral tremors affecting entire limbs and possibly the head.

Significant past research has been done analyzing involuntary hand tremor with the twin goals of finding the cause of the tremor and then stopping it. Alleviating the tremor can be done by either curing the source (preferred) or symptomatic treatment. Several methods have been used to quantitatively analyze tremors, primarily using electromyography (EMG) analysis and accelerometer sensors (less common methods include video analysis and signals from potentiometers). EMG records the electrical activity of muscles causing the tremor, while accelerometer sensors measure the tremor acceleration. Analysis of tremors comparing EMG signals from the muscle and signals from accelerometer sensors shows the correlation between the two signals is very good.[24] As EMG recordings are generally considered the "gold standard" in tremor analysis, the good correlation of accelerometer sensors to EMG analysis indicates accelerometer sensors are a simple and non-invasive (EMG studies often use intra-muscular recording needles) way to study tremor.

Many studies have been done to analyze the origins of hand tremor and how to relieve its symptoms. Two such studies are described below: the effect of neurologically active chemicals on hand tremor, and the effectiveness of pharmaceuticals targeted to decrease the amplitude of tremor.

B. Measuring Chemical Effects on Involuntary Hand Tremor

The pre-ganglionic receptors in the parasympathetic nervous system are called nicotinic receptors because they can be stimulated by nicotine in addition to the normal parasympathetic neurotransmitter acetylcholine. The parasympathetic nervous system is only one-half of the

autonomic nervous system; the sympathetic nervous system is the other half. Increasing the concentration of a neurotransmitter (such as nicotine) which only affects one-half of the system will cause an imbalance in the nervous system. Data correlating finger tremor amplitude (measured with an accelerometer) and cigarette smoking shows a two-fold increase in tremor amplitudes between 1 and 25Hz while cigarette smoking. [25] The control in this study was inhaling through an unlit cigarette, known as sham smoking.

Caffeine is a neurotransmitter that is commonly ingested through coffee and other caffeinated beverages. Caffeine stimulates many neuroreceptors, including adenosine receptors in the central nervous system. One common side effect of caffeine is shaky hands, or an increase in hand tremor. Many studies[26,27,28] have been done quantitatively correlating hand tremor with caffeine intake. One study[26] measured finger tremor in healthy people with an accelerometer sensor and found that 150 mg of caffeine (equivalent to 3 cups of coffee) taken while fasting caused finger tremor to increase significantly, while the same amount of caffeine taken with a normal diet didn't change the amplitude of tremor.

A very common symptom with alcohol or narcotics addiction withdrawal is hand tremor, which has been quantitatively analyzed with an accelerometer sensor.[29] Hand tremor was measured for several weeks during verified abstinence. The results showed alcohol-dependent patients had abnormally high hand tremor while doing a pointing task (trying to hold their hand steady) during early withdrawal, but the tremor amplitude decreased with continued abstinence. The cocaine-dependent patients had abnormally high hand tremor while resting, but when doing a pointing task the tremor temporarily went away; the resting tremor did not improve with continued abstinence (cocaine has a very similar effect to Parkinson's disease). The results were interpreted as showing alcohol and cocaine affect different parts of the nervous system: alcohol temporarily effects the cerebellum, and cocaine more permanently affects the extrapyramidal nervous system.

Hand tremor is a common side effect with many pharmaceuticals. One study analyzed the hand tremor side effects with two drugs that are inhaled to improve lung function in asthmatic patients, salmeterol and salbutamol.[30] The study found salbutamol significantly improved in lung function after just two minutes, while salmeterol took 7 minutes for significant improvement. Similarly, hand tremor as measured with a linear accelerometer sensor had a much more rapid onset with salbutamol than salmeterol.

C. Measuring Efficacy of Essential Tremor Treatment

A pharmaceutical called propranolol is the treatment of choice for essential tremor. Essential tremor is most common in the hands, but can slowly spread up the arms to the head. Several studies have been done to quantitatively determine the efficacy of propranolol treatment.

One study analyzed the minimum dose of propranolol needed to decrease tremor, especially in the head but also in the hands.[31] Accelerometer sensors were fixed to the forehead and hands to measure the amplitude of head and hand tremor. The results showed doses at 80 milligrams/day or below were not effective. Comparing the tremor amplitudes of the head and the hand showed improvement of tremor in the head corresponded well over time to improvement of tremor in the hand.

A second study analyzed the time course of the effect of a single oral dose (120 mg) of propranolol on hand tremor as measured with an accelerometer over several hours.[32] Tremor reduction peaked at 2 hours, with a mean reduction of tremor amplitude of 50%, and the tremor amplitude remained suppressed for as long as 8 hours. There was no change in the frequency of tremor resulting from propranolol treatment.

Another possible method of alleviating the hand tremor resulting from essential tremor is applying a local anaesthetic to the skin. In one study,[33] xylocaine was used to desensitize the skin. In all patients the amplitude of tremor (as measured by EMG and an accelerometer) was reduced, with an average reduction of 40%. There was again no change in the frequency of tremor.

D. Applications Measuring Voluntary Hand Motion

Accelerometer sensors also have applications measuring voluntary hand motion by directly converting hand movement to the input of a control system. Three common examples of computer control using conventional hand movement sensors are a keyboard, joystick, and the computer mouse. Keyboards send a signal based on the location of a finger pressing a button. Joysticks use two potentiometers to sense two-dimensional tilt of a lever controlled by the hand. A conventional computer mouse uses rotational encoders to measure x and y movement of the ball under the mouse, and sends the change in mouse position as a signal to the computer.

Voluntary hand motion can be sensed using accelerometer sensors, and the signal from the sensors can be filtered to detect tilt or linear acceleration. Digital Equipment Corporation (recently acquired by Compaq) has designed a personal digital assistant (PDA) called the Itsy,[34] similar to but smaller than the Palm Pilot. The Itsy is small enough to fit comfortably into the palm of the user's hand, and has an onboard accelerometer (the Analog Devices ADXL202,[35] a

two-axis accelerometer sensor) to sense how the unit is tilted. When the Itsy is rolled side to side or pitched fore and aft, the text on the screen scrolls left, right, up, or down appropriately, and the magnitude of tilt sets the scroll speed.[36] Filtering the accelerometer signal avoids the effects of unwanted motion such as hand tremor. In addition, four different predefined functions can be indicated by momentarily dipping the appropriate edge of the PDA. The tilting and gesturing input used in the Itsy allows one-handed operation of the PDA using intuitive control directly from the hand motion instead of more a more artificial control using buttons or levers.

Another new device developed by British Telecommunications measures linear hand acceleration. It is an electronic pen called the SmartQuill[37] that has an onboard accelerometer sensor (also the ADXL202) and uses a handwriting recognition algorithm to directly enter text into a computer. By measuring the acceleration of the pen as the user writes the text, the pen decodes the acceleration into words and sends the signal into the computer. Such a computerized pen is more convenient and portable than a digitizing tablet, which measures the location of the tip of a pen on a pad.

A final significant commercial application of measuring hand acceleration is more realistic controllers for computer games. The keyboard, joystick, and mouse are effective at converting hand movement into computer signals, but pressing buttons or moving hand position over a flat plane is a natural method of control. Very small and lightweight multi-dimensional accelerometer sensors (such as the one developed in this project) can be used to directly measure hand motion with a transparent user interface.[38] Movements such as punching or turning a steering wheel can be directly converted into inputs to a computer. Accelerometer sensors can also be mounted on the head to detect tilt or other head movement, and when coupled with gyroscopes for direction sensing, the movement of the head or any other object can be fully characterized.

E. Summary of Present Measurements of Hand Acceleration

Measurement of voluntary and involuntary hand motion represents an important application for accelerometer sensors. Involuntary hand tremors are quite common and accelerometer sensors are frequently used for quantitative measurement of tremor in medical research. Voluntary hand movement is the universally used method for inputting signals into a computer system. Accelerometer sensors have the potential of making the computer input interface much more transparent.

In applications measuring either voluntary and involuntary hand movements, the ideal sensor is as small and light as possible to avoid interfering with the motion. Although some movement

will still be measured using heavy sensors, the measurement will not be an accurate representation of movement in the unencumbered system. With involuntary movement, loading the hand will increase the amplitude of tremor while decreasing the frequency.[14] With voluntary movement, more work is required to operate the sensor and the sensor interface is less subtle.

The ideal sensor of hand motion is completely transparent to the user—the mass negligible, the size small enough not to interfere with motion, and the wires (if necessary) light and flexible. The sensor developed in this project for measuring hand movement is designed to be small and light enough for measuring involuntary movement, with the connecting wire very fine gauge and flexible. As the requirements for measuring voluntary hand motion are so similar to measuring involuntary hand motion, the sensor created here also can be used in measuring voluntary hand movement.

Chapter 3. Accelerometer sensors

A. Basic Theory of Operation

Accelerometer sensors convert either linear or angular[39] acceleration to an output signal. Accelerometer sensors use Newton's second law of motion, $\vec{F} = m\vec{a}$, by measuring the force from acceleration on an object whose mass is known. There are many ways to measure the force exerted on the mass, called a proof mass, but the most common method used in accelerometer sensors is measuring the displacement of the mass when it is suspended by springs. The mass-spring system is diagrammed in Figure 3-1.

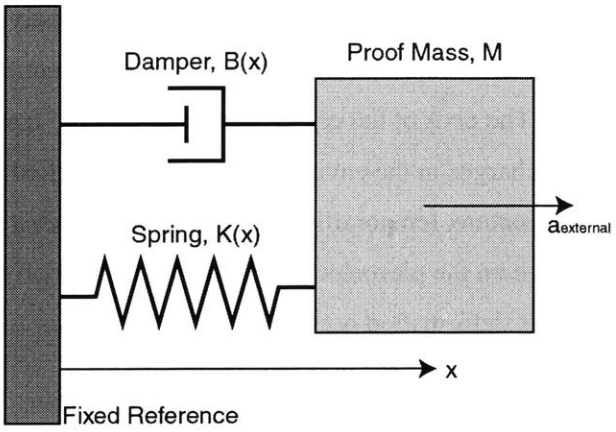

Figure 3-1. Diagram of differential capacitive layout.

Forces acting on the proof mass include the force from external acceleration, the force from damping (proportional to velocity), and the restorative force of the spring (proportional to position).

$$\vec{F} = M\vec{a}_{external} = M\frac{d^2\vec{x}}{dt^2} + B(\vec{x})\frac{d\vec{x}}{dt} + K(\vec{x})\vec{x} \qquad \text{(Eqn. 3-1)}$$

In accelerometer sensors operating far from the resonant frequency of the mass-spring system, the effect of damping can be largely ignored. Some high precision accelerometer sensors operate near the resonant frequency to mechanically amplify the displacement from acceleration. For example, the JPL seismic accelerometer described in Section 1b is designed to have the resonant frequency at 10 to 25 Hz, and the bandwidth (operating range) of the sensor is 0.05 to 50 Hz.[12] Furthermore, in the JPL sensor the cavity around the proof mass is evacuated to reduce the damping coefficient as much as possible, increasing the mechanical amplification. However, all sensors discussed hereafter are operating far from their resonant frequency.

For sufficiently small displacements, the spring constant K(x) can be assumed to be constant. (An analysis of the actual spring linearity is in Section 3e.) In equilibrium when the mass is not moving, the restorative force exerted by the spring is equal to the force from acceleration on the proof mass. The displacement of the spring, x, is a parameter that can be converted to an electrical signal by a variety of methods. The two common methods are measuring a change in resistance of a piezoresistive material and measuring a change in capacitance between moving and fixed electrical elements. An alternative way of directly measuring the acceleration force exerted on the proof mass is measuring a change in the charge of a piezoelectric material.

B. Three Types of Accelerometer Sensors

Piezoelectric materials produce a transient charge on their terminals proportional to the amplitude of compressive or shear force.[40] The charge arises from internal dipole polarization, as diagrammed in Figure 3-2. The ends of the crystal have a net charge from the dipoles, which is quickly neutralized by free charges in the environment. A force applied to the crystal causes a deformation in the dipole structure, temporarily altering the surface charge until it is re-neutralized. Thus, the charge on the piezoelectric material is a function of both the amplitude of deformation and how fast the deformation occurs.

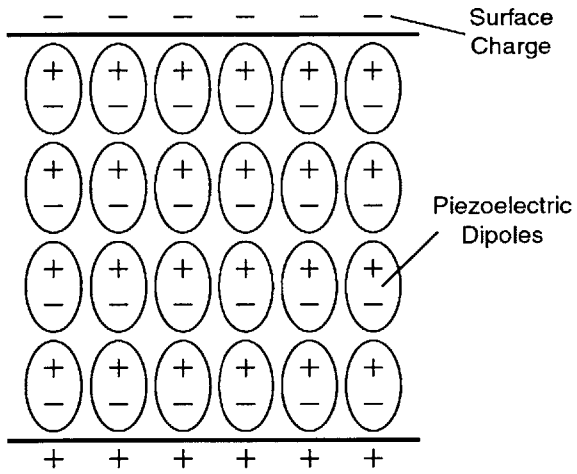

Figure 3-2. Diagram of dipoles in a piezoelectric material.[41]

Piezoelectric materials have a very high internal resistance, so the two ends of the material look like capacitor plates. The voltage across the plates is a function of the charge and the capacitance, related in the constitutive equation for a capacitor.

$$V = \frac{Q(\text{force})}{C} \qquad \text{(Eqn. 3-2)}$$

Crystals such as quartz are naturally piezoelectric but have a low sensitivity (Coulomb charge / Newton force). Man-made ferroelectric ceramics are more sensitive and consequently more widely used in piezoelectric accelerometer sensors. Overall, piezoelectric materials are an effective way to measure acceleration force, but they have the disadvantages of an inability to measure DC acceleration and a complex relationship between output voltage and acceleration amplitude and frequency.[42] Piezoelectric sensors are typically better applied measuring high amplitude and high frequency acceleration, such as shocks. Ferroelectric material can be deposited on a silicon wafer to create a piezoelectric MEMS accelerometer.[43]

Piezoresistive materials are solid-state resistors functioning as strain gages. As the mechanical stress applied to piezoresistors changes, their resistance changes also. Typically the conductance of the piezoresistive material is linearly proportional to the force, or the resistance is inversely proportional to the force.

Diagrams of two types of piezoresistive arrangements are in Figure 3-3. In the figure on the left, the piezoresistor is constructed by laying out conductive traces over a resistive film. As the silicon substrate under the film deforms, the resistance through the resistive film between the traces will change as well. A piezoresistor such as this can be made on the surface of a spring element, to measure deformation of the spring as the proof mass moves.

Another way to arrange piezoresistors is like microscopic wire strain gages, as diagrammed on the right of Figure 3-3. The freestanding conductors deform from mechanical stress. Usually the piezoresistor is arranged to have exclusively tensile or compressive stress, and the resistance of the piezoresistors is a function of the width of the gap the piezoresistors bridge.

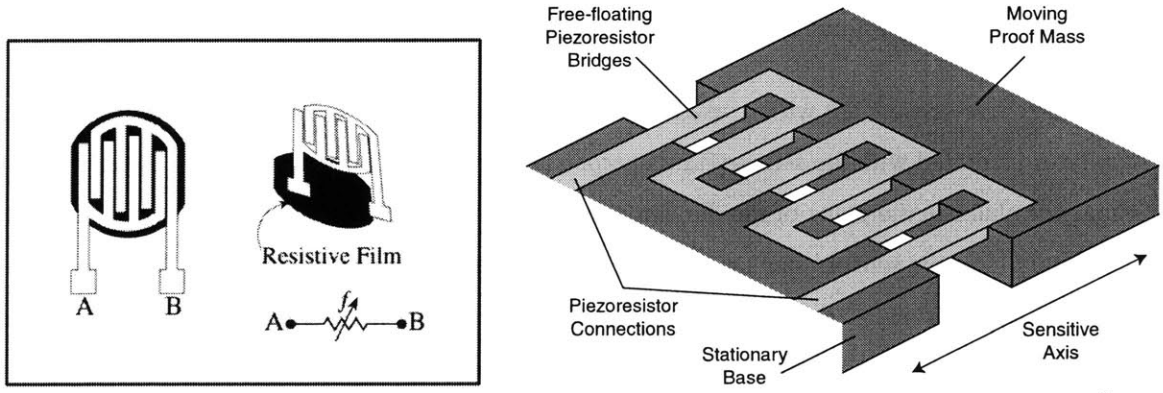

Figure 3-3. (a. Left) Diagram of a piezoresistive layout using resistive film backing.[44] (b. Right) Diagram of a free-standing piezoresistive strain gage.

Using either of these two methods for applying piezoresistors, the displacement of a proof mass in an accelerometer sensor can be measured. Commonly, multiple piezoresistors are used

with the same mass-spring system, and arranged in a bridge circuit to increase sensitivity and reduce thermal variations.

Finally, the capacitance between the moving proof mass and some fixed object on the base of the sensor can be measured. As the displacement of the proof mass changes relative to the base, the gap between the two sides of the capacitor will increase or decrease. The equation for capacitance is an inverse function of the gap (d).

$$C = \frac{\varepsilon A}{d} \qquad \text{(Eqn. 3-3)}$$

The capacitance can either be arranged as single-sided or differential pair. A diagram of a differential capacitive pair is in Figure 3-4. In a setup as shown in the diagram the entire proof mass is conductive, and a connection through the spring to the proof mass serves as the electrical connection to the floating capacitor plate.

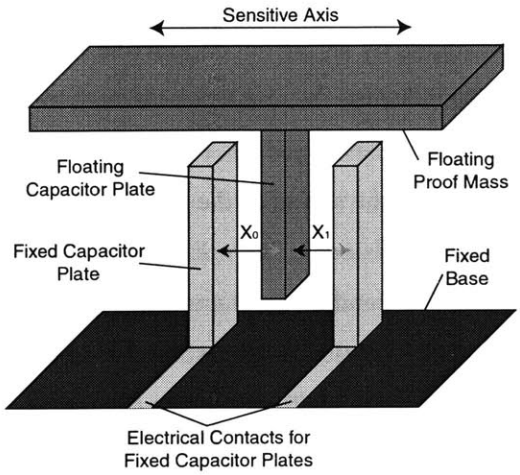

Figure 3-4. Diagram of differential capacitive layout.

Capacitive sensors are widely used in accelerometers. Single-sided capacitive accelerometers can be constructed with the sensitive axis perpendicular to the plane of the silicon die and the capacitor plates in the plane of the die, allowing a very large capacitor area and resulting in a high sensitivity (seismic sensors such as the JPL sensor often use this arrangement[12]). More conventional sensors use differential pair capacitors and are constructed with the sensitive axis in the plane of the device. Another advantage of differential capacitive accelerometer sensors is an electrostatic force-feedback system can be used to avoid non-linearities in the springs and capacitors by keeping the mass position nearly fixed. (The force-feedback system is described more below.)

C. Three Commercially Available Micro-Accelerometer Sensors

Three examples of commercially available accelerometer sensors will demonstrate different methods of measuring acceleration. These three sensors were selected to display a variety of technical solutions to acceleration measurement, and they have the necessary specifications to measure hand acceleration (although in general they are too big and heavy). The three examples are the PCB Piezotronics 352C67[45] (piezoelectric), the Endevco 7265A-HS[46] (piezoresistive), and the Analog Devices, Inc. (ADI) ADXL105[47] (differential capacitive). The accelerometer sensor used in this project is similar to the ADI sensor, so discussion of the ADXL105 will be more extensive. Specifications for all the sensors are in Table 3-1 at the end of this section.

The PCB Piezotronics 352C67 piezoelectric accelerometer is not a MEMS; the sensor is encased in a titanium housing and hermetically sealed. Most MEMS piezoelectric accelerometers have insufficient sensitivity for accurately measuring hand movement because the amount of piezoelectric material is extremely small. The piezoelectric element in the PCB Piezotronics device is used in shear mode, which reduces the noise floor and sensitivity to thermal transients arising from the center post. Cross-sectional diagrams of the sensor are in Figure 3-5. A pre-tensed metal ring is placed around the piezoelectric material to cause initial deformation in the dipole matrix, increasing the sensitivity.

The sensor includes an amplifier inside the housing to amplify the piezoelectric voltage and produce a low impedance output. The output signal of the amplifier gives the sensor a sensitivity of 100 mV/g. As with all piezoelectric sensors, there is no response at DC; the lowest acceleration frequency that can be measured is about 0.5 Hz.

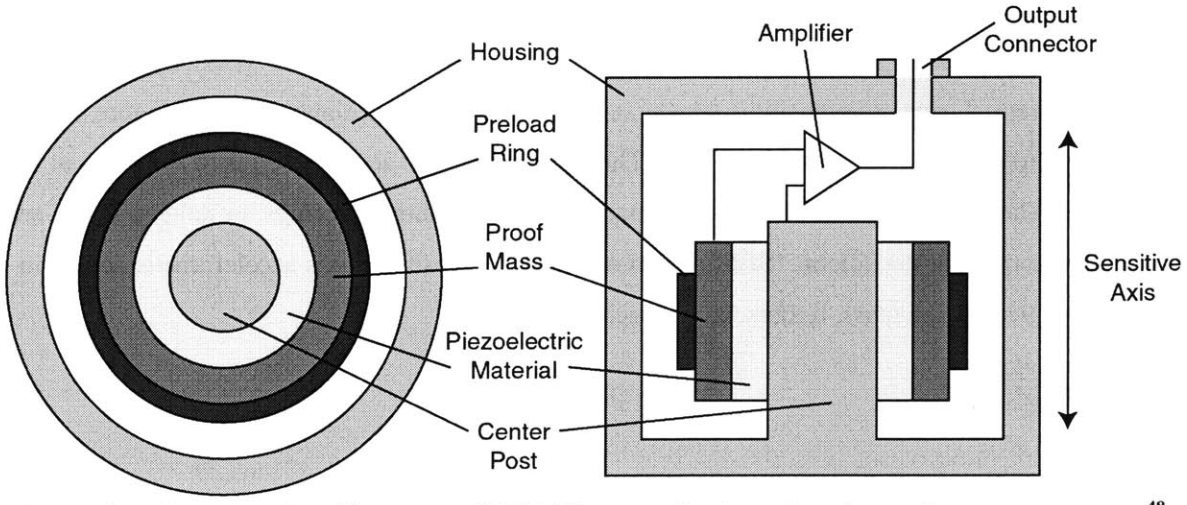

Figure 3-5. Cross section diagrams of PCB Piezotronic piezoelectric accelerometer sensor.[48] (a. Left) Top view. (b. Right) Side view.

The Endevco 7265A-HS piezoresistive accelerometer sensor is constructed on a single chip and then packaged inside an aluminum alloy housing. The device uses a MEMS mass-spring system in which the mass is suspended along one edge by a silicon hinge. A top-view diagram of the sensor layout is in Figure 3-6. The axis sensitive to acceleration is in the plane of the device. The hinge acts as a rotational spring that applies a force proportional to the angle between the proof mass and the rest of the sensor, to counteract the acceleration force. Near the ends of the mass are the piezoresistive strain gage sensors, arranged in a differential pair on either side of the hinge. As the sensor is accelerated the mass rotates, and the strain gages detect the magnitude of rotation.

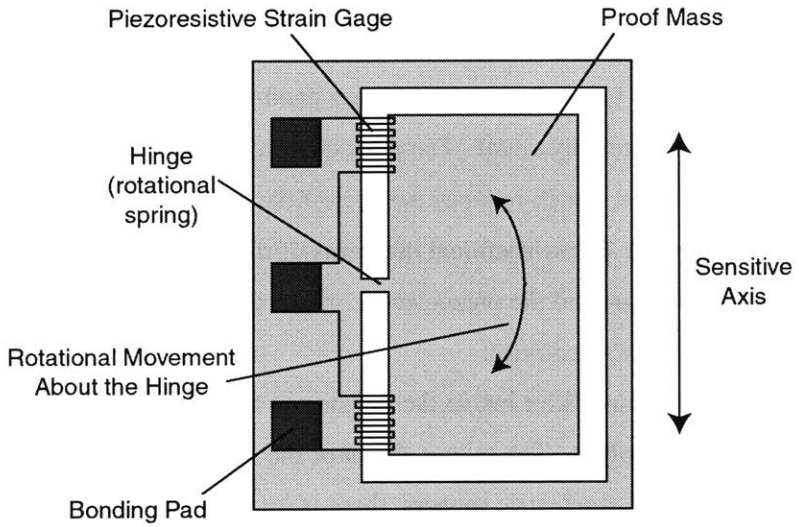

Figure 3-6. Diagram of Endevco piezoresistive accelerometer sensor.[49]

The ADI ADXL105 accelerometer sensor is packaged as a standard integrated circuit: a 10 lead ceramic package or a metal can. The mass-spring system used in the ADXL105 is MEMS and differential capacitive position sensing is used. The system is diagrammed in Figure 3-7 and a die photo of the sensor is in Figure 3-8. The axis sensitive to acceleration is in the plane of the device. The mass is a piece of the wafer attached at the corners by springs, or tethers, which are also formed out of the silicon. SEM photos of another ADI single-axis accelerometer sensor in Figure 3-9 show the mass, tethers, and capacitive elements.

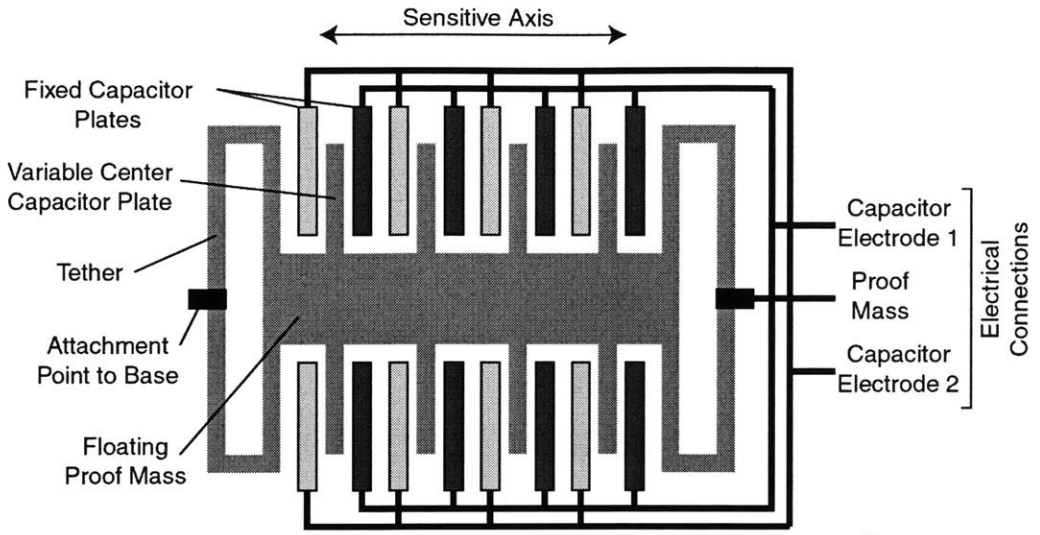

Figure 3-7. A diagram of the ADXL105 MEMS layout.[50]

On the single silicon die there is the mass-spring system and also the entire electrical circuit to calculate the acceleration from the measured displacement of the mass. This is the circuit seen on the die surrounding the proof mass in figures 3-8 and 3-9. ADI calls this technology iMEMS, for integrated MEMS.[51] The final output of the chip is an analog voltage ranging from zero to five Volts and linearly proportional to acceleration.

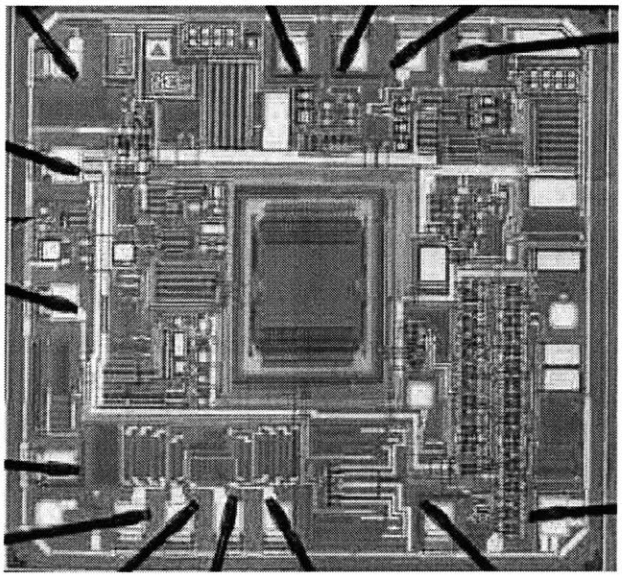

Figure 3-8. Die photo of the ADXL105 accelerometer sensor.[52]

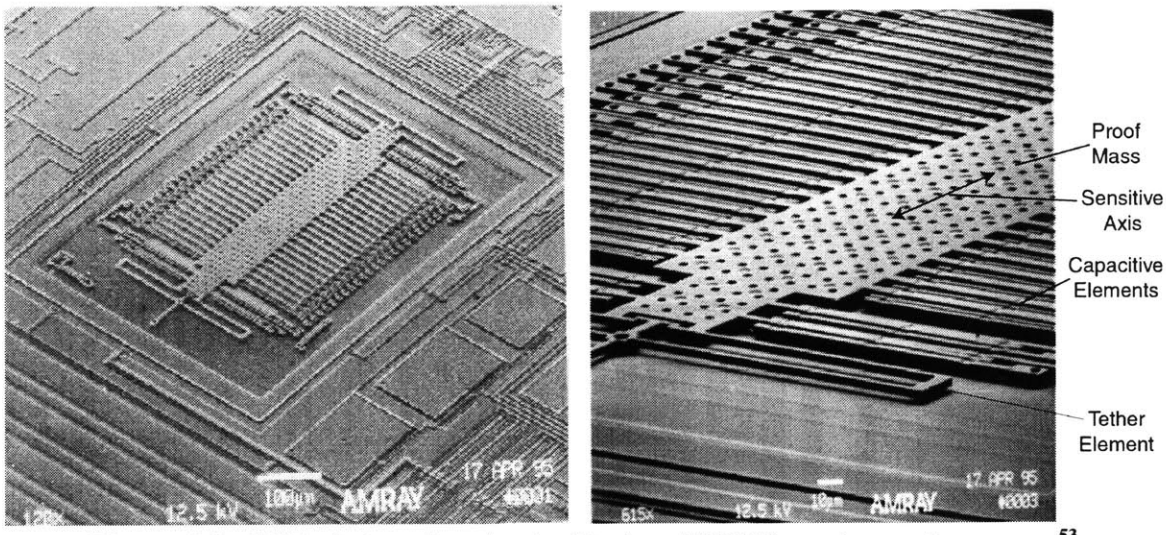

Figure 3-9. SEM photos of an Analog Devices iMEMS accelerometer sensor.[53]

The ADXL105 uses a force-feedback loop, to avoid non-linearities in the springs and capacitive sensors. The two fixed sets of capacitor plates are held at DC bias voltages, $\pm V_0$. Then the voltage on the proof mass is changed to alter the net electrostatic force between the floating capacitor plates on the proof mass and the fixed capacitor plates on the base. The appropriate electrostatic force is applied to keep the position of the proof mass fixed, independent of the external applied acceleration. The equation for the electrostatic force of attraction between two capacitor plates is

$$F = \frac{CV^2}{2d} \qquad \text{(Eqn. 3-4)}$$

where C is the capacitance, V is the voltage difference between the plates, and d is the gap between the capacitor plates.

The net force with a differential capacitive arrangement is the sum of two oppositely directed electrostatic forces. Expanding the equation for capacitance and assuming the two sets of capacitor areas are equal (an excellent assumption), the equation for net electrostatic force is

$$F_{net} = \frac{\varepsilon A}{2}\left[\frac{(V_0 - V_{mass})^2}{(d_0 - x)^2} - \frac{(V_0 + V_{mass})^2}{(d_0 + x)^2}\right] \qquad \text{(Eqn. 3-5)}$$

Essentially the force-feedback circuit measures a small displacement of the proof mass, modifies its guess of the external acceleration force based on the equation for the spring (Equation 3-1), and then applies the V_{mass} necessary to restore the mass to its resting position. The output voltage is linearly proportional to the net electrostatic force applied, as this is equal to the acceleration force in equilibrium. The force-feedback method keeps displacements of the

mass extremely small to minimize mechanical non-linearities and also allows the above equations to be linearized.

ADI accelerometers also are available in two-axis versions; the two axes are perpendicular and in the plane of the die. There are two ways two-axis sensors can be constructed: two different single-axis accelerometer sensors laid out with the two axes perpendicular, or a single proof mass which can freely linearly translate along both axes in the plane of the die. A single mass needs to have capacitive sensors arranged to measure movement along both axes. Die photos of each of these constructions are in Figure 3-10. Three-axis accelerometer sensors on a single die can be constructed in a similar manner: separate single-axis accelerometer sensors with separate proof masses for each of the three axes,[54] or using fewer proof masses (two or even one[55]) and multiple sensitive axes on the proof masses. For measuring out of plane motion, the sensor can use a single sided capacitance, as described above in Section 3b.

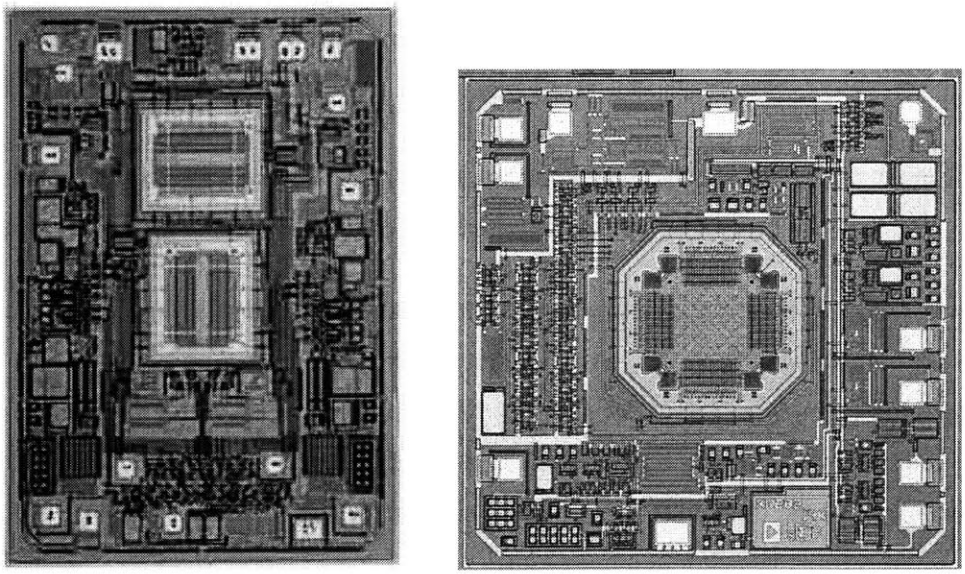

Figure 3-10. Die photos showing different ways of creating two-axis accelerometer sensors. (a. Left) Two proof masses: the ADXL250.[52] (b. Right) One proof mass: the ADXL210.[56]

There are no commercially available single-chip three-axis accelerometer sensors available. When using a single proof mass to measure all three axes, it is very difficult to constrain the motion of the proof mass to purely linear translation along all three axes: building the tether design is too hard. Three-axis accelerometer sensors using three separate proof masses are limited by the technology used to measure out-of-plane acceleration, which isn't developed enough to be applied commercially. However, within the next few years ADI will undoubtedly mass-produce a single-chip three-axis accelerometer sensor.

Since the commercial introduction of the first ADI iMEMS accelerometer sensor in 1993, the resolution of the sensors has increased while the cost of the sensors has decreased. As shown in the left plot of Figure 3-11, the resolution of the accelerometer sensors has improved from 30 mg in 1993 to 0.3 mg today. At the same time, the cost of each axis per mg resolution (a metric for the cost of performance) has dropped from about $500 down to less than $5 today, as shown in the right plot of Figure 3-11.

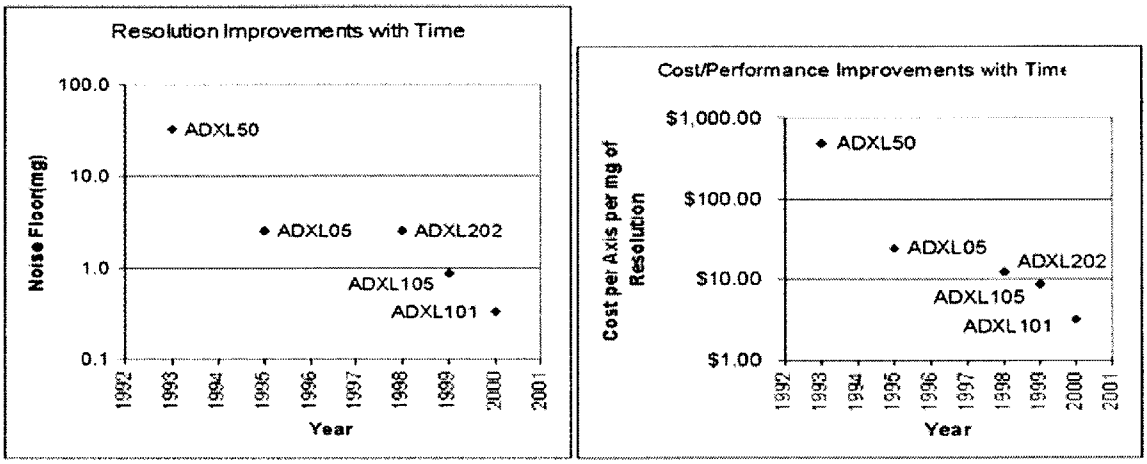

Figure 3-11.[52] (a. Left) The resolution of ADI accelerometer sensors over time. (b. Right) The cost of performance in ADI accelerometer sensors over time

The overall specifications of the piezoelectric, piezoresistive, and differential capacitive sensors are compared in Table 3-1. Also included in the table are the specifications for the MIT Microsystems Technology Laboratory (MTL) differential capacitive accelerometer sensors used in this project. Two of the key reasons for using the MTL accelerometers are the small size and mass, which allow the final three-dimensional sensor to be small and lightweight.

Table 3-1. Comparison of Endevco, PCB Piezotronics, Analog Devices, and MIT MTL Accelerometer Sensors

Device Type	Piezoresistive	Piezoelectric	Differential Capacitive	
Manufacturer	Endevco	PCB Peizotronics	Analog Devices	MIT MTL
Part Number	7265A-HS	352C67	ADXL105	Type 2
Normal Range	+/- 20 g	+/- 50 g	+/- 5 g	+/- 5 g [2]
Sensitivity	25 mV/g	100 mV/g	250 mV/g	938 mV/g [2]
Resolution	2 mg	0.16 mg	2 mg	2.5 mg [2]
Frequency Range (+/- 5%)	0 to 500 Hz	0.5 to 10,000 Hz	0 to 5,000 Hz	0.1 to 25 Hz [2]
Resonant Frequency	1400 Hz	35 kHz	18 kHz	2 kHz
Nonlinearity	2%	5%	0.20%	1.3% [3]
Transverse Sensitivity	5% max	5% max	5% max	3.75% max [3]
Max Acceleration	2000 g	5000 g	1000 g	45 g [4]
Mass	< 5.9 grams [1]	2.0 grams	0.934 grams	.036 grams [5]
Size	11.9 x 7.4 x 7.4 mm [1]	11.4 x 7.1 x 7.1 mm	10.5 x 10.6 x 4.3 mm	5 x 5 x 0.7 mm [5]

Notes: [1] Removing bolt attachments reduces the weight by a gram or two and reduces the volume to that indicated. The MEMS device inside the aluminum housing is 3 x 1 x 1 mm.
[2] Unknown; dependent on the electrical circuit. Values given are results in this project.
[3] Previously unknown. Determined in Section 7e of this project.
[4] No specification exists. Rough calculation made in Section 3e.
[5] The size and mass of the raw die.

D. The MTL Accelerometer Sensor

The MTL accelerometer sensors (including those used in this project) were fabricated over the past few years in several iterations by visiting researcher Kei Ishihara and graduate student Chi-Fan Yung. The MTL accelerometer sensor is similar to the ADI accelerometer sensor described above in that it uses differential capacitors with a mass-spring system. There are several significant differences between the MTL and the ADI accelerometer sensors, however. ADI accelerometer sensor fabrication uses polysilicon deposition over a sacrificial oxide layer and later removal of the sacrificial layer allows free movement of the proof mass. The MTL accelerometer sensor was fabricated using deep reactive ion etching (DRIE) to remove sections of the silicon wafer all the way through. These cuts create gaps around the proof mass allowing it to move as designed. The cuts in the wafer require a second wafer underneath to support the different pieces: the lower "handle" wafer supports the accelerometer components and provides electrical traces to connect the capacitor electrodes, and the upper "device" wafer is the wafer cut by DRIE. A diagram of the MTL accelerometer sensor layout is in Figure 3-12.

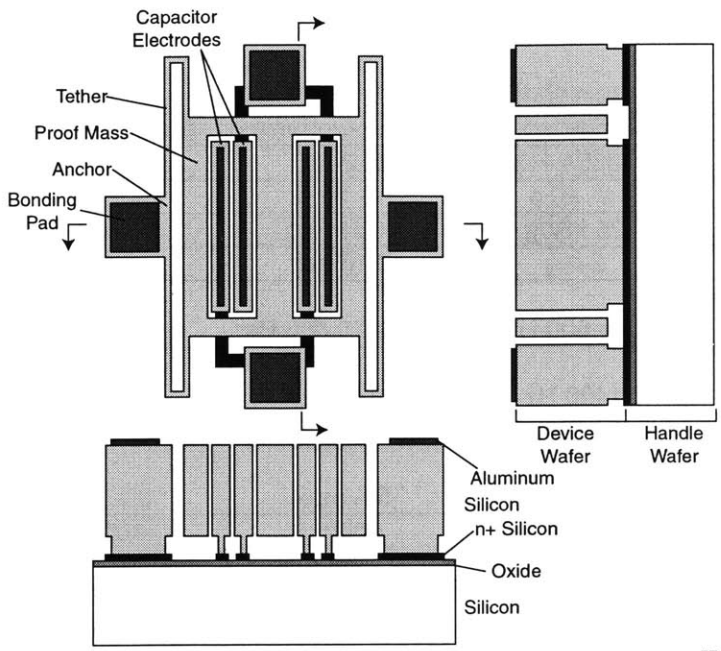

Figure 3-12. Layout of the MTL accelerometer sensor.[57]

The MTL accelerometer sensors don't have on-chip electronics like the ADI sensor. The capacitor plate geometry the MTL accelerometer sensors use is much different than the geometry used on the ADI sensor. The MTL accelerometer uses only five or seven capacitor plates arranged on inner surfaces of the proof mass. The ADXL105 has over 50 capacitor plates arranged around the exterior periphery of the proof mass. The connections between the internal capacitor electrodes on the MTL accelerometer occur through the electrical traces on the handle wafer. Die photos of five and seven capacitor MTL accelerometers are in Figure 3-13.

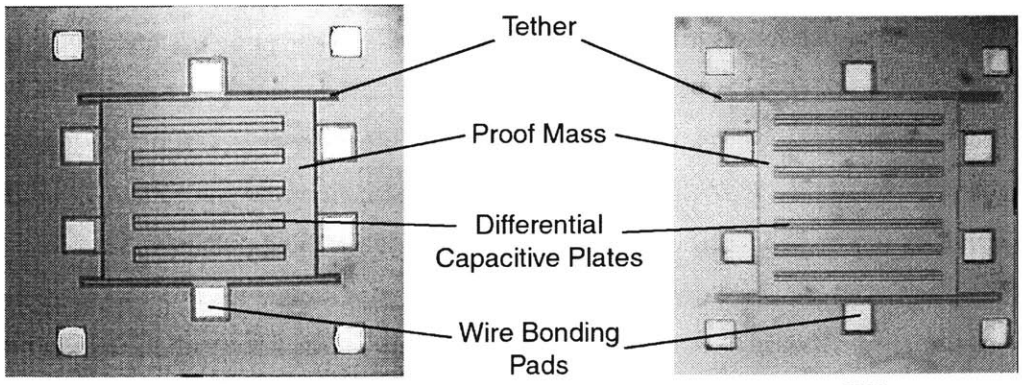

Figure 3-13. Die photos of MTL accelerometer sensors.[58,59]

There are six connected wire bonding pads on the die arranged in three pairs of redundant connections. One pair connects to the proof mass through the tether elements. The other two pairs connect to each of the two sets of capacitor electrodes. The layout for wire bonding

contacts is shown in Figure 3-14; the same pattern is used for all of the different types of MTL accelerometer sensors.

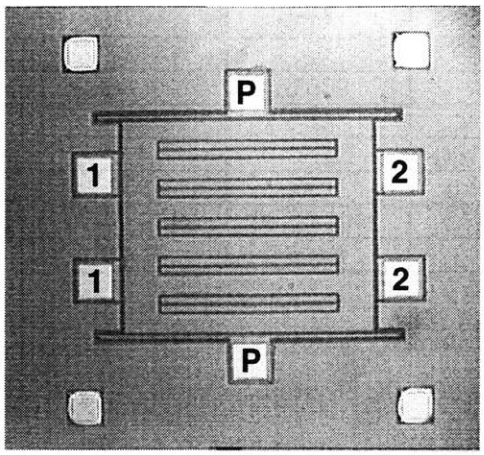

Figure 3-14. Layout of the MTL accelerometer sensor bonding pads.[60]
Legend: P: proof mass, 1: capacitive electrode 1, 2: capacitive electrode 2

There are several advantages of using DRIE fabrication as in the MTL accelerometers instead of polysilicon deposition over sacrificial oxide as in the ADI accelerometers. One reason is maintaining a single silicon crystal avoids any potential material stability problems associated with the bonding of polysilicon on monocrystalline silicon. Another reason is the ratio of the thickness of the sensor to the horizontal dimensions of the mechanical elements, called the aspect ratio, on the sensor is increased.

Increasing the aspect ratio has many benefits. The capacitance between the proof mass and the capacitor electrodes is increased from the higher surface area, increasing the sensitivity (Farads capacitance / Newtons force) of the sensor. The cross-sensitivity (sensitivity to acceleration along perpendicular axes) is reduced because the tethers have more depth and have more mechanical strength to constrain the proof mass motion to the desired axis. Susceptibility to Brownian noise is reduced because the proof mass is more massive.

There are several different versions of the MTL accelerometer with different mass, spring, and capacitor geometries. The specifications of the different models are in Table 3-2. The type 2 sensor was the version selected for this project for several reasons. The large capacitance and high sensitivity makes signal processing easier. The small die size reduces the required package size and the final volume of the sensor. Finally, the type 2 accelerometer dies were available in adequate quantity: a fabrication cycle to produce more accelerometers was not desired.

Table 3-2. Comparison of different MTL accelerometer models.

Accelerometer	Type 1	Type 2	Type 3	Type 4
Number of capacitor plates	7	7	7	5
Sensitivity (fF/g) (each set)	31	90	31	53
Total Spring Constant (N/m)	141.6	141.6	140.8	108.8
Gap spacing (um)	5	3	5	3
Proof mass (ug)	965.3	965.3	965.3	750.5
Resonant Frequency (kHz)	2	2	2	2
Capacitance (pF) (each set)	2.5	4.2	2.5	2.5
Proof mass thickness (um)	100	100	100	100
Proof mass area (um^2)	2400x2400	2400x2400	2400x2400	1750x2400
Die size (mm^2)	5 x 5	5 x 5	5 x 5	5 x 5

E. MTL Accelerometer Linearity Analysis and Specification Calculations

As will be seen in Chapter 5, the electronics that convert the differential capacitance signal in the sensor results in an analog voltage that is linearly proportional to the proof mass position in the sensor. This is very convenient because the proof mass position is linearly proportional to external acceleration and thus the analog voltage will be linear with acceleration. Consequently an important aspect of analyzing the sensor is considering how linear the output is with acceleration. This section investigates the proportionality between the proof mass position and external acceleration. Section 5d looks at linearity in the electronics.

Analyzing linearity of the physical mass-spring system is equivalent to asking how strongly the spring constant K(x) in Equation 3-1 is a function of the mass displacement x. Accurate estimates of the restorative force of the spring can be made using numerical techniques such as finite element analysis or solving analytical equations. One analytical method commonly used is minimization of energy in the system. The derivation of the force necessary for beam deflection (applicable to the tethers that hold the mass in place) is described elsewhere,[61] and only the results of the calculation are presented here.

The restorative force at the end of a long deflecting beam is given in Equation 3-6. E is Young's modulus for the material (silicon: E = 1.525 x 10^{11} N/m^2), d is the deflection, and D is the depth, L is the length, and W is the width of the beam (width is in the direction of displacement). The first term of the summation is linear with displacement; this term represents the ideal spring constant K, associated with beam bending. The second term is nonlinear with displacement and is associated with stretching the beam.

$$F = \frac{ED\pi^4}{32L^3}\left[\frac{W^3 d}{3} + \frac{Wd^3}{4}\right] \qquad \text{(Eqn. 3-6)}$$

At each of the four corners of the mass are tethers, consisting of two beams in series. (The two beams act as springs in series, which add like capacitors in series.) The dimensions of the two tethers are given in Table 3-3.

Table 3-3. MIT MTL type 2 accelerometer tether geometry.

Dimension	Size
Length 1	1500 um
Length 2	500 um
Depth (1 and 2)	100 um
Width (1 and 2)	20 um

Using just the linear term in Equation 3-6, the restorative force related to the ideal linear spring coefficient for two beams in series with the geometries in Table 3-3 can be calculated. The total force on the mass is equal to the restorative force from each tether times the number of tethers. The resulting total force corresponds to a spring coefficient of 141.6 N/m, which is the specification for type 2 accelerometers in Table 3-2.

Now the contribution from the nonlinear term in Equation 3-6 is considered. By solving the complete equation for a variety of displacements, the range of displacement corresponding to the ± 5 g acceleration range is determined. The nonlinearity is a cubic polynomial and becomes more significant with larger displacements; a plot of the contribution from the nonlinear term is in Figure 3-15. The effect of the nonlinear term is to create an error in the output ranging from ± 1.0 mg over the range of displacements from ± 5 g acceleration.

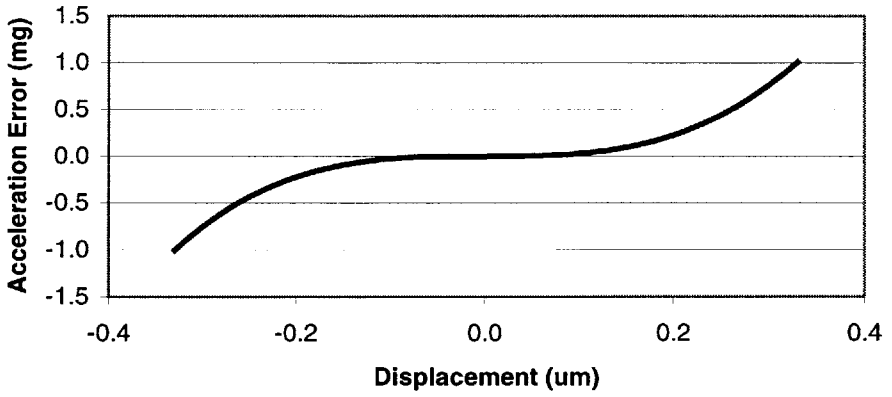

Figure 3-15. Nonlinear error in the accelerometer sensor response over the ± 5 g acceleration range.

As will be seen in Section 5b, the sensitivity (output / acceleration input) of each accelerometer sensor must be calibrated to compensate for variations in resistances internal to the

die. Consequently, an applicable measure of nonlinear error is the maximum integral linearity error (MILE), which is the largest difference between the actual output and a straight line between the minimum and maximum outputs. The straight line corresponds to the sensitivity calibration. With the type 2 accelerometer, the MILE peaks at ± 2.9 g acceleration, and the error is 0.388 mg. Given the full-scale range of ± 5 g, this corresponds to a nonlinearity of 39 parts-per-million (ppm). The nonlinearity of the mass-spring system is fairly good given the ideal specification of 1 mg resolution for the sensor (from Section 1d), and the relative nonlinearity in the electronics (discussed in sections 5b and 5d).

There is an additional potential non-linearity from the electrostatic force and the voltage differences between the proof mass and the capacitor electrodes, as in Equation 3-5. This force will not be important as long as the frequency of the voltage signals is much different than the resonant frequency of the mass-spring system. This is the case in this project: the signal frequency is 20 kHz, but the resonant frequency is only 2 kHz.

The sensitivity of the physical accelerometer is the change in capacitance with the change in acceleration. Sensitivity increases as the displacement increases, because the capacitance is inversely related to the displacement so the capacitance changes faster for small displacements. Over the full scale range of ± 5 g, the displacement is ± 0.33 μm (as in Figure 3-15). Calculating capacitance from Equation 3-3, the capacitance varies from 3.78 to 4.73 pF over the ± 0.33 μm, for a difference of 947 fF over ± 5 g, or a sensitivity of 94.7 fF/g over the full scale. For very small displacements, the sensitivity is lower because the capacitance changes less quickly: the sensitivity is only 93.5 fF/g for the ± 0.5 g acceleration range. These results are close to the 90 fF / g specification for type 2 accelerometers in Table 3-2.

An approximation for the maximum acceleration range of the sensor can also be calculated. When the proof mass has moved so far that the two capacitor electrodes are touching, then that acceleration can be considered to be the maximum acceleration the sensor can safely experience. Using the gap spacing of 3 um for the type 2 sensor, this acceleration is 45.6 g. However, mechanically the sensor may be able to take much higher accelerations before there is permanent mechanical damage. Still, ± 45 g is much higher than the ± 20 g maximum survivable acceleration specification for the final sensor from Section 1d.

F. MTL Accelerometer Fabrication

About forty MTL accelerometer sensors were fabricated on each four-inch diameter silicon wafer. The handle and device wafers were processed separately, bonded together, and then the

top surface of the bonded pair was worked on. The wafers were standard thickness, 500 to 550 μm. The accelerometer sensor fabrication took place at the MIT MTL fabrication facilities.[62]

The handle wafer originally had a thin conductive layer over an insulating layer on the top surface. The first processing step was etching global alignment marks on the top and bottom surfaces, for alignment with photolithography and wafer bonding. Next, the thin conductive layer was selectively etched away to form the traces connecting the capacitive electrodes together. The locations of the remaining conductive traces are shown in Figure 3-15a. Finally, a protective oxide layer was added to cover the conductive traces where they might have been exposed in the final DRIE step after the two wafers were bonded together.

The device wafer was a fairly conductive n-doped silicon wafer. The first step in processing the device wafer was again placing global alignment marks, although this time exclusively on the bottom surface which would be contacted with the handle wafer (the upper surface is polished later, which would remove the marks). Then 20 μm cavities were formed by DRIE. The locations of the DRIE cavities are shown in Figure 3-15b. This etch step creates the separation between the proof mass on the device wafer and the top surface of the handle wafer, and hence determines the parasitic capacitances between the proof mass and the capacitor interconnect traces. A 20 μm etch depth was chosen to minimize the parasitic capacitance while maintaining the capacitor surface area. Areas where no etch occurred became the anchors that supported elements on the device layer over the handle wafer.

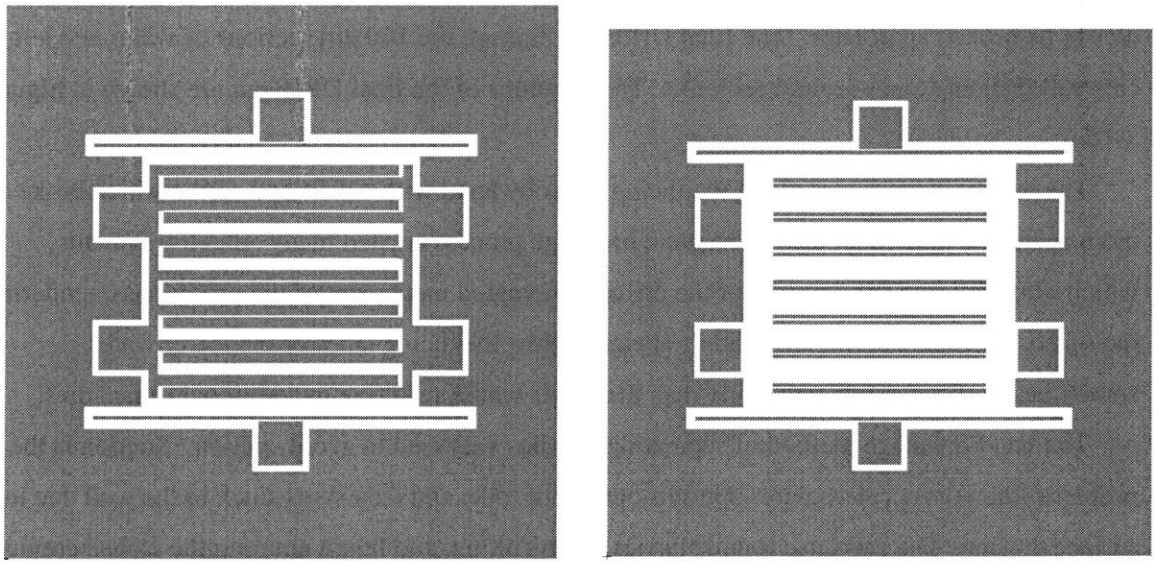

Figure 3-16. MTL accelerometer fabrication photoplots.[63] (a. Left) Conductive traces on the handle wafer interconnect layer. (b. Right) Device wafer DRIE cavity etch locations.

Next the handle and device wafers were bonded together. Wafer bonding is a three-step process: preparing the surface, contacting the two wafers together, and finally annealing.[64] The surface is prepared by ensuring the contacting surfaces are very smooth and flat, and then cleaning the wafers to form hydrated surfaces. The wafers are carefully aligned using the etched alignment marks. Contact occurs by pressing the two wafers together at a central point, and then a contact wave is initiated that sweeps across the entire surface. Finally, the contacted pair is annealed at elevated temperature to increase the bond strength.

After bonding, the device wafer half of the bonded pair was thinned down to 120 μm by mechanical polishing, leaving 100 μm thick device elements (the other 20 μm had been previously removed by DRIE from the other side). The 100 μm element thickness was chosen because this is a depth for which DRIE works well. Thicker elements would be preferred, and as the DRIE technology improves the thickness can be increased.

After polishing, new global alignment marks were created on the top surface, positioned by looking at the relative orientations of the prior three alignment marks using infrared photography to see through the wafers. An oxide layer was thermally grown on the surface of the device wafer, and then the oxide was selectively removed over the sites of the bonding pads where a 1μm thick aluminum layer was deposited. The locations of aluminum deposition are shown in Figure 3-16a. An additional protective oxide was added over the new aluminum pads. The oxide was then selectively removed for the final DRIE: exposed were the locations where the wafer would be cut through to free the proof mass, and between adjacent dies to allow the individual dies to be broken apart later. The final DRIE cut through the 100 μm sections of wafer and left cuts called dicing lanes around each die. The locations of the final DRIE cut are shown in Figure 3-16b.

The wafers were scored along the dicing lanes by hand with a diamond scribe which broke them apart into individual dies. The hand breakage process created many silicon fragments, which often fell into the crevices of the die and prevented movement of the proof mass, rendering the sensor useless. Scoring also didn't always follow the dicing lanes or the lower wafer sometimes broke at a different angle than the upper wafer, resulting in additional ruined dies.

The hand-breakage method of separating the dies was used to avoid stiction. Stiction is the problem when the accelerometer bottoms out to one side, and then stays stuck to the wall due to surface tension. Die saws use liquid slurries when cutting, and liquid entering the etched crevices increases the surface tension and the probability of stiction. Hand breaking the wafers avoids liquids, but induces other significant problems with quality.

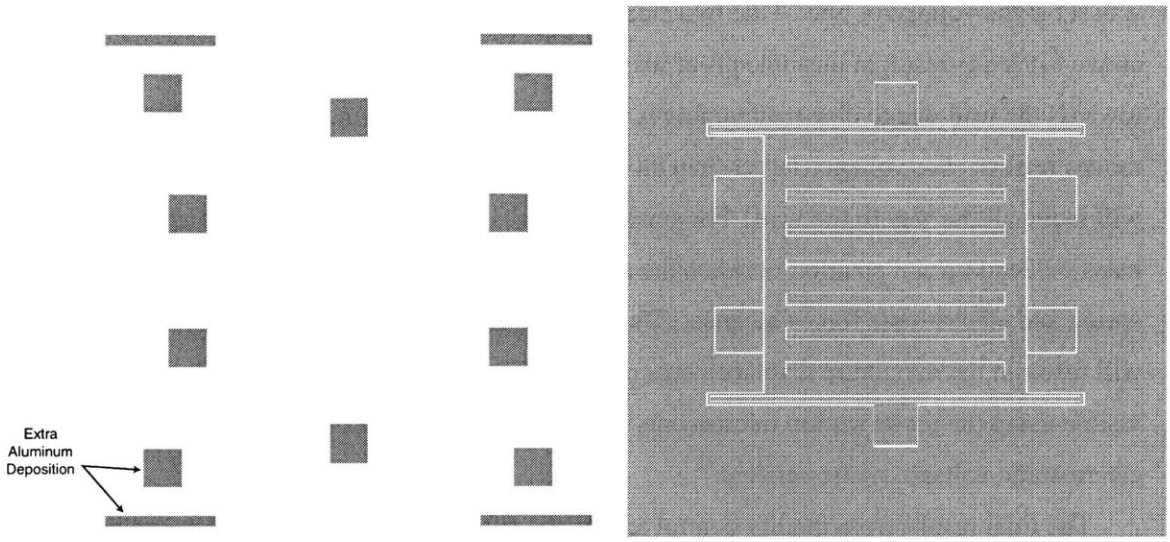

Figure 3-17. MTL accelerometer fabrication photoplots.[63]
(a. Left) Metal deposit sites. (b. Right) Inverted DRIE location.

G. MTL Accelerometer Quality Control

The process of packaging and testing the functionality of accelerometer sensors is expensive and time-consuming, and the fraction of functional MTL accelerometers out of those fabricated was known to be low due to the hand breakage problems. Consequently, a simple quality-control test was performed on the dies before selecting which ones to use.

The test was performed at a probe-station. Probes were used to contact the pads on the die, and by changing the relative voltage on the proof mass and the capacitive electrodes, electrostatic forces were created that caused movement of the die, visible through the microscope of the probe station. Although this process didn't explicitly test the response of the accelerometer to acceleration, the test did indicate which accelerometers were clogged with silicon fragments or otherwise broken, which were the expected problems with the accelerometer sensors.

Three probes were touched to three pads on the die: one pad for each of the two sets of capacitor electrodes, and one pad connected to the proof mass through the tethers. The capacitor electrodes were biased to plus and minus fifteen Volts, and the voltage on the proof mass was varied between plus and minus fifteen Volts.

Numerical analysis was used with the equation for net electrostatic force on the proof mass (Equation 3-5 above) and the parameters for the type 2 accelerometer sensors to calculate the proof mass position from the applied voltage. The analysis was iterated multiple times to account for movement of the proof mass and changes in the net electrostatic and restorative spring forces. Analysis was restricted to symmetric capacitor electrode voltages, ±V, and the proof mass voltage

was set at the voltage of one of the two electrodes. The analysis results show voltage amplitudes above 6.1 Volts result in unstable proof mass movement. That is, as the proof mass moves towards the wall due to electrostatic forces, the electrostatic force increases, and the proof mass moves further. For voltages larger than this threshold, the feedback is positive and the proof mass will move all the way to the wall. For smaller voltages the feedback is negative and the proof mass will end up at a position between the zero-force resting position and the wall where the spring and electrostatic forces balance. Thus, proof mass voltages of plus or minus fifteen Volts will result in the maximum displacements possible. Such a displacement magnitude is clearly visible using the probe station microscope, and proper response of the accelerometer to the electrostatic voltage can be verified.[65]

The final results from quality control testing the fifteen accelerometer sensors are in Table 3-3. There were four accelerometer sensors that had large and regular displacements when the voltage on the proof mass was flipped between plus and minus fifteen Volts. Such a response was expected for a properly functioning accelerometer and the accelerometer was called good response, good quality. There were three accelerometers that either moved well to only one side, or seemed to get stuck often. This was probably due to small silicon fragments caught in the gaps; these accelerometers are referred to as good response, poor quality. There were three accelerometers that had very little movement (poor response). Finally, there were five that had no movement at all (no response).

Table 3-4. Quality Control Testing Results of MTL Accelerometer Dies

Category	Number of Dies	Percentage of Total
Good Response, Good Quality	4	27%
Good Response, Poor Quality	3	20%
Poor Response	3	20%
No Response	5	33%
Total	15	100%

Of the fifteen accelerometers tested, twenty seven percent were operating correctly. When trying to calculate the overall yield from fabrication, additional accelerometers that were obviously damaged after hand breaking would need to be included in the total count as well, decreasing the overall yield further. Twenty-seven percent is an already an extremely low yield, but acceptable for fabricating an experimental device to show proof-of-concept.

If a higher yield of accelerometers were required such as in a commercial production, then a different die-separation process would be needed. One idea previously suggested[64] is bonding a third wafer over the present two to act as a capping wafer. The capping wafer would prevent any fluid from the die saw cutting process to enter the gaps in the accelerometer sensor. An

additional advantage of capping is if the wafer bonding is done in a vacuum, the environment around the proof mass will remain in a vacuum. A vacuum will reduce the damping coefficient of the mass-spring system, as described in Section 3a.

H. Accelerometer Sensor Conclusions

The MTL accelerometer sensors were selected for use in this project for many reasons. The foremost reason is the MTL accelerometers allow the smallest mass and volume of the fingertip sensor. In comparison to the ADI accelerometer sensors, by not placing sensor electronics on the same chip the required die size is decreased, decreasing package size and eventual sensor volume. Unpackaged MTL accelerometer dies were available and could be placed in very small chip-scale packages, whereas the other commercially available sensors were already in fairly large and heavy packages.

In addition, this project serves as a demonstration system for the MTL accelerometer sensors. Up to now the accelerometer sensors have been designed, fabricated, and tested, but not applied in a project.

Although the results of the quality control test showed a surprisingly low yield, the test results were accurate. Of the four accelerometer sensors that the test indicated were working properly, all four were packaged, tested, and found to have the correct change in capacitance with acceleration. The three accelerometers used in the three-axis fingertip sensor continued to work throughout construction and testing of the sensor.

Chapter 4. Packaging the MTL Accelerometer

A. Package Selection

As part of the initial MTL research project fabricating the accelerometers,[66] the response of the accelerometer to various combinations of amplitudes and frequencies of acceleration was characterized. For testing purposes the die was packaged in a 69-connection pin grid array (PGA) package. The PGA package is quite robust, easy to handle, and allows solid connections in a standardized, temporary testing socket. The package used for the MTL testing is made by Kyocera (Kyoto, Japan) and has a size of 25.4 x 25.4 x 6.6 mm and a mass of 5.00 grams.

For the sensor application in this project the PGA package is not a reasonable solution. It is far too massive to put one, much less three for the three different sensor axes, on a person's fingertip, and expect to measure normal finger motion. Thus, a smaller and lighter package was required.

Leadless chip carriers (LCCs) are the smallest chip-scale packages available that still have the leads accessible from the perimeter of the package. Accessible leads were an important requirement because a hand soldering iron was going to be used to connect to the packages as no alternative soldering methods were readily available. An even smaller package than the LCC would be the ball grid array (BGA) package, which has a small array of surface mount contacts on the bottom side of the package. A uniform heating source is required to make the solder flow properly under a BGA package, such as hot air or infrared heaters. However, LCCs are not significantly bigger than BGA packages given the size of the die that must fit inside.

When selecting the smallest package for a die, two important features must be considered: the size of the package cavity and the number of external connections. The number of external interconnects required for this application is only six (although three would be theoretically possible) plus one or more ground plane connections. Consequently, the area of the package cavity restricted the smallest package size possible. In contrast, the primary benefit of BGA packages is a higher density of lead connections by moving the connections from the perimeter of the package to the entire bottom surface.

After looking at packages from several different vendors, the Mini-Systems, Inc. (Plainville, MA) C4LN28CM LCC was selected. The two reasons for choosing this specific package were the availability of the correct size (the size desired is unusually small) and the moderate cost ($36.60/package). The LCC package with the accelerometer die is diagramed in Figure 4-1.

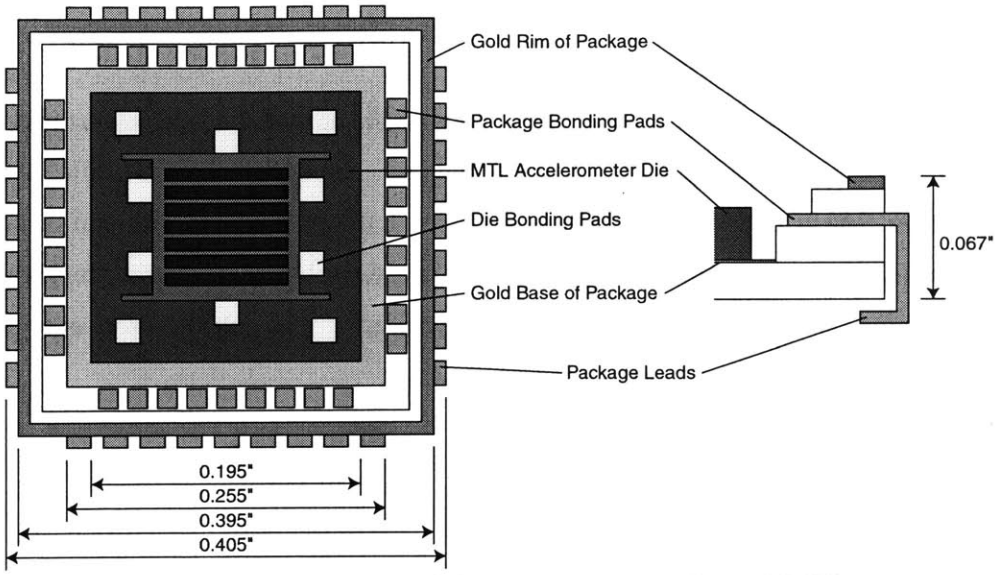

Figure 4-1. Diagram of the accelerometer die and LCC.
(a. Left) Top view. (b. Right) Side cross-section.

There was 0.030" of clearance left between the die and the edge of the cavity inside the package to allow fairly easy insertion of the die. Also, if the hand breakage separating the dies was not clean and there was a piece of the adjacent die still attached (as was the case for one of the four accelerometers packaged), the die would still fit in the package.

B. Fixing the Die Inside the Package

Dies are fixed to the bottom surface of package cavities with conductive epoxy, which was also used in this project. Conductive epoxy electrically as well as mechanically connects the silicon die to the thin layer of gold covering the bottom of the package. By electrically connecting the two surfaces, a good ground plane is formed.

The conductive epoxy used was Epoxy Technology[67] (Billerica, MA) compound H20E. The two parts were mixed in a one-to-one ratio, and then lightly spread on the gold surface on the bottom of the package cavity. The die was aligned as accurately as possible by hand with the base of the package, and then pushed down gently but firmly to make good mechanical contact.

The alignment of the die with the package is an important factor in the cross-sensitivity of the final sensor. The accelerometer sensor will be more sensitive to acceleration along an unexpected axis if the sensor is slightly rotated. An analytical compensation is theoretically possible, and is discussed more in the future work section of Chapter 8.

The packages and dies were cooked in an oven for 15 minutes at 115°C to cure the epoxy. The epoxy was very hard afterwards and the dies were well attached to the packages.

C. Gold Wire Bonding the Die to the Package

Electrical connections between the bonding pads on the die and the leads on the package were made using gold wire bonds. A gold ball wire bonding machine (Kulicke and Soffa[68] 4124, Willow Grove, PA) in the MIT MTL Integrated Circuit Lab was used. A picture of the machine is in Figure 4-2. The gold ball bonder uses 0.001" diameter gold wire.[69] The technology of gold wire bonding is well known and described well elsewhere,[70,71,72] so only a cursory overview of the gold wire bonding process used in this project follows.

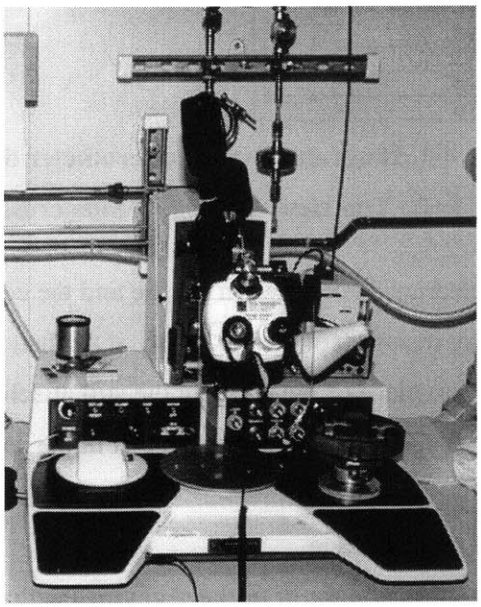

Figure 4-2. Photograph of the Kulicke and Soffa 4124 gold ball wire bonder.[73]

The bonding machine uses a chessman to manually move the package small distances in the horizontal plane: the hand piece has a mechanical lever to decrease the amplitude of movement of the stand supporting the package with the die inside. The first gold wire bond is made by pushing a small ball of gold at the head of the gold wire onto the aluminum bonding pad on the die, and then melting part of the ball into the pad using a thermosonic actuator. Then the wire is strung out to the location of the package pad while under moderate tension to prevent excess loop in the wire, and a crush bond is made by pushing the wire against the pad and melting it in with the thermosonic actuator. Finally, the wire is quickly pulled back while in tension, and the wire breaks at the weak part of the crush joint. The free wire end is melted by an electronic discharge and reforms the ball. The machine is then ready to make the next bond.

At little experimentation was required to determine the proper parameters for the downward force during the bond, the intensity of the ultrasonic generator, and the duration of the ultrasonic

pulse to form strong wire bonds between the aluminum pads on the die and the gold pads on the package. The final settings used are in Table 4-1.

Table 4-1. Kulicke and Soffa 4124 Gold Wire Bonder Settings[74]

Bond	Force	Time	Power
First (Ball)	5.0	5.0	170
Second (Crush)	7.0	7.0	900

The gold wire between the two bonds was left slightly long so as to theoretically curve up between the two connections and not have any physical contact with the die. However, my wire bonding technique often allowed the loops to touch the edge of the die. As later resistance testing determined (described in Section 4f), the accidental contact with the die did not have a significant effect. This is probably because the silicon die was covered with silicon oxide, an insulator, and the area of contact was extremely small.

Connections were made from all six pads on the die to the inner package pads. In addition, four test connections were made just before the six important connections using the four unconnected die pads, to verify that the gold wire bonding machine was working correctly. Finally, four more gold wire bonds were made between the gold inner ground plane of the package and the package pads to allow good connection to the ground plane of the package. The final connection pattern is in Figure 4-3.

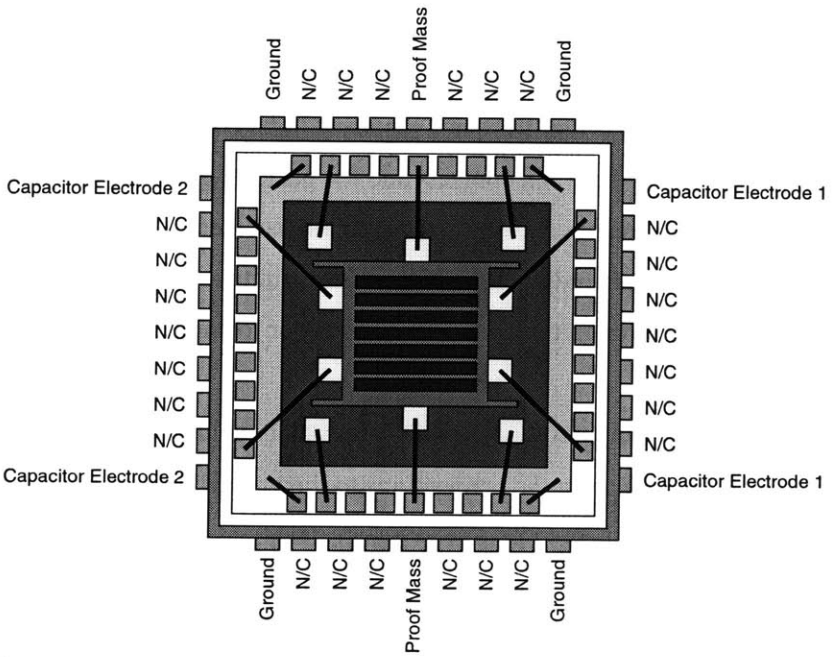

Figure 4-3. Diagram of gold wire bonds interconnecting the accelerometer die and the LCC.

D. Completing The Package

The final step in packaging the accelerometer sensors was putting a cover on the package. The metal lid serves two purposes: a second ground plane for the package, and a hard physical barrier to prevent damage to the accelerometer die or the gold wire bonds. Package covers could have been purchased from the company that made the package but they were quite expensive. Instead, small sections of 0.005" thick copper-beryllium alloy were used. A piece of the metal was cut to the appropriate size of the package, and the piece was soldered down to the gold rim of the package.

In the completed fingertip sensor, the package lid was electrically connected to the ground plane of the package and the ground of the electrical system. By sandwiching the die and gold wire bonds between two ground planes, noise from RF interference was minimized.

E. Resistance Testing

A significant concern for the overall quality of the packaged accelerometer sensors was poor gold wire connections: a high impedance or open circuit, or an accidental short to another electrically active element. An open circuit would prevent good contact to the die, although there is some redundancy with two connections to each active element on the die. Alternatively, an accidental short to another gold wire, the lid, or base of the package would render the accelerometer useless. Consequently, resistance testing was performed between all of the occupied pins on the LCC, and between the pins and the package lid.

The resistance testing results were satisfactory for all four packaged accelerometer sensors. The resistance between contacts that were not supposed to be connected to each other was infinite, as was the resistance between contacts and the package ground plane or lid. This result indicates there was no significant connection through any accidental contact between poorly looping gold wire bonds and the edge of the die, as some finite resistance would have been seen to either the ground plane through the conductive epoxy, or to another lead that was also touching slightly.

The resistance between any two LCC contacts internally connected to the package ground plane was less than 1 Ω, indicating the connections to the ground plane were good and the gold wires had very low resistance (<0.5 Ω per wire bond). The resistance between leads connected to die bonding pads that were supposed to be connected together (such across the proof mass) fluctuated considerably, however. The resistance data for connected elements are in Table 4-2. All resistances were in the range of 400 to 800 kΩ. In general the resistances between connected elements varied together with the die; i.e. on some dies all of the internal resistances were higher

for all connected elements than on other dies. The change in resistance did have an effect on accelerometer performance; analysis concerning the effect of die internal resistance is described more in the fingertip electronics section of Chapter 5.

Table 4-2. Resistance testing results. All values in kΩ. (n=4)

Element with Two Connections	Mutual Resistance	Standard Deviation
Mass	684	118
Electrode	657	109

F. Weight Analysis

A step-by-step weight analysis of the accelerometer sensors was done as the packages were assembled. The package was weighed after each step of the packaging process to calculate the mass added in that step, and the results are in Table 4-3.

Table 4-3. Weight analysis of accelerometer sensor packaging.

Component	Mass (grams)
Package	0.2615
Type 2 Accelerometer Die	0.0357
Conductive Epoxy	0.0013
Gold wire	0.0008
Copper lid + solder fixative	0.1069
Total	0.4062

The empty LCC package comprises about 60% of the final weight; the accelerometer die is only 8%. The total weight for three packaged accelerometers (as would be present in the fingertip sensor) is 1.2 grams, considerably less than the original 5 gram specification (discussed in Section 1d).

The lid is a significant fraction of the total weight: 26%. If the weight of the sensor needs to be absolutely minimized, in the future a thinner copper-beryllium lid (possible 0.002") or an aluminum lid of comparable thickness to the current lid could be used. The thinner lid would weigh 0.0428 grams, leaving the final packaged accelerometer 84% of its present weight. Comparing the relative densities between copper (which comprises 97% of the copper-beryllium alloy) and aluminum, a 0.005" thick aluminum lid would weigh 0.0322 grams, resulting in a final weight 82% of the present. However, a disadvantage of using an aluminum lid is the lid couldn't be soldered down to the package. Instead, a conductive epoxy could be used, and the weight of the epoxy would probably be negligible.

Chapter 5. Sensor Electronics

A. Electronics Overview

The MTL accelerometer sensor converts acceleration into changing differential capacitors. An electrical circuit is used to convert the differential capacitive signal into an electrical signal for computer acquisition. The block diagram of this circuit is in Figure 5-1.

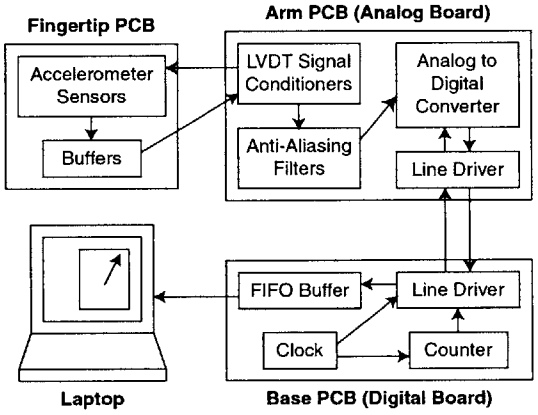

Figure 5-1. Block diagram of the sensor electrical circuit.

There are three accelerometers in the fingertip sensor to sense three-dimensional motion. Each accelerometer is connected to a linear variable differential transformer (LVDT) signal conditioner IC, which converts the differential capacitance into an analog voltage proportional to the proof mass position in the die. Proof mass position is proportional to external acceleration by the springs attached to the proof mass. The LVDT signal conditioner has a sinusoidal voltage output connected to the proof mass. The corresponding voltages on the dual capacitor electrodes will also be sinusoidal, but the amplitudes will vary depending on the spacing between the proof mass and the capacitor electrodes. Voltage followers used on the fingertip sensor buffer the capacitive signals immediately out of the accelerometers to prevent excessive noise in the wires between the fingertip and the LVDT signal conditioners on the nearby analog signal processing board.

The analog outputs of the LVDT signal conditioners from each acceleration axis are passed through anti-aliasing filters and then into separate channels of a 4-channel 16-bit analog-to-digital converter (ADC). The serial digital output from the ADC is passed to a first-in-first-out (FIFO) buffer on the digital board, which both buffers the data and converts the serial signal into a parallel signal. The parallel data from the FIFO is sent into the parallel port of a laptop computer, and a program (described in Chapter 6) displays and stores the data on the laptop.

B. Converting Differential Capacitance to Acceleration and Linearity Analysis

An LVDT signal conditioner IC is used to convert the accelerometer differential capacitance signal into an analog voltage proportional to the acceleration. LVDTs are used in manufacturing and robotics as precise linear position sensors. An LVDT is a set of three wire coils collinear with each other, as diagrammed in Figure 5-2. One central coil is the primary of the transformer, and the other two are secondary coils. A paramagnetic metal rod is placed partially in the core of the coils and allowed to slide freely in and out of the cores. As the position of the metal slug moves, the relative transformer ratios between the primary and the secondary coils will change. The LVDT signal conditioner provides the AC excitation voltage to the LVDT's primary and outputs an analog signal proportional to the position of the metal slug by measuring the relative secondary voltages.

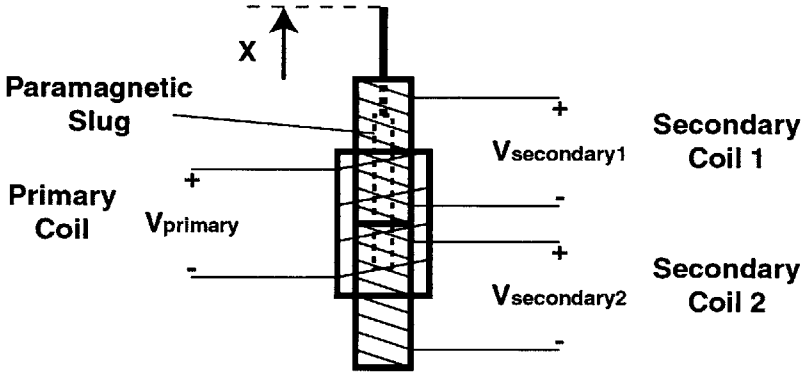

Figure 5-2. Diagram of an linear variable differential transformer (LVDT).

The equation for voltage across a transformer coil is that the ratio of voltages is equal to the ratio of coil turns (Equation 5-1). The presence of a paramagnetic element in the core of the secondary coils increases the magnetic flux density and thus increases the effective turns ratio, increasing the coil voltage.

$$\frac{V_1}{V_2} = \frac{N_1}{N_2} \qquad \text{(Eqn. 5-1)}$$

The LVDT signal conditioner IC produces an AC voltage of constant amplitude connected to the LVDT primary coil. The amplitudes of the two secondary coil output voltages vary depending on the metal slug position. The signal conditioner takes the voltages from the two secondary coils and calculates the voltage magnitudes. The output of the signal conditioner is an analog voltage linearly proportional to the position of the slug in the core of the LVDT. The specific equation for the signal conditioner output is the ratio of the difference between the two

amplitudes divided by the sum of the two amplitudes (Equation 5-2; the output is a function only of amplitude, not of phase). K_1 and K_2 are constants set by external passive components.

$$V_{out} = K_1 \frac{|V_A| - |V_B|}{|V_A| + |V_B|} + K_2 \qquad \text{(Eqn. 5-2)}$$

In the LVDT, the differential voltage magnitude from each secondary is linearly proportional to the amount of metal in the respective core. The voltage in each coil is in Equation 5-3, where N is the turns ratio between the primary and secondary coils, d is the length of the slug in the coil core, and B is the effective multiplier of the turns ratio for each unit length of metal slug in the core.

$$V_{secondary} = V_{primary} \cdot N \cdot d \cdot B \qquad \text{(Eqn. 5-3)}$$

The depth of the slug in the two secondary coils is inversely related: as the slug moves out of one core it moves into the other core by the same amount. Substituting Equation 5-3 into Equation 5-2 results in the effective LVDT signal conditioner output Equation, 5-4, where x_0 is the one-half slug length that starts in each core.

$$V_{out} = K_1 \frac{V_i NB \cdot (x_0 - x) - V_i NB \cdot (x_0 + x)}{V_i NB \cdot (x_0 - x) + V_i NB \cdot (x_0 + x)} + K_2 \qquad \text{(Eqn. 5-4)}$$

This equation reduces to the simple result in Equation 5-5, which shows the output voltage is linearly proportional to the position of the slug in the LVDT. This is the basis for using LVDTs to measure linear position.

$$V_{out} = K_1 \frac{-x}{x_0} + K_2 \qquad \text{(Eqn. 5-5)}$$

The conversion of differential voltage amplitudes to an analog voltage output is also applicable to the differential capacitors in the MTL accelerometer sensor. The equivalent circuit for the accelerometer sensor is diagrammed in Figure 5-3. R_{mass}, R_{cap1}, and R_{cap2} are the resistances on the die, as measured in Section 4e. C_{cap1} and C_{cap2} are the differential capacitances between the proof mass and the fixed capacitor electrodes. R_{ext} is external resistance added to each side of the system that creates a highpass filter in conjunction with the differential capacitance. The highpass filter keeps the capacitance electrode voltages with a DC value of zero, preventing the voltages from going outside the range of the amplifier. R_{fet} is the input impedance of the FET-input voltage followers used on the fingertip to buffer the voltage before sending the signal to the analog board.

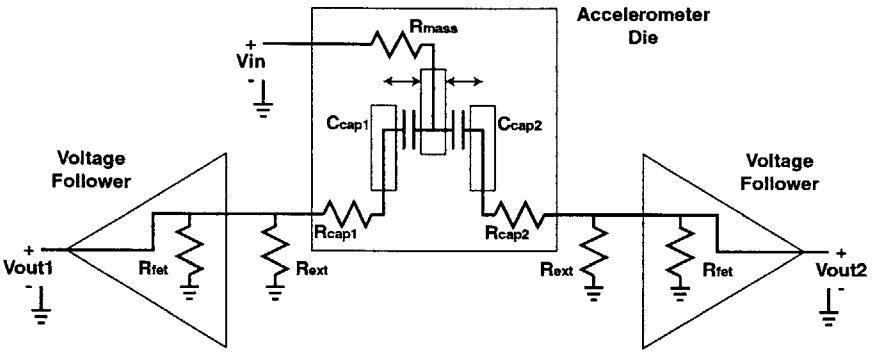

Figure 5-3. Accelerometer sensor equivalent circuit.

The two sides of the accelerometer circuit act as voltage dividers (Equation 5-3), where ω is the angular frequency of the input voltage and the capacitance C_{cap} is a function of the capacitor's changing gap as the proof mass moves (Equation 3-3). For now, ignore the effect of the parasitic resistances in the circuit: R_{fet}, R_{mass}, and R_{cap}.

$$|V_{out}| = V_{in} \frac{R_{ext} \| R_{fet}}{R_{ext} \| R_{fet} + \frac{1}{\omega C_{cap}} + R_{mass} + R_{cap}} \qquad \text{(Eqn. 5-6)}$$

Similar to the amount of metal in each coil in the LVDT, the two capacitances in the accelerometer have an inverse relationship because the sum of the two capacitor gaps is a constant. Inserting Equation 3-3 into Equation 5-3, and substituting twice (for the two output voltages) into Equation 5-2 for the LVDT output and simplifying, the result is that the output voltage is a linear function of proof mass position (Equation 5-4). In this equation, x is the distance the proof mass moves, d_0 is the original spacing, and C_0 is the original capacitance.

$$V_{out} = K_1 \frac{-x/d_0}{\omega R C_0 + 1} + K_2 \qquad \text{(Eqn. 5-7)}$$

Now the effects of R_{fet}, R_{mass}, and R_{cap} can be considered one at a time to avoid making the overall model too complicated. R_{mass} affects both sides of the accelerometer sensor equally by scaling down the input voltage to the proof mass. The common-mode output voltage of both amplifiers is decreased, and conveniently in the equation for the output of the LVDT signal conditioner (Equation 5-2) any multiplier of both amplitudes cancels out. Indeed, upon numerical analysis of the system, changing R_{mass} has no effect on the output of the signal conditioner.

R_{cap} has a more complicated effect because the resistances of the capacitor output on the two sides of the sensor are different. Upon numerical analysis of the system, it is found that changing the resistances of the capacitor electrodes keeps the system linear, but the zero-acceleration output voltage changes as does the sensitivity (Volts/g). The parallel resistances between the

capacitor electrodes and the two bonding pads will probably be about the same as the resistance between the two bonding pads measured in Section 4e. The largest difference between the two resistances of the four accelerometers packaged and tested in Section 4e is capacitor electrode resistances of 444 and 554 kΩ. With these resistances, the sensitivity decreases 14.8% and the new zero-acceleration output is where the output previously indicated 1.19g. These are significant changes indicating each accelerometer sensor needs to be individually calibrated for zero-acceleration output and sensitivity.

R_{fet} is the FET-input resistance to the op-amp buffering the capacitor electrode voltages. A dual op-amp package is used for the two sides of the accelerometer, so the two input resistances in the single package will be almost identical. The nominal value for R_{fet} is 10^{10} Ω in the op-amp used. When R_{fet} is included in the numerical analysis and set to its nominal value on both sides of the circuit, the linearity is not significant and sensitivity and the zero-acceleration output remain unchanged. If one resistance is set to the nominal value and the other is set at one-tenth nominal (a difference far greater than would be reasonably expected), the output becomes slightly non-linear: the maximum integral linearity error (MILE)[75] is 0.15 mg, the sensitivity increases by 0.02%, and the zero-acceleration output becomes the prior output for 18 mg.

A similar effect will be seen if the two external resistors have slightly different values. Using 1% resistors (as was used building the circuit board), the worst case error results when one resistor is higher than its nominal value by 1% and one is lower by 1%. Numerical analysis shows with this arrangement the MILE is 3.76 mg, the sensitivity is unchanged, and the zero-acceleration output becomes the prior output for 0.45 g. If the circuit were built using 0.1% resistors the errors reduce by a factor of 10: the MILE is 0.38 mg, sensitivity is unchanged, and the zero-acceleration output is what 45 mg was previously.

Overall, numerical analysis shows the output characteristics of the accelerometer are good given all of the parasitic resistances in the circuit. Parasitic capacitances will also be present (such as between the capacitor electrodes and ground), but the effect will be similar to the resistances described above and the resultant error very small. To compensate for the parasitic effects, each accelerometer will have to be initially calibrated for sensitivity and zero-acceleration output. Depending on the temperature sensitivity of these parameters and the operating temperature range, temperature changes may cause the sensor to loose calibration.

The nonlinearity of the fingertip electronics is greater than the 1 mg resolution specification discussed in Section 1d. If the project were redone using 0.1% resistors on the fingertip nonlinearity would be improved significantly. Additional substantial nonlinearities in the system arise from nonlinearities in the mass-spring system (as the spring constant varies with mass

position, resulting in a MILE of 0.39 mg, discussed in Section 3e) or nonlinearities farther down in the electronics.

C. Electronics on the Fingertip

A very small two-sided printed circuit board (PCB) was fabricated to accompany each accelerometer LCC package. The layout schematic of the fingertip PCB is in Figure 5-4. Plots of the two copper layers are in appendix A. On one side of the fingertip PCB the LCC packaged accelerometer is attached, and on the other side of the board there is the dual op-amp buffer.

The fingertip PCBs are about 12mm by 12 mm, restricting the total volume of the sensor to be larger than $(12\ mm)^3$. This is considerably larger than the original volume specification of $(7\ mm)^3$, but still very usable.

The LCC packaged accelerometer is soldered to the upper copper layer of the board. There are ten connections made between the LCC and the PCB: the six connections for the accelerometer elements (two connections each for the two capacitor electrodes and the proof mass) and four ground connections to the ground plane in the package cavity. In addition, a separate wire is soldered between the PCB ground and the lid of the package. Overall, the mechanical connection between the LCC and the fingertip PCB is very strong due to the many solder joints.

On the bottom copper layer of the PCB is the dual op-amp, capacitors and resistors, and the connections to the wires running off the board. The op-amp is the OPA2137[76] (Burr-Brown) connected as two voltage followers. The OPA2137 was selected because it was the smallest dual FET-input op-amp found, to avoid increasing the mass and volume of the fingertip sensor excessively. There are two 0.1 μF capacitors to buffer the power to the op-amp (± 15 V) and the two external 910 kΩ resistors. There is also a very small LED and resistor in series with the + 15 V power supply to indicate when the sensor is powered. Finally, there is a small array of six plated through-holes for solder connections to the wires connecting the fingertip PCB to the analog board.

The wires to the analog board are 40 gauge-- the smallest diameter electrical wire manufactured. The six wires carry the signal conditioner's AC signal to the proof mass, two buffered signals returning from the capacitor electrodes, power (± 15 V) for the op-amp, and ground. The 6 wires are all wrapped together tightly to prevent undesired RF interference from causing excessive noise in the analog buffered signals and also to make the physical characteristics of the wire bundle convenient. The wire bus runs about 1 meter to the analog PCB.

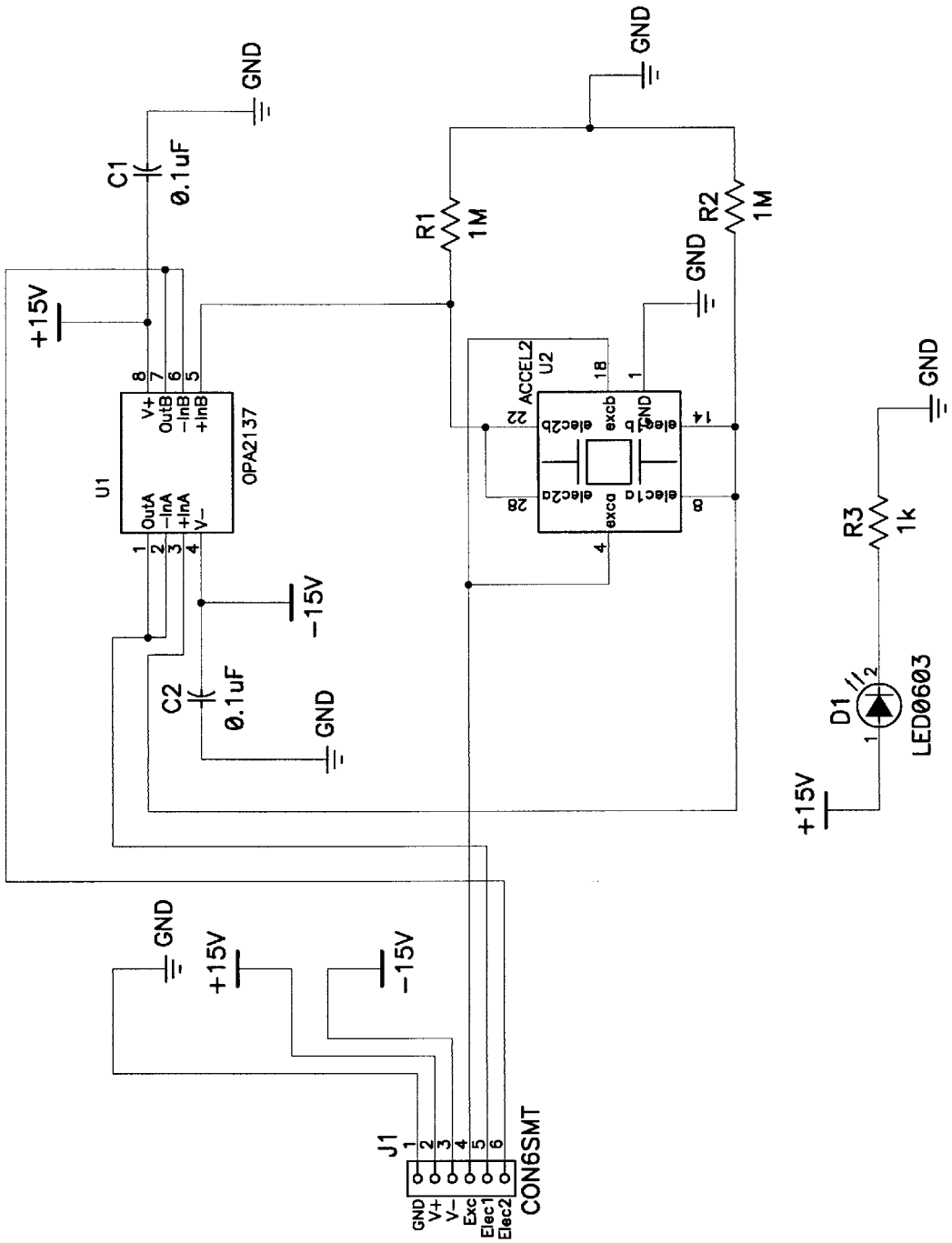

Figure 5-4. Layout Schematic of the Fingertip PCB

There is one wire bundle for each of the accelerometers, and the 3 wire bundles in the final sensor are all wrapped lightly around one another to connect to the three-axis sensor. In total, eighteen 40 gauge wires connect the sensor on the fingertip to the analog PCB. The weight of 40 gage wire is 7.1 milligrams/cm, so the bundle of 18 wires will weigh 0.13 grams/cm. The wire bundle could potentially be reduced to 10 wires by using the same proof mass excitation, power connections, and ground for all three sensors. This would reduce the bundle weight to 0.071

grams/cm. However, 0.13 grams/cm is already extremely small, and the 18 wire bundle is extremely flexible. Consequently, the wires connecting the fingertip sensor don't significantly affect finger or hand motion, meeting one of the significant physical design criteria of the sensor.

D. The Analog Board

The wire bus connects the fingertip PCB to the analog PCB that would theoretically be located on the upper-arm, in a backpack, or sitting nearby. The analog PCB was designed as a two-layer board; a schematic of the analog board is in Figure 5-5 and plots of the two copper layers are in appendix A. There is a large ground plane on the bottom layer of the board, divided into a power ground plane and an analog ground plane. The analog ground plane is the reference ground for the analog signals between the signal conditioner outputs and the ADC inputs, and it is connected to the power ground plane underneath the ADC. In a loop around the analog ground plane is the power ground plane, which has a cut in one side to prevent circular currents.

There is a separate six-pin connector on the PCB for each of the three accelerometer channels. Simple header connectors were used for ease of assembly with soldering to the thin 40 gauge wire. The three signal wires for each accelerometer are routed directly from the connector to the LVDT signal conditioner, the Analog Devices AD598.[77]

Resistors and capacitors select the amplitude and frequency characteristics of the sinusoidal proof mass excitation voltage from the LVDT signal conditioner. The sinusoidal output was set to be 20 kHz and 20 Volts peak-to-peak. The frequency was chosen because it is well above the 2 kHz resonant frequency of the mass and spring in the accelerometer sensor. Exciting the sensor proof mass near the resonant frequency could possibly induce proof mass motion by electrostatic forces, which could make the system very non-linear. The amplitude was selected experimentally: the signal conditioner specification has a desired voltage range for the signals from the capacitor electrodes, and an AC voltage on the proof mass of 20 Volts peak-to-peak gave an amplitude in the middle of the range.

The output of the signal conditioner is given in Equation 5-2. The two constants K_1 and K_2 can be selected with external passive components. The analog system was designed to operate on $\pm$15V, so the constant K_2 was set to zero. Depending on the specific parameters of the accelerometer sensor, there can be a significant zero-acceleration offset voltage. A potentiometer with each signal conditioner allows the voltage offset to be set to zero: the accelerometer is positioned with the sensitive axis perpendicular to the acceleration of gravity (so there is no acceleration on the proof mass) and the potentiometer is adjusted to set the output voltage to zero.

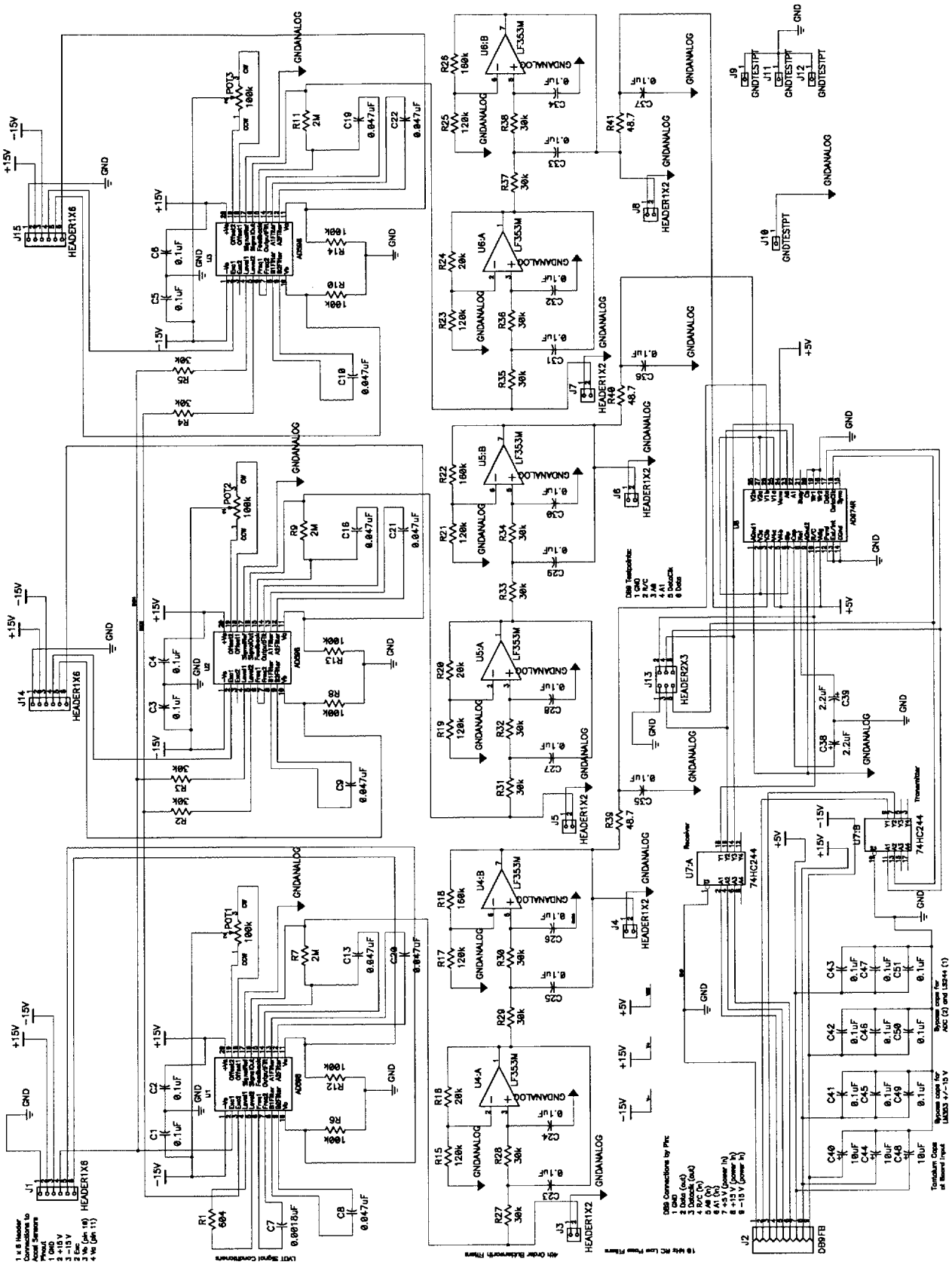

Figure 5-5. Layout Schematic of the Analog PCB.

The constant K_1 was selected to give a reasonable sensor sensitivity considering both the desired resolution (1 mg) and the maximum range to be measured (± 5g). The AD598 can support output voltages of ± 11V. However, more significant was the range of the ADC, ± 10V, and the gain in the anti-aliasing filter, which is 2.5. The signal conditioner output amplitude is in Equation 5-5, where R_2 is an external resistor value.

$$V_{out} = \frac{|V_A| - |V_B|}{|V_A| + |V_B|} \times 500\mu A \times R_2 \qquad \text{(Eqn. 5-8)}$$

Using Equation 5-7 and the nominal spring constant of the accelerometers, the theoretical voltage ratio was calculated to be 0.0150 for every g of acceleration when there are no parasitics (parasitics generally decrease the sensitivity). Consequently, R2 was selected to be 100 kΩ, which makes V_{out} 0.75 V/g acceleration. The input to the ADC will then be 1.875 V/g, and the maximum range of acceleration that can be measured is ± 5.33 g, meeting the specification for maximum measurable acceleration amplitude. Keeping the sensitivity high reduces noise in the system and helps improve the resolution.

The specifications for the AD598 state the maximum nonlinearity in the output is 500 ppm of full scale with a typical value of 75 ppm. With a full-scale range of 29.3 g over the ± 11 V scale, the MILE is 14.6 mg, and a typical nonlineariy is 2.2 mg. The specification for output voltage ripple is a maximum of 4 mVrms, which corresponds to a noise floor of ± 7.54 mg with an output sensitivity of 0.75 V/g. Only the middle third of the AD598 full-scale range will be used (10 g out of the 29.3 g range), so actually the MILE will probably be better than the 2.2 mg specification for the full-scale range.

The anti-aliasing filters are four-pole Butterworth filters with a cutoff frequency of 45 Hz, allowing frequencies up to 25 Hz to be measured without distortion while still removing some 60 Hz noise from the environment. The Butterworth topology was selected because it works well to solve the opposing goals of preserving the signal up to 25 Hz (thereby meeting the maximum frequency specification of the sensor) and removing as much noise as possible at 60 Hz and above. Preserving the signal below cutoff frequency is best done using a Bessel filter, and removing noise above the cutoff frequency is best done with an elliptical filter, but the Butterworth filter is a good compromise between the two.

The design of the filter was done with the assistance of a filter design book.[78] The filter is built around the dual op-amp LF353M[79] (National Semiconductor) and has a two-stage Sallen-Key configuration. Frequency analysis of the anti-aliasing filter was done in HSPICE, and the code is in appendix B. A Bode plot of the filter's frequency response is in Figure 5-6.

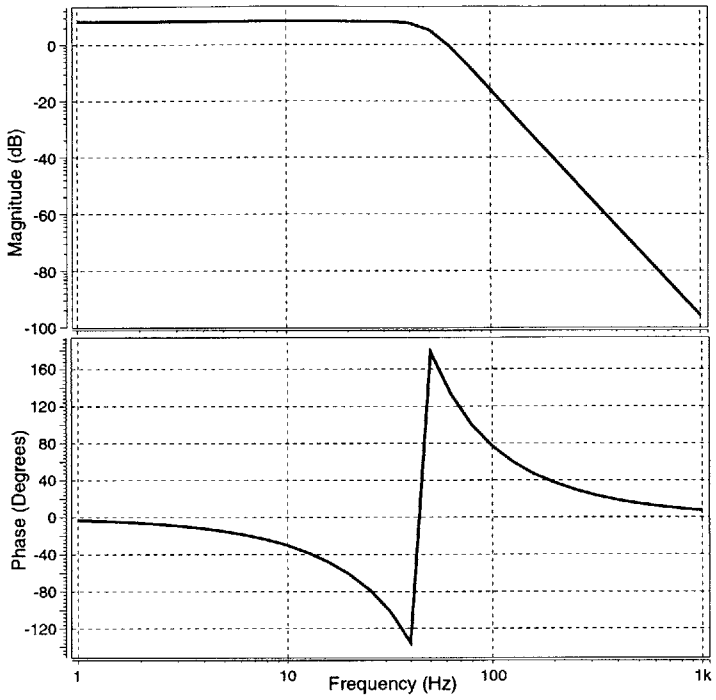

Figure 5-6. Bode plot of the frequency response of the anti-aliasing filter.

The phase is not important for this application, which is more concerned with the amplitude of acceleration. The gain calculated in HSPICE is 2.59 at 0.1, 1, 10, and 25 Hz, showing how flat the amplitude response is in the bandwidth of interest (0.1 to 25 Hz). The gain at 60 Hz is 1.12—there is some filtering function of powerline noise, but more aggressive 60 Hz filtering would have to be done subsequently with the digital data. The anti-aliasing filter clearly falls off at –80 dB/decade at frequencies above the cutoff frequency of 30 Hz, as the filter has four poles.

As further discussed in Chapter 6, one feature of the data acquisition system is a variable sampling frequency, allowing the sampling frequency to be increased as fewer real-time data processing functions are used and the computer can process data faster. The range of sampling frequencies on each channel varies from 250 to over 800 Hz, and consequently the smallest Nyquist frequency is 125 Hz. This is high enough that 60 Hz noise and its first harmonic isn't aliased back into the frequency ranges of interest, and significant digital filtering can be performed to reduce this noise.

The filtered analog signal leaves the Butterworth filter and enters the ADC, the AD974[80] (Analog Devices), a 16 bit successive-approximation switched-capacitor ADC. The ADC operates at DC, meeting the minimum measurable frequency specification of 0.1 Hz. The specification for the AD974 is a MILE of ± 3 least-significant bits (LSB), where each LSB is 305 μV with the ± 10 V range. This is equivalent to an error of ± 0.49 mg, where the sensitivity at the input to the ADC is 1.875 V/g.

Just prior to entering the ADC, the signal passes through a final RC lowpass filter with a cutoff frequency of about 32 kHz to remove any noise in the signal either injected from the active anti-aliasing filter or added in the final trace between the filter and the ADC. The circuit diagram for the system between the anti-aliasing filter output and the ADC input is in Figure 5-7.

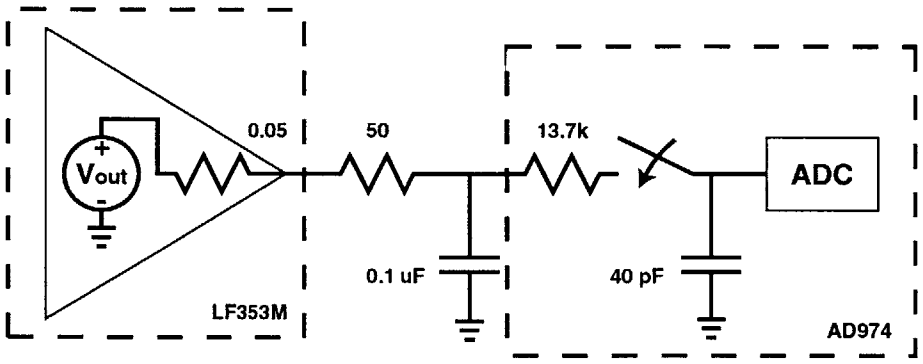

Figure 5-7. Equivanent ADC input electrical circuit.

The resistance in the RC filter was chosen to be 50 Ω. A low series resistance is extremely important because the ADC uses a switched capacitor method of sampling the signal. When the capacitor inside the ADC is switched to sample the signal, if the series input resistance is high then the voltage on the capacitor will drop as the capacitor charges, and when the capacitor voltage is converted the voltage will be lower than the correct voltage. The ADC uses an on-chip resistive network to scale the inputs to allow a range of ± 10V, but the input resistance is fairly low: 13.7 kΩ. A 50 Ω series resistance will create a voltage divider that decreases the voltage amplitude only 0.4%, although the actual response will be better because as the 40 pF sampling capacitor charges (the duration of the sampling time is 1 μsec) the current into the capacitor will decrease. The 50 Ω series resistance will not load the active filter output (which has a resistance of 0.05Ω at the frequency and gain for the anti-aliasing filter) excessively—the voltage divider there only drops the voltage 0.1%. Both of these voltage dividers will only decrease the sensitivity of the accelerometers, but will be corrected for with the sensitivity calibration already required (Section 5b).

The ADC has four channels—three are used for each of the three accelerometer channels, and the fourth is used as a parsing channel. The fourth channel is railed to above the valid input range, so the ADC output for that channel will always be the maximum. As the four channels are sampled in sequence in an endless loop, each time a channel is the maximum value the data acquisition program can recognize this channel as the parsing channel and correctly process the following three data channels correctly.

The ADC makes its channel selection by two signals from the digital board. The two signals are created by a two-bit counter, which steps through the four channels one at a time. There is also a read/convert signal sent to the board, which alternately triggers the ADC to acquire an analog voltage from the appropriate channel (selected by the two channel bits), and then convert the signal and output the serial digital result. (A timing diagram is in Figure 5-8.)

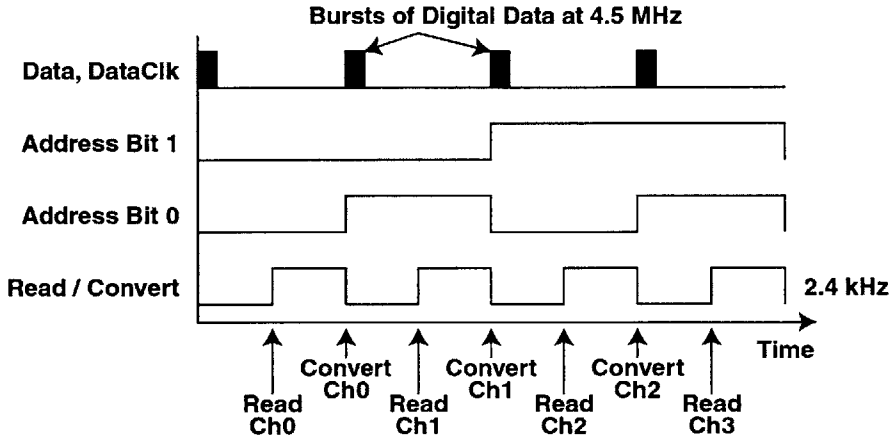

Figure 5-8. Timing diagram of the ADC functions.

A 4.5 MHz clock internal to the ADC clocks out the ADC digital output. The ADC output is two brief signals after conversion is complete: the data signal and the clock signal. The clock signal is sixteen consecutive clock signals for the sixteen bits of data. The data, least significant bit first, has each bit valid on the falling edge of each clock pulse.

The two ADC digital output signals are passed into a buffering line-driver/line-receiver, the 74LS244[81] (Fairchild Semiconductor). The ADC digital outputs are buffered to provide the necessary power to drive the cable between the analog and digital boards. The buffer also receives the read/convert and channel-select signals from the digital board and sends them to the ADC. The line-driver has a maximum frequency of 80 MHz, which is more than fast enough for the 4.5 MHz signal from the ADC.

The cable connecting the analog and digital boards is a standard 9-conductor serial cable with DB9 connectors at each end. The pinout of the cable is in Table 5-1.

Table 5-1. Analog to Digital Board Cable Pinout

Pin	Function	Direction [1]
1	Ground	D -> A
2	Data Signal	A -> D
3	Dataclock Signal	A -> D
4	Read/Convert Signal	D -> A
5	Channel Bit 0 Signal	D -> A
6	Channel Bit 1 Signal	D -> A
7	+ 5 V Power	D -> A
8	+ 15 V Power	D -> A
9	- 15 V Power	D -> A

Note 1: A -> D: analog board to digital board;
D -> A: digital board to analog board

E. The Digital Board

The primary function of the digital PCB is converting the serial digital data from the ADC to a parallel signal suitable for passing into a computer through the parallel port. The other important functions of the digital board are creating the clock and channel signals for the analog board, and connecting to the power source and delivering the power to the analog board. The schematic of the digital board is in Figure 5-9, and plots of the two copper layers (again, a two-layer board) are in appendix A. The lower copper layer has a very large ground plane to minimize noise. A 9-pin connector receives the cable from the analog board, and a Centronix 36-pin connector connects to a standard printer cable running into the parallel port of the laptop computer. A small section of header is used to connect to the power supply, delivering + 5 V, ± 15 V, and ground.

The key element on the digital board is a first-in-first-out (FIFO) buffer, the IDT72132L50P[82] (Integrated Device Technology). The FIFO buffer has an externally clocked serial input and an 8-bit parallel output, with 2,048 bytes of memory. Another 74LS244 line-driver/line-receiver on the digital board receives the ADC data and clock signals from the analog board and sends them directly to the FIFO input. The sixteen bits of serial data fill up two successive bytes in the FIFO memory. The maximum serial input rate is 40 MHz, which is more than adequate for the 4.5 MHz signal from the analog board.

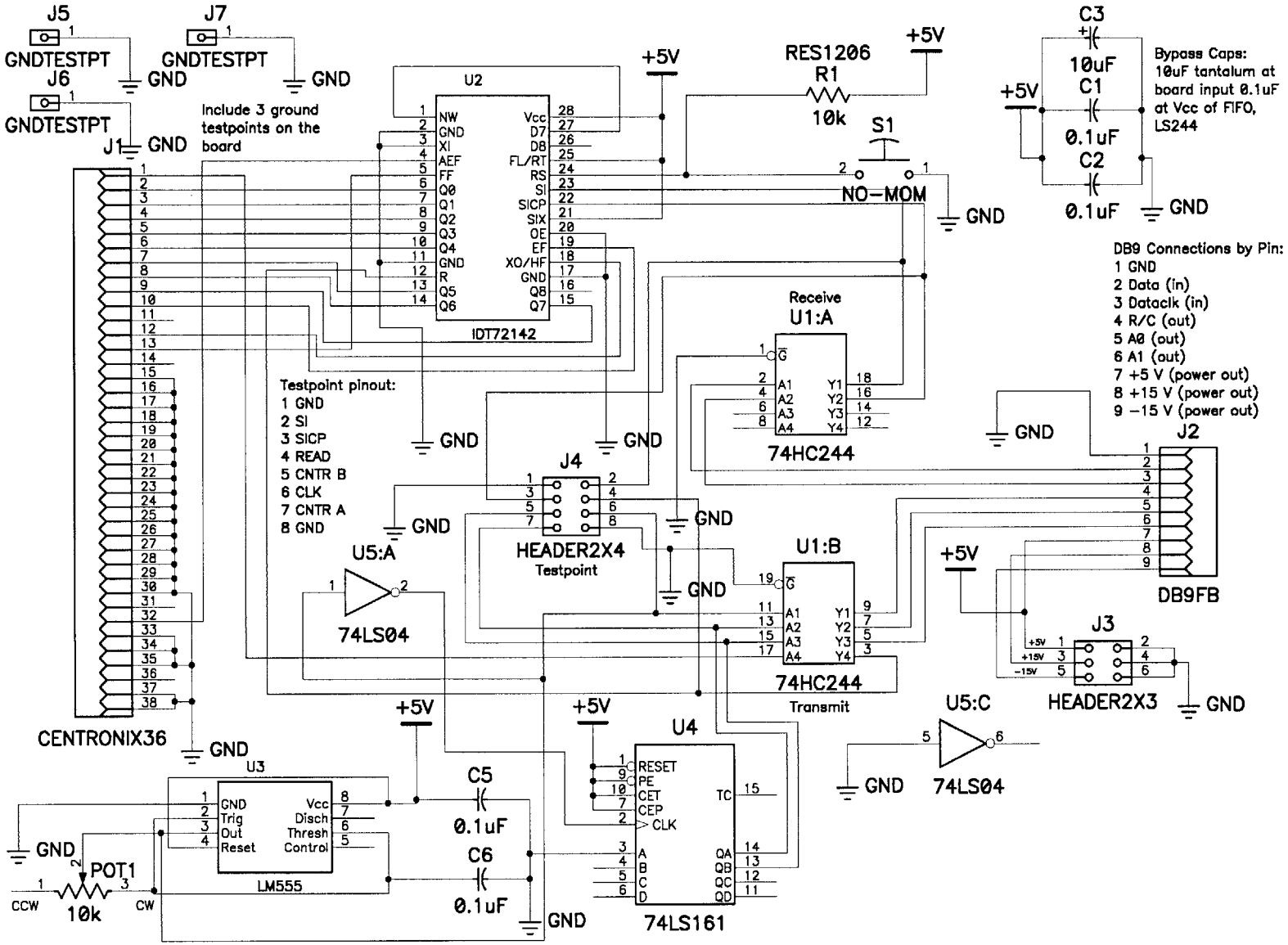

Figure 5-9. Schematic of the digital board.

The FIFO has four output pins that are flags to show the available FIFO memory. The computer software monitors these flag signals and when the FIFO has data in its memory the data is recovered. The laptop sends a read signal on a control line of the parallel port to the digital board. The signal is buffered through the 74LS244 to avoid spurious read requests, and then sent to the read line of the FIFO. When the read line goes low the first byte of data is displayed at the eight output registers of the FIFO. When the read line goes high and then low again, the next byte of data is displayed. To access all sixteen bits of the ADC data, two successive reads are required. The output registers are connected through the printer cable to the parallel port of the computer.

A clock on the digital board is the source for the channel counter and the read/convert signal for the ADC. The clock is a simple 555 timer[83] (National Semiconductor). As mentioned above, the frequency of the clock is variable, but it has a range of 1 to 3.2 kHz and has a duty cycle of 70%. The clock frequency is divided by the number of channels (four) for the sampling rate per channel, and when optimizing the clock frequency the limiting factor is the software's acquisition speed. The FIFO receives 2000 to 6400 bytes per second, which allows the computer software to delay acquiring the data 1 to 0.31 seconds before the buffer overflows and data is lost.

The counter for the ADC channel-select is a 74LS161[84] (National Semiconductor) 4 bit counter. Only the first two bits of the counter are used to cycle through the four channels of the ADC. The clock signal is inverted before going into the counter with a single channel of a simple 74HC04[85] (Fairchild Semiconductor) inverter. Consequently, when the clock goes high (indicating start-conversion on the read/convert line to the ADC), the channel increments. (See the timing diagram in Figure 5-8.) Inverting the clock signal prevents the channel from changing at the same time the ADC reads the data, which could possibly violate the setup and hold times for the acquisition. The ADC can operate at up to 200,000 samples per second, which is more than sufficient for the data rates used in this project.

The clock, counter, and inverter are located on the digital board to reduce the required area and weight of the analog board, which is potentially located on the arm. The digital board is located next to the laptop computer, which already fairly large and bulky so the digital PCB is not a significant addition.

F. Electronics Conclusion

The electrical circuit for the three-axis accelerometer sensor converts the differential capacitances on the MTL accelerometer dies to three analog voltages representing the acceleration, and then the analog voltages are sequentially sampled with an ADC and acquired

into a computer. The nonlinearity in the system is most significant in the LVDT signal conditioner, which can have a nonlinearity of up to 14.6 mg. A summary of the different sources of noise and nonlinearity in the sensor system is in Table 5-2.

Table 5-2. Summary of noise and nonlinearity in the accelerometer system.

Source	Noise	Nonlinearity	Text Section
Accelerometer Springs		+/- 0.39 mg	3e
FET Input Resistors		+/- 0.15 mg	5b
External Resistors		+/- 3.76 mg	5b
LVDT Signal Cond. [1]	+/- 7.54 mg	+/- 2.20 mg	5d
Analog to Digital Converter		+/- 0.49 mg	5d
Total	**+/- 7.54 mg**	**+/- 6.99 mg**	

Note 1: The typical LVDT signal conditioner has a nonlinearity of ± 2.2 mg. The worst case for the LVDT signal conditioner nonlinearity is ± 14.6 mg.

The typical system will have a nonlinearity of 7.0 mg and a noise floor of 7.5 mg. Over-sampling the analog voltages and then digitally lowpass filtering the signals can reduce the noise but not the nonlinearity. The present system is over-sampled at thirteen times the cutoff frequency, allowing significant digital filtering. Potentially using very systematic characterization of the accelerometer sensor the nonlinearity could be corrected in post-processing in the computer system.

Chapter 6. The Computer Program

A. Program Overview

A computer program was written in Visual Basic[86] (from Microsoft, Inc.) to download, process, and display the accelerometer data collected in the first-in-first-out (FIFO) buffer on the digital board. The program was implemented on a laptop computer connected through the parallel port to the digital board of the sensor. This chapter describes the theory of how the program operates and the general method of implementation; the complete code is listed in appendix C.

The software is the final component of the complete accelerometer sensor. The program stores and displays the acceleration data from the accelerometer sensor when the sensor is tested or used in a more practical setting. Testing results are included in Chapter 7.

There are three sections to the program. First the data is collected through the parallel port of the laptop computer, which accesses the data in sequential bytes from the FIFO. The data is then processed, which includes dividing the data into separate channels for each of the three axes of the sensor and also digitally filtering the data. Finally the data is displayed on the computer screen and optionally stored to disk. The computer program runs sequentially in an endless loop through these steps.

B. Data Acquisition

The connection between the laptop computer and the digital board is made with a standard 25-wire printer cable, which has a 36-contact Centronix connector on the side of the digital board and a 25-contact connection at the computer's parallel port. The connections in the parallel port of a computer are divided into several different groups: eight data lines, four control lines, four status lines, and the remainder are grounds. The overall pinout for the parallel port lines used in this project is in Table 6-1.

The control lines are transmit only: the computer sends out signals on these lines. The status lines are receive only: on these lines the computer receives information from the peripheral (typically a printer). The data lines can be used for transmitting or receiving, and the method of selecting between the two directions depends on the computer hardware system. The laptop used in this project has a bit in a register inside the computer that can be set high or low to respectively receive or transmit data over the data lines.

Table 6-1. Parallel Port Pinout for Used Lines

Line Type	Pin by Connector Type		Function	Direction [1]
	Parallel Port	Centronix		
Control	1	1	Read Command	C -> D
Data	2	2	Data Bit 0	D -> C
Data	3	3	Data Bit 1	D -> C
Data	4	4	Data Bit 2	D -> C
Data	5	5	Data Bit 3	D -> C
Data	6	6	Data Bit 4	D -> C
Data	7	7	Data Bit 5	D -> C
Data	8	8	Data Bit 6	D -> C
Data	9	9	Data Bit 7	D -> C
Status	10	10	Almost Flag	D -> C
Status	12	12	Full Flag	D -> C
Status	13	13	Half Flag	D -> C
Status	15	32	Empty Flag	D -> C

Note 1: C -> D: computer to digital board; D -> C: digital board to computer

The algorithm for the data acquisition section of the program is diagrammed in Figure 6-1. The FIFO buffer on the digital board has eight parallel output registers connected to the eight data lines in the parallel port. There are four FIFO status pins that are memory capacity flags connected to the four parallel port status lines, and together indicate if the FIFO is empty, almost empty, less than half full, more than half full, almost full, or full.

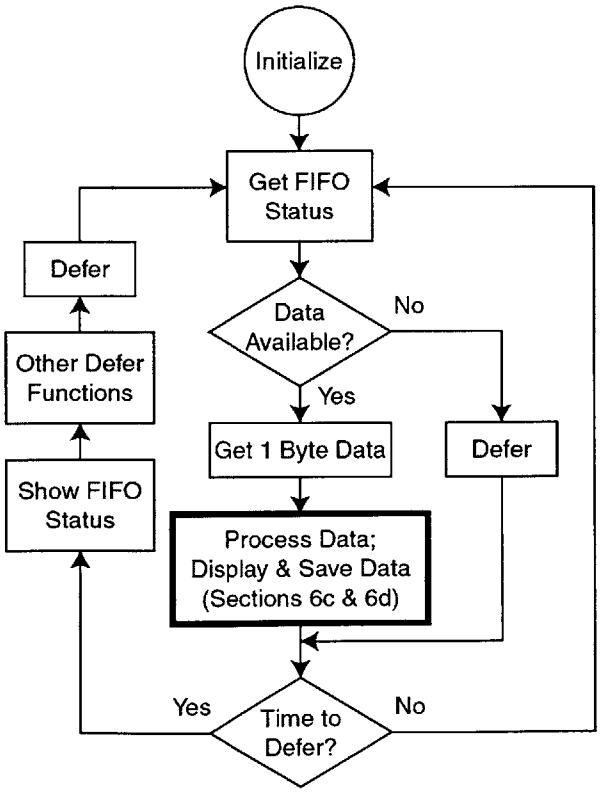

Figure 6-1. Flowchart of acquisition algorithm.

The first step to data acquisition is checking the FIFO status lines. If the memory capacity flags indicate the FIFO has data available, a parallel port control line connected to the read pin on the FIFO is switched, loading the next byte of data into the FIFO output registers. The program acquires that byte of data through the data lines of the parallel port and proceeds on to the next section of the program: processing the data.

Visual Basic programs need to periodically defer use of the computer's CPU to allow low-level processes to run, such as responding to keyboard data entry or mouse clicks. In this program, deferral occurs once each second. Just before the program defers, the computer screen displays the FIFO memory status indicated by the status lines. The program also has other functions it does just before deferring, such as calculating and displaying the rate of data acquisition, which is done by counting the number of bytes downloaded in that second. In addition, if there is no data in the FIFO, the program defers to kill time.

C. Data Processing

The data processing step has many components, including determining each byte's channel, digitally filtering the data, and calculating standard deviations for the data from each channel to quantify jitter. The processing section is diagrammed in Figure 6-2.

In the hardware of the sensor, the first bit to enter the FIFO's serial input is the least significant bit (LSB) from the ADC. However, the connection between the FIFO and computer hardware flips the byte: the LSB from the FIFO becomes the MSB (most significant bit) of the data, and so on for all the bits. Consequently, the first step in the processing algorithm is flipping the data byte back, bit by bit.

The next step in the process algorithm is identifying each byte's channel, done using the parsing channel on the ADC: the one channel pinned permanently high. The channel identification subroutine monitors the bytes of data coming from the FIFO, and whenever there are two consecutive high bytes (16 high bits, or the maximum output of the 16-bit ADC), the channel counter is set to zero. Each subsequent bit is then assigned to a channel: the next two bytes following the reset belong to channel A, then the next two are channel B, and finally two from channel C. After channel C the parsing channel is resampled and there are two high bytes again, the channel counter is reset to zero, and the channel identification subroutine repeats. If there are no high bytes then the data is invalid until two consecutive high bytes reset the counter.

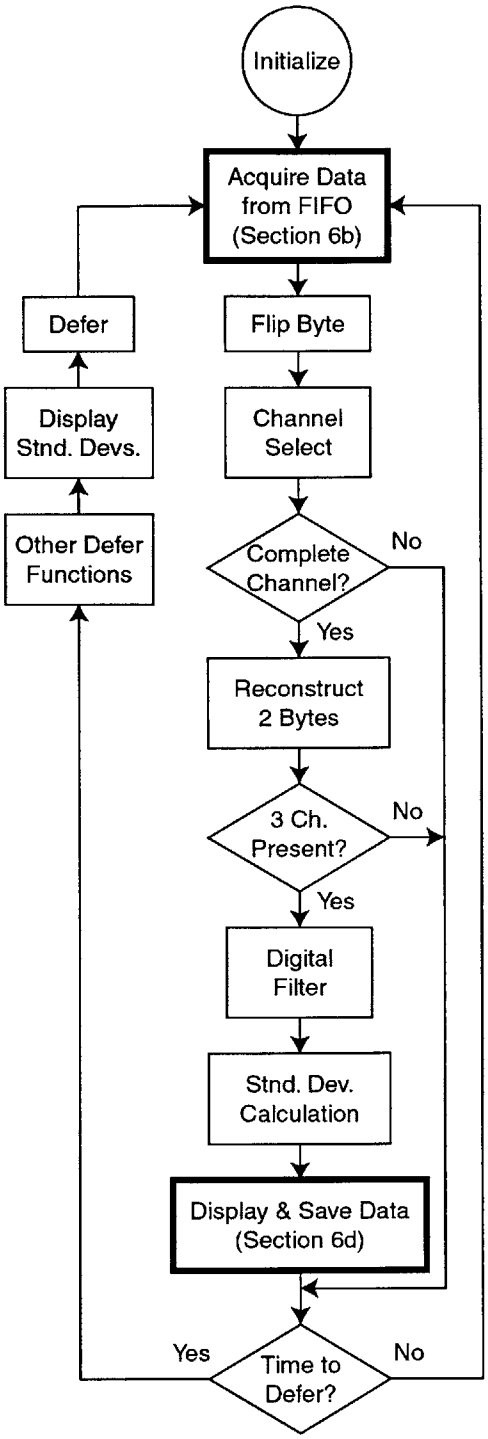

Figure 6-2. Flowchart of process algorithm.

The program waits for both bytes from each channel before proceeding. After both bytes for the channel are present, the program combines the two bytes together to reconstruct the full 16 bit output from the ADC by multiplying the newer, more significant byte, by 256 and then adding the result to the previous, less significant byte.

The process routine then waits for complete data from all three channels before moving on to the filtering and standard deviation calculations. The user has the option of selecting the type of low-pass digital filter: rectangular or Hanning. The user can also select the length of the filter; a special case is a rectangular filter of length 1, which is equivalent to no filter. The cutoff frequency of the filter is dependent on both the filter length and the sampling frequency of the system, so as the sampling rate is calculated just before deferral every second, the frequency of the first zero of the digital filter is also calculated and displayed for the user. Bode plots of the frequency response for typical digital filters are in Figure 6-3.

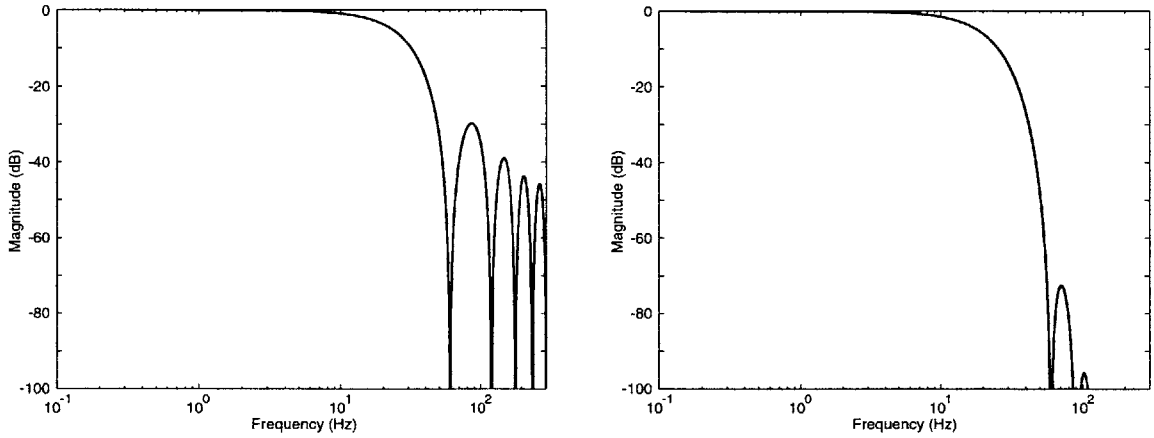

Figure 6-3. Digital filter Bode plots. (a. Left) Rectangular filter, n=10, Fs = 600 Hz (b. Right) Hanning filter, n=19, Fs = 600 Hz

The user also selects how often the filter output is passed on to the plotting section and displayed on the computer screen. This is a feature that allows the computational time required for displaying the data to be decreased by decreasing the screen update rate, increasing the possible rate of data acquisition. The filter output rate can vary from once every new data point to each time the filter is filled with new data. Just before deferral, the display rate is also calculated every second and presented to the user.

After digital filtering, standard deviation calculations for the data from each of the three axes are made to quantify jitter of the sensor. The user can select three different methods to make the standard deviation calculation. The first calculates the standard deviation of the dataset of every data point acquired in each channel for the entire second between deferrals. The second calculates the standard deviation for each small set of data points used in the filter to calculate a point that is displayed, and the result for each channel is the average of all of the channel's standard deviation calculations for one second. The third calculates the standard deviation of the

dataset of all of the filtered output points displayed for each channel for the entire second between deferrals.

Averaging standard deviations for many short times is best used to measure jitter during voluntary movement. The frequency range of normal voluntary movement is much lower than the frequency spectrum for hand jitter, and consequently calculating the standard deviations for short samples of data will not make voluntary hand movement a significant component in the standard deviation calculations. The other two methods calculating the standard deviation over the duration of a second are more applicable for measuring small involuntary jitter when the sensor is being kept as still as possible.

D. Data Display and Storage

This section displays the data, and if the user desires, the raw or filtered data can also be saved. Due to the constraints of the two-dimensional computer screen, the user can select only two accelerometer channels to display at any one time: one on the horizontal axis and one on the vertical axis. A diagram of the data display and storage section of the program is in Figure 6-4.

The user has the option of saving the acquired data two different ways: either the unfiltered raw data after being sorted into the three different channels, or the filtered output data: the same points displayed on the screen. When the user indicates they want to save data, they first create the file to save the data into. After preparing the data file, the user can start acquisition at any time. By keeping a delay between creating the file and starting acquisition, the data that filled the FIFO to overflowing while the dialog box was presented can be processed, and data acquisition can start with the FIFO almost empty.

The format of the data file is comma separated variable. After the file name is specified the file is created and a few lines of header are written to the file. The first five lines of the file are the date and time of acquisition, the file name, a line of text specified by the user, the sensitivity calibrations for each channel (described below), and the headers for the four columns. The four columns of data are the time and the three channels of acceleration data, which are scaled to acceleration in g's. If the user has selected saving raw data, then immediately after the filtering section of the program the points in each channel that were just inserted into the filtering function are scaled and written out as the next line in the output data file.

The display and saving section proceeds if the filter output is ready to be displayed. If the user has selected saving filtered data, then the filtered data output is scaled and saved as the next line in the data file at this time.

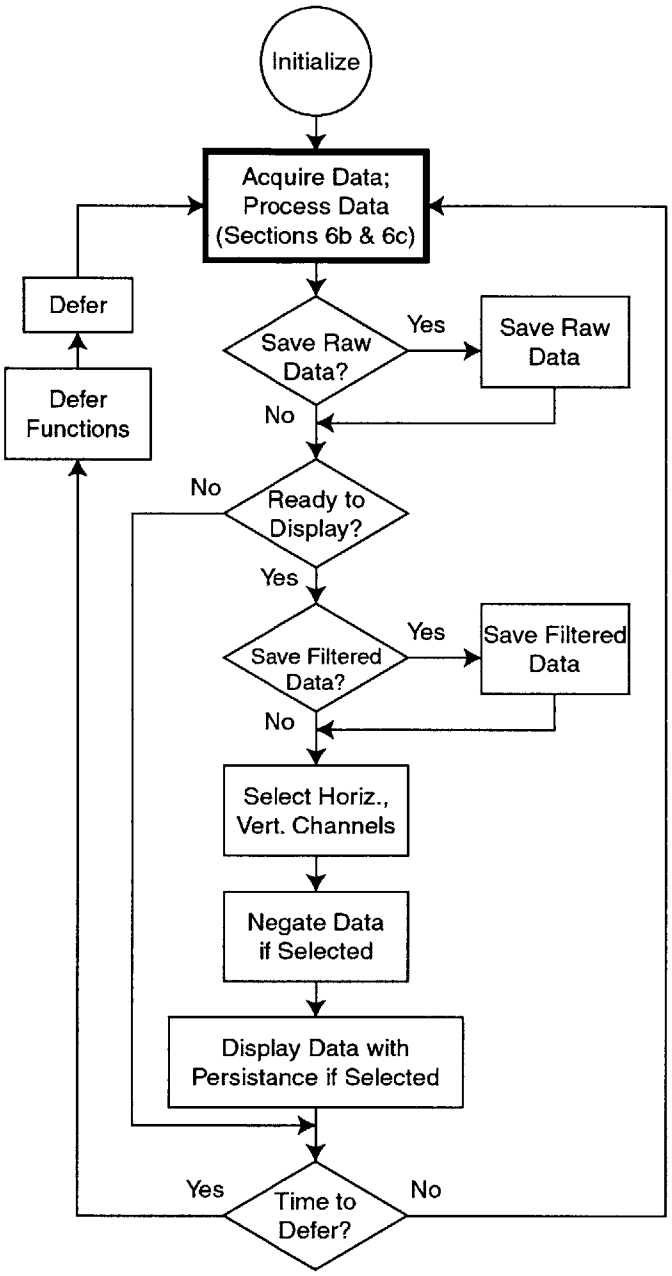

Figure 6-4. Flowchart of data display and storage algorithm.

Then the data display is updated. The user selects which of the data channels (A, B, or C) to be displayed on the horizontal and vertical axes. In addition, the data on either axis can be negated to flip the data displayed. The user can also select if the data plotted is just the most recent point, or a fading persistence using the last 20 points from the filter. If the persistence is selected, the previous points are displayed with a color that gradually fades from black into the white background as the data becomes older. The newest data point is displayed as a line from

the center of the display to the point, and the older data can either be displayed as lines from the center or just points.

The user can set different gains for the data from the three axes to calibrate the individual sensitivity of the three sensors. The calibration is easily done using the 1 g acceleration of gravity. The user calibrates the sensitivity of an axis by rotating the sensor so the axis is horizontal, perpendicular to the acceleration from gravity, and then the output from that channel (the zero-g output) is set to zero by adjusting the zero-output potentiometer on the analog board for that channel. The user then rotates the sensor so the axis is parallel to the acceleration of gravity. A 1 g amplitude ring is displayed on the screen and the sensitivity calibration for that axis is adjusted until the data displayed lies on the 1 g amplitude ring.

The data from each channel is multiplied by the channel's sensitivity calibration before saving or displaying the data. The scaling factors are saved in the header of the data file. A separate gain for just the data displayed allows magnification of the display for small accelerations.

E. Conclusion

The computer program acquires the data from the sensor hardware, separates the data into the three accelerometer channels, digitally filters the data, calculates the jitter in each channel, optionally saves the raw or filtered data, and displays in real-time the acceleration data for two dimensions.

One of the features of the sensor system is a variable sampling frequency. The limiting factor of the sampling rate is the rate of data acquisition and processing by the software. Depending on the number and type of functions the user wants to run real-time in software, the program can run very slowly and consequently the sampling frequency needs to be decreased to avoid overflowing the FIFO. Functions that make the software run slowly include long digital filters, jitter calculations, saving raw data, and frequent displaying of the data. If the software were run on a faster computer, the sampling frequency could be increased as the computer computation speed increases.

The sampling frequency is adjusted by hand by changing a potentiometer on the digital board, which changes the clock speed of a 555 timer. The FIFO free memory availability is displayed every second, allowing the sampling frequency to be adjusted before the FIFO overflows and data is lost. However, changing the sampling frequency changes the filter cutoff frequency of the digital filter, which is corrected by changing the digital filter length.

Overall the software works well but fairly slowly. The program performs many simple functions, but the slow speed of Visual Basic and the fairly slow computer it runs on limits the possible sampling frequency. More complex functions such as calculating the frequency spectrum can be done with the saved data in post processing.

Chapter 7. Hardware Construction and Testing

A. Construction and Testing Overview

The three-dimensional accelerometer sensor system described in the previous chapters was constructed and tested. The complete system includes the three-dimensional accelerometer array for the fingertip, the analog and digital boards, and the software developed for this project.

As construction of the sensor components progressed, the subsystems were tested frequently to ensure all of the parts of the system worked together. Several revisions of the original hardware and software designs were required to make the overall sensor operate properly, and the final designs are those described in the previous chapters.

One key goal of testing the sensor system was confirming the theoretical performance of the accelerometer sensor described in previous chapters is accurate in practice. In addition, acquisition and analysis of involuntary hand tremor data was also performed, as measuring involuntary human hand acceleration is the intended application of the sensor.

B. Construction of the Accelerometer Sensor Hardware

Single-axis MIT Microsystems Technology Laboratory (MTL) accelerometer sensors (described in sections 3d and f) had been previously fabricated, and fifteen were quality control tested as discussed in Section 3g. The four high-quality accelerometers identified were packaged in leadless chip carriers as described in Chapter 4. The fingertip, analog, and digital printed circuit boards (PCBs) described in Chapter 5 were fabricated (at Alberta Printed Circuits[87]) and populated with the specified components. Single-axis accelerometer sensors consisting of a packaged accelerometer die and a fingertip PCB were constructed.

Affixing three single-axis accelerometer sensors to a small balsa wood cube formed the three-dimensional accelerometer sensor array. The cube provides a rigid support for the sensor array and keeps the single-axis sensors mutually perpendicular. The adhesive used was hot glue because it is repairable although fairly heavy. The single-axis sensors were hand-aligned on the faces of the cube and consequently there was some misalignment between sensors so in the final array the three axes weren't quite mutually perpendicular. However, as with misalignment of the accelerometer dies inside the LCC packages (Section 4b), misalignment of the packages on the cube could theoretically be corrected by extensive testing and characterization of the sensor, and then post-processing the data.

As the weight of the sensor on the fingertip is a critical aspect to the system, a detailed analysis of the mass added by each component of the final sensor is in Table 7-1. The table lists

the weight added to each single-axis sensor and the contribution to the final three-axis sensor array. Weights of the package components are repeated from Table 4-3. The individual single-axis accelerometer sensors weighed an average of 1.06 grams, with a range of 1.04 to 1.08 grams. The measured mass of each single-axis sensor is higher than the predicted mass from adding up the components, possibly due to the solder used to attach the different components together.

Table 7-1. Detailed weight analysis of completed sensor (all units grams).

Component	Mass for 1-D Sensor	Mass for 3-D Sensor
Package		
LCC package (empty)	0.2615	0.7845
MTL Accelerometer Die	0.0357	0.1071
Conductive Epoxy (post-cure)	0.0013	0.0039
Gold for wire bonding	0.0008	0.0024
Copper lid and solder to attach	0.1069	0.3207
Packaged accelerometer total	*0.4062*	*1.2186*
PCB Components		
Resistors (0603, each, 3 per PCB)	0.0024	0.0024
Capacitors (0806, each, 2 per PCB)	0.0086	0.0086
LEDs (0603, each, 1 per PCB)	0.0015	0.0015
OPA2137 (dual buffer, each, 1 per PCB)	0.0255	0.0765
Total component mass	*0.0514*	*0.1542*
PCB Overall		
PCB (unpopulated)	0.4200	1.2600
PCB total	*0.4714*	*1.4142*
Packaged accel + PCB (theoretical)	0.8776	2.6328
Packaged accel + PCB (measured)	*1.0603*	*3.1808*
3-dimensional sensor		
Balsa wood cube		0.1255
Hot glue to attach sensors		0.4156
Total mass of 3-D array (measured)		*3.7218*
Fingertip connection		
Plastic thimble (new)		1.2937
Plastic thimble (w/ lightening holes)		1.0406
Hot glue to connect thimble		0.1176
Total fingertip sensor (measured)		***4.8800***

The total weight of the three-dimensional fingertip sensor on the balsa wood cube is 3.72 grams. The balsa wood cube was hot glued to a plastic thimble to allow easy mounting on a fingertip. Initially the thimble weighed 1.29 grams, but six holes drilled in the thimble reduced its weight to 1.04 grams. Thus, the total weight of the sensor including the thimble is 4.88 grams, slightly less than the 5 gram maximum weight specification from Section 1d.

The true weight of just the fingertip sensor is difficult to measure because the wires connecting the sensor to the analog board have significant mass. The wires were already soldered to the single-axis sensors when the three-axis sensor was assembled, and the wires couldn't be easily removed for weighing purposes. However, weighing the sensor with a few inches of wiring (which is the 4.88 gram specification) provides a good estimate of the total mass added to the finger.

The weight of the wiring is separated into individual components in Table 7-2 for the connections to a single-axis sensor and the final three-axis sensor. In addition to the eighteen 40 gauge wires connecting the fingertip PCBs to the analog board, a plastic sheath (0.100" diameter, 0.020" thick) from a coaxial cable was placed around the wires to prevent damage. The sheath was carefully cut down the side to form a split-loom cover, and the wires were tucked inside.

Table 7-2. Detailed weight analysis of the sensor wiring.

Component	Mass for 1-D Sensor	Mass for 3-D Sensor	Units
40 ga. wire linear density	0.0071	0.0071	grams / cm
Wire count	6	18	
Sheath linear density		0.027	grams / cm
Total linear mass	*0.043*	*0.155*	*grams / cm*
Total wire length	97	97	cm
Total wire mass	*4.10*	*14.96*	*grams*

The size of the three-dimensional sensor array on the balsa wood cube is 17 mm on a side, for a total volume of 4913 mm^3. This is 14 times more volume than the original specification of $(7\ mm)^3$ from Section 1d. A listing of the key components contributing to the final volume of the fingertip sensor is in Table 7-3. The LCC package dimensions determine the horizontal size of each single-axis sensor, and the PCB is only slightly larger than the package to allow the package contacts to be soldered to the PCB. The thickness of the package, the PCB, and the PCB components sum to the height of each single-axis sensor. The final three-dimensional sensor edge length (17 mm) is equal to the horizontal dimension (12.3 mm) of a single-axis sensor plus the thickness (4.6 mm) of another sensor mounted perpendicular.

Overall the fingertip sensor has a mass slightly less than the target specification and a size considerably larger than the volume specification. The added mass of the wiring connecting the fingertip PCBs to the analog board was not specified but turns out to be very significant: the meter of wiring used weighs 15 grams.

Table 7-3. Detailed volume analysis of the fingertip sensor size.

Component	Dimensions (mm)
Accelerometer die	5.0 x 5.0 x 0.6
LCC Package	10.3 x 10.3 x 1.7
Fingertip PCB (unpopulated)	12.3 x 12.3 x 1.6
Single-axis sensor	12.3 x 12.3 x 4.6
Three dimensional sensor on cube	17 x 17 x 17

C. Analyzing DC Operation of the Sensor

The operation of the sensor system with constant (DC) acceleration can be observed by following the signal path from the sensors on the fingertip through the LVDT signal conditioner, the anti-aliasing filter, and the analog-to-digital converter (ADC) while the acceleration on the sensor is kept known and constant. A known and constant acceleration is easily produced by resting the sensor on a stationary tabletop in known orientations relative to the acceleration of gravity.

The first processing step is the LVDT signal conditioner. The LVDT signal conditioner converts the buffered sinusoidal signals from the accelerometers on the fingertip to an analog output voltage. The output voltage is given by Equation 7-1 (which is Equation 5-8 repeated), where V_A and V_B are the sinusoidal amplitudes of the input signals, R_2 is 100 kΩ, and V_{out} is the DC output voltage.

$$V_{out} = \frac{|V_A| - |V_B|}{|V_A| + |V_B|} \times 500\mu A \times R_2 \qquad \text{(Eqn. 7-1)}$$

Using a Keithley 2000 digital multimeter[88] the input voltages and the output voltage were measured on a channel of the system when the accelerometer axis for that channel was pointed either in or opposite the direction of gravity. The signal amplitudes for the data from one channel are in Table 7-4. The theoretical change in the voltage ratio calculated in Section 5d is 0.0150/g, but that can change ± 20% depending on the sensitivity of the specific accelerometer, which is a function of the physical parameters of the die.

Table 7-4. Confirming the LVDT signal conditioner function (Channel A data).

Acceleration (g)	1	-1
Vb measured (VAC rms)	0.2668	0.2600
Va measured (VAC rms)	0.2520	0.2590
Vout measured (VDC)	0.334	-0.331
(Va-Vb)/(Va+Vb) (0 g offset to 0 V)	0.0133	-0.0133
Vout predicted (VDC)	0.665	-0.665
Vout predicted / Vout measured	1.99	2.01

The measurements show that the voltage ratio sensitivity is within 20% of the theoretical value. However, the LVDT signal conditioner has a gain too low by a factor of two. The data for the other channels is similar. Consequently the effective sensitivity at the output from the LVDT signal conditioner is one-half the 0.75 V/g sensitivity predicted. Sensitivity calibration is still required for each accelerometer due to differences in the individual dies. The reason for the erroneous gain is unknown, but is internal to the LVDT signal conditioner, an off-the-shelf part. The low gain will increase the active range of the accelerometer sensor but also increase the noise floor (both by a factor of two).

The signal path proceeds on to the anti-aliasing filter and the ADC, ending with the digital data. The measured results for this section are in Table 7-5.

Table 7-5. Confirming the anti-aliasing filter and ADC function (Channel A data).

Acceleration (g)	1	-1
Anti-Aliasing Filter Input (VDC)	0.334	-0.331
Anti-Aliasing Filter Output (VDC)	0.888	-0.919
Digital Data (VDC)	0.863	-0.927
Anti-Aliasing Filter Gain	2.66	2.78

The measured gain of the anti-aliasing filter is about 2.7, which is close to the theoretical gain of 2.59 from HSPICE simulation (Section 5d). The ADC correctly converts the analog signal to digital data without significantly changing the value. The other channels have similar data.

Overall, the signal path works as expected for constant acceleration except for the LVDT signal conditioner, which has a gain one-half that of its specification making the effective sensitivity of the analog system 0.938 V/g. The active range of the sensor is also increased, but that is not important for measuring involuntary hand acceleration because the amplitude of involuntary hand acceleration does not exceed ± 5 g's.

D. Measuring the Noise Floor

One of the key parameters in the system is the noise floor, which determines the precision of an acceleration measurement. The sensor was rested on a tabletop, and the software acquired and

saved a section of data. An oscilloscope was used to simultaneously measure the signal on the input and output of the anti-aliasing filter to determine the analog noise. The digital data was scaled to the voltage range of the ADC input, ± 10 Volts. The measurements from this test are in Table 7-6.

Table 7-6. Comparing analog and digital noise floors.

	Noise Floor (mVp-p)				Standard Deviation (mV)	
	Analog Signal		Digital Data		Digital Data	
Chan.	Before AAF	After AAF	Unfiltered	Filtered [1]	Unfiltered	Filtered [1]
A	40	10.4	3.0	2.0	0.8	0.6
B	60	11.5	7.0	5.0	1.7	0.9
C	50	10.6	5.0	3.5	1.1	0.6

Note 1. Digital filter: 9 point Hanning filter, cutoff frequency= 60 Hz.

The noise floor at the output of the LVDT signal conditioner is 40-60 mVp-p, considerably higher than the noise floor specification of 11.3 mVp-p for the LVDT signal conditioner as discussed in Section 5d. However, the higher than expected noise could be due to the bandwidth of the measurement: the analog noise floors were measured with a 0 to 20 MHz bandwidth on the oscilloscope. Indeed, after the anti-aliasing filter reduces the bandwidth to 0 to 45 Hz, the noise floor is reduced to 11 mVp-p even though the signal has been amplified 2.7 times.

The noise floor of the LVDT signal conditioner output was observed to vary greatly from unit to unit. The noise is independent of the accelerometer connected, as swapping which single-axis accelerometer sensor is connected to which LVDT signal conditioner does not affect the noise floor for that LVDT signal conditioner. The LVDT signal conditioner used in channel B for testing was new, and had a reduction in the noise floor of 10 mVp-p compared to the prior LVDT signal conditioner used.

The noise in the digital data is lower than the noise in the analog signal after the anti-aliasing filter, due to the final RC lowpass filter immediately before the ADC input.

Finally, the measured noise floor in the filtered digital data is 3 to 5 mVp-p. The filter used for this part of the testing was a nine point Hanning filter with the first zero falling at 57 Hz with an acquisition rate of 250 samples per second per channel. The accelerometer sensor sensitivity is 0.938 V/g, so the noise floor for the channels corresponds to about ± 2.5 mg—slightly larger than the 1 mg noise specification for the accelerometer. The standard deviations for the unfiltered and filtered digital data is included in Table 7-6, and is equivalent to the RMS noise in the signal. There are additional effects from non-linearity and cross-sensitivity (discussed in the next section) that add to the inaccuracies of the sensor.

Plots of the noise spectrum of the digital data before and after filtering are in Figure 7-1. The spectra show most of the noise is at lower frequencies, due to the analog anti-aliasing filter which has a cutoff frequency at 45 Hz. There is significant noise in particular near 60 Hz. The noise between about 20 and 80 Hz is strongly attenuated by the digital lowpass filter. However, the noise amplitude at higher frequencies is increased slightly.

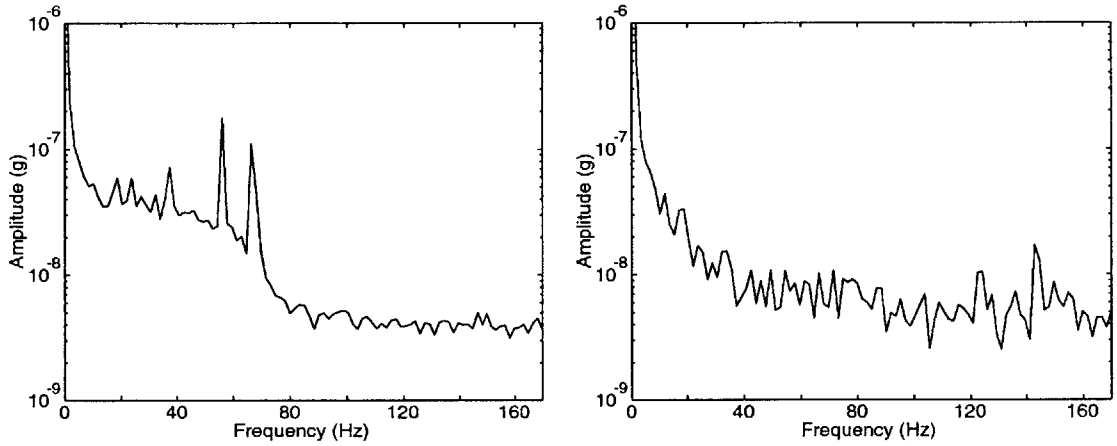

Figure 7-1. Noise power spectral density of channel A. F_s = 340 Hz. (a. Left) Before filtering. (b. Right) After filtering with a 11 pt Hanning filter, 1st zero at 60 Hz.

The effect of the digital filter reducing noise in the system is reflected in the decrease of the noise power (the standard deviation of the signal) as seen in the data in Table 7-6. To fully preserve the 0.1 to 25 Hz bandwidth of interest, the cutoff frequency of the filter would need to be increased slightly, increasing the noise in the system as well. Alternatively, a more sophisticated filter with a sharper cutoff could be used with the data.

E. Calibrated Acceleration Source Testing

Two important parameters characterizing the accelerometer sensor system are linearity and cross-sensitivity. Linearity indicates how the sensitivity of the system varies with acceleration amplitude. Cross-sensitivity characterizes how sensitive the accelerometer sensor is to acceleration perpendicular to the intended axis.

Linearity and cross-sensitivity testing is done using an acceleration source that can produce a variable but known acceleration. The source used for testing in this project was a Ling Dynamic Systems[89] V450 vibrator with a PA1000 power amplifier. A signal generator supplies a sinusoidal signal to the power amplifier, which drives the vibrator. The vibrator is a large

electromagnet system similar to an audio speaker that moves a small test stand up and down in a sinusoidal manner.

A Brüel & Kjær[90] 4383 piezoelectric reference accelerometer is mounted on the test stand to measure the acceleration. The reference accelerometer allows repeatable determination of the system acceleration. However, the sensor has a calibration only accurate to ± 1.2%, indicating the sensor can be up to 1.2% nonlinear itself.

The linearity test is made by positioning a single-axis sensor on the test stand with the sensitive axis of the sensor parallel to the axis of the vibrator. The amplitude of sinusoidal acceleration is increased from 0 to ± 5 g (or 10 g peak-to-peak). The standard deviation of acceleration measured by the accelerometer sensor system is calculated at each of the different acceleration amplitudes and the data is plotted against the output from the reference accelerometer which indicates the actual acceleration. A straight line is drawn from the intercept at zero acceleration to the sensor output at maximum acceleration (± 5 g), and the error between the line and the measured acceleration is the non-linearity of the acceleration signal. The measured data and the error is plotted in Figure 7-2.

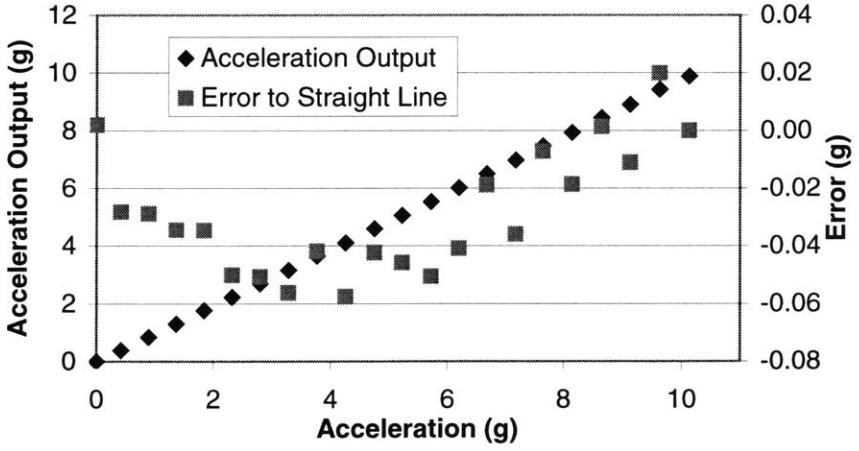

Figure 7-2. Linearity analysis. Accelerations are measured peak-to-peak.

The maximum nonlinearity in the system is at about 4 g (± 2 g) of acceleration, when the output is about 57 mg's below the amplitude of the acceleration as measured by the reference accelerometer. However, the reference accelerometer is only accurate to ± 1.2%, which is 48 mg's at 4 g of acceleration amplitude. In addition, the amplitude cannot be measured more precisely than ± 2.5 mg's due to the noise floor. Thus the nonlinearity of the developed accelerometer system is at least 7 mg's, and undoubtedly slightly more. Overall the nonlinearity is probably as good as or better than the nonlinearity of the reference accelerometer.

The theoretical nonlinearity is ± 7 mg, as calculated in Chapter 5 and summarized in Section 5f. Thus the experimental data indicate the actual nonlinearity is at least as large as the theoretical nonlinearity. The theoretical nonlinearity can be as high as ± 20 mg's depending on the particular LVDT signal conditioner. This amount of nonlinearity is perhaps more reasonable given the experimental data, but cannot be confirmed using the testing setup with this reference accelerometer.

The cross-sensitivity test is identical to the linearity test, except the accelerometer is rotated 90 degrees so the intended axis sensitive to acceleration is perpendicular to the axis of the vibrator. The cross-sensitivity is the ratio of the output acceleration indicated by the sensor system and the input acceleration as measured by the reference accelerometer. The data from the cross-sensitivity test is plotted in Figure 7-3.

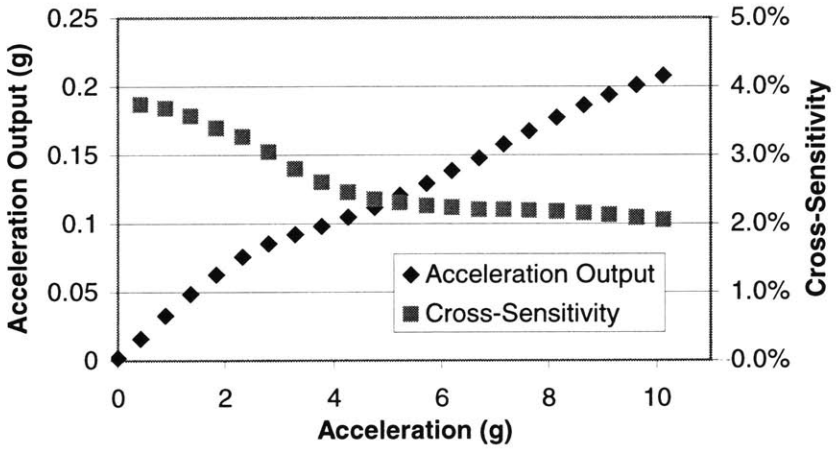

Figure 7-3. Cross-sensitivity analysis. Accelerations are measured peak-to-peak.

Commercial accelerometers (such as the three described in Section 3c) typically have maximum cross-sensitivity specifications of 5%. The MTL accelerometer is slightly better than these specifications: the maximum cross-sensitivity on the ± 5 g range is only 3.75%. The cross-sensitivity decreases down to just 2% as the acceleration amplitude is increased. An important factor in the low cross-sensitivity specification of the MTL accelerometer is the geometry of the tether elements holding the proof mass in place. The geometry arises from the deep reactive ion etch (DRIE) fabrication technique, described in Section 3d, used to make the MTL accelerometers. The DRIE allows the tether elements of the accelerometer sensor to be much thicker then the tethers of conventional accelerometer sensors fabricated with sacrificial oxide, which prevents much of the tether flexing in unintended directions.

F. Rotation Analysis

One other important characteristic of the sensor system is how the three-single axis accelerometer sensors are mounted with respect to each other. Ideally the axes are mutually perpendicular, but in actuality they will not be quite perpendicular and thus an axis of the sensor will be unexpectedly sensitive to acceleration along another axis.

A simple test can be used to see the effect of not having the sensors mutually perpendicular by slowly rotating the sensor and watching the combination of the accelerometer outputs; the data from this test is in Figure 7-4. The data has had the zero-acceleration output set to zero and has been correctly calibrated for sensitivity.

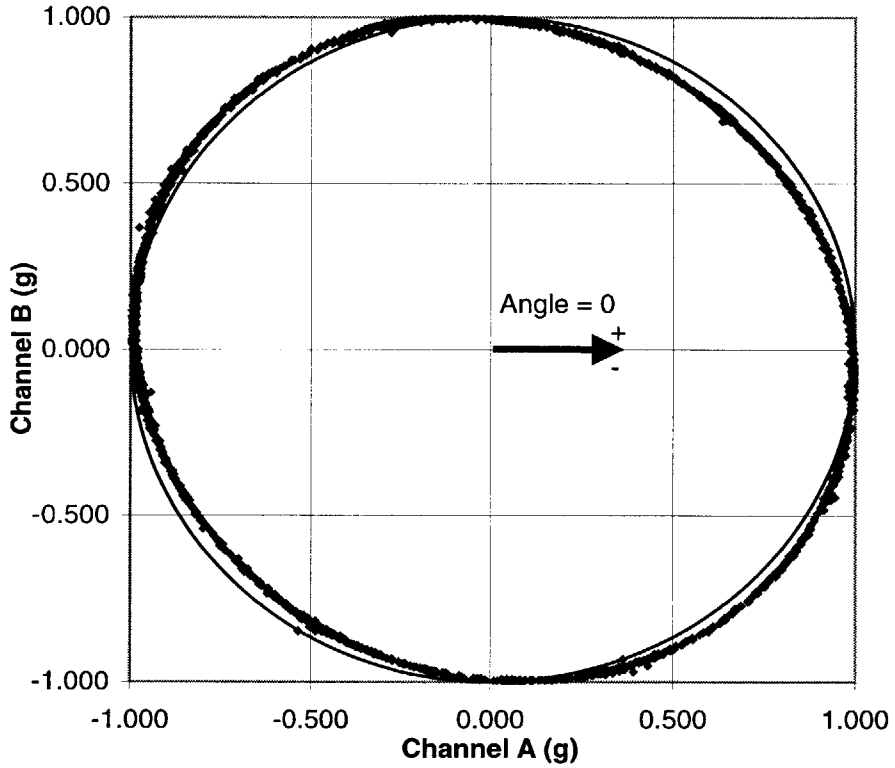

Figure 7-4. Acceleration from gravity as the sensor is rotated in a circle. (The thin black line is a perfect circle.)

The vector sum of the acceleration amplitudes should theoretically trace a perfect circle as the finger is rotated. However, the plot of data is slightly elliptical. The magnitude of the vector sum of acceleration for the two axes is in Figure 7-5. The plot shows the magnitude of measured gravitational acceleration slowly changes as the sensor is rotated.

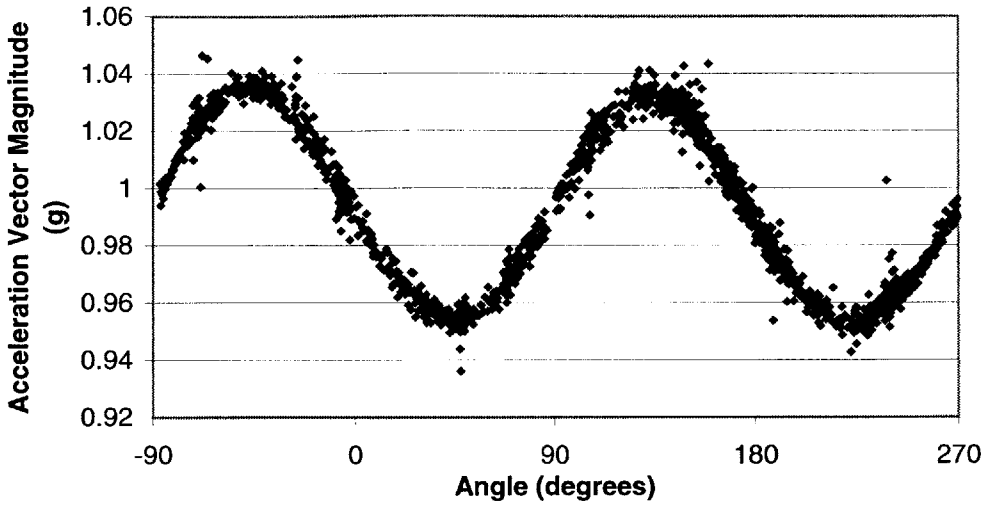

Figure 7-5. Magnitude of gravitational acceleration as the sensor is rotated in a circle using the data from the two axes in Figure 7-4.

One reason the plot is elliptical is the two axes of the sensor are not maintained exactly in the vertical plane. To do this test the thimble was mounted on a dowel, and the dowel was slowly rolled along the edge of a table with the sensor rotating at the end of the dowel. If the sensor was not perfectly aligned on the dowel, the two axes plotted will tip forward and backward slightly. Including the data from the third axis in the magnitude calculation can compensate for this effect, and the result is shown in Figure 7-6. However, as seen in the plot, this effect only contributes to a small part of the variation in magnitude seen with a change in angle.

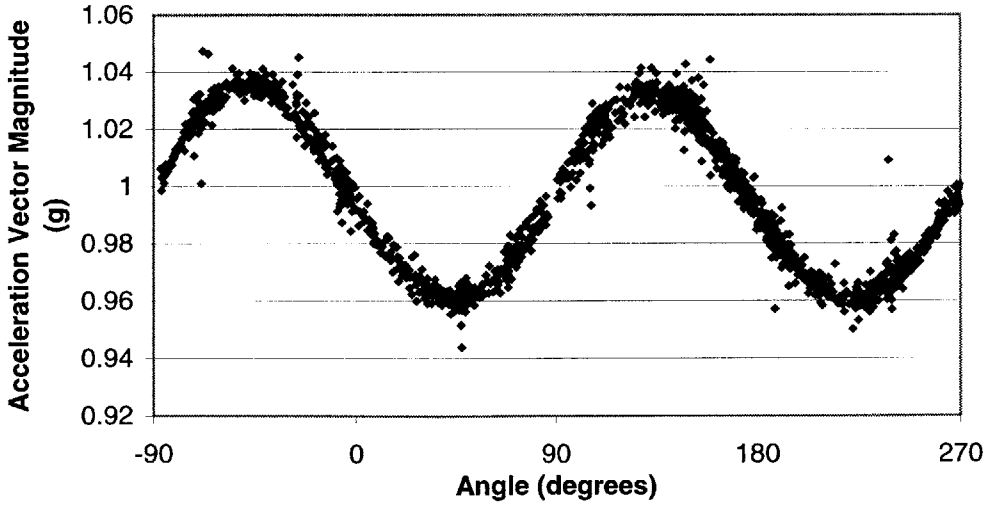

Figure 7-6. Magnitude of gravitational acceleration as the sensor is rotated in a circle, including the acceleration from all three axes.

The second reason the data in Figure 7-5 is elliptical is the different axes of the sensor are not quite mutually perpendicular. When the sensor array is rotated to –45 degrees (referenced to Figure 7-6), the axes of the two acceleration sensors are both slightly closer than 45 degrees to the direction of gravity. Consequently, the vector sum of the two accelerations measured is more than 1 g.

The relative angle between the axes can be calculated from the magnitude of acceleration measured, which peaks at about 1.035 g at –45 degrees. At that amplitude, both accelerometer sensors are experiencing about 0.735 g instead of the 0.707 g sensors would sense when positioned at a perfect 45 degree angle to gravity. Taking the inverse cosine of this value, the angle of each sensor to the vector of gravity is only 43 degrees, so the two axes are only about 86 degrees apart instead of 90 degrees. The observed angle between the two packages is about 85 degrees. However, measurement of the angle between packages does not reveal the orientation of the dies inside the packages, and consequently the analytical method used to calculate the mutual angle is more accurate than simply measuring the relative package orientations.

The cross-sensitivity of the accelerometer sensors will also contribute to the elliptical gravitational acceleration. Using the cross-sensitivity specification calculated in the previous section, the estimate of the mutual angle between sensors could be compensated for cross-sensitivity resulting in a higher accuracy angle calculation.

The two axes tested on the three-axis sensor array are not quite mutually perpendicular. The third axis will not be exactly perpendicular to these two axes either, and the same measurement could be made to calculate the relative angles between the other axes pairs. Using this technique, the overall configuration of the three axes could be analytically reconstructed. As discussed in the future work section of the next chapter, the complete characterization of the sensor could be used to theoretically compensate in post-processing the acceleration data from axes that are not quite mutually perpendicular, and reconstruct the true original three-dimensional acceleration signal.

G. Finger Tremor Analysis

The goal of this project is development of a sensor capable of measuring human hand acceleration. There is considerable prior research in hand acceleration, and a brief review of the literature is in Chapter 2. One of the important tests of this project is demonstrating the sensor is capable of measuring involuntary hand acceleration and would be useful in applications measuring involuntary hand acceleration.

The involuntary hand motion test was made by mounting the sensor on the fingertip of a normal subject. The test subject held their hand as still as possible with the hand kept horizontal, and data was acquired at a rate of 330 Hz. The standard deviations of the accelerations of all three axes were measured relative to a control test with the sensor stationary on a tabletop. The standard deviations from involuntary human hand jitter are in Table 7-7. A digital lowpass Hanning filter built into the software was used with a length of 12 points, placing the first zero of the filter at about 55 Hz.

Table 7-7. Standard deviations of acceleration from hand jitter (in mg).

Axis	Control on Tabletop	Mounted on Fingertip
A	0.5	31
B	1.1	6
C	0.9	17

Axis A was oriented parallel to the acceleration of gravity. The hand jitter amplitude was highest on this axis, indicating most of the jitter is along the axis of gravity. The lowest jitter is on axis B, which was oriented in the direction of the finger, indicating there is very little jitter in that direction. Finally, axis C was the other axis in the horizontal plane, and had a moderate amount of acceleration from jitter.

One example of how the sensor could be used to measure hand acceleration is recording data with astronauts to see how the human body's control system changes in microgravity. A previous experiment with this purpose was done during long duration space flight on the Russian space station MIR using a single-axis piezoresistive accelerometer sensor mounted on the subject's wrist.[91] Acceleration data was acquired before leaving Earth, during space flight (over 150 days in length), and after returning to Earth. The data shows an oscillation of about 8 Hz is dominant before and after flight, but in space the 8 Hz signal disappears and instead a 3-4 Hz signal becomes dominant. The researchers hypothesize the body's control system for limb position changes to use different muscle reflexes depending on the presence or absence of gravity.

With the accelerometer sensor developed in this project, a related experiment can be easily made. A 35 second duration segment of hand tremor data (without digital filtering) from a normal subject was acquired for spectral analysis. The power spectral density of the data from two axes is plotted in Figure 7-7. The data in the plot on the left is from channel A and is parallel to gravitational acceleration. Three main frequencies are present: 9.5, 16, and 3 Hz in decreasing amplitude. The data from channel C (in Figure 7-4b) is perpendicular to gravitational acceleration and has the same frequencies, but the amplitudes of the 9.5 Hz and 16 Hz signals are considerably decreased. The 3 Hz signal is decreased as well, but much less so. These results

indicate the body control system for hand position may be sensitive to the orientation of gravity, as the amplitude and frequency characteristics of hand tremor along specific axes depend on the relative orientation of gravity to that axis. The hand tremor spectra seen in Figure 7-7 is very similar to that reported elsewhere in the literature,[14,19,92] with frequency peaks in the ranges of 3-5 Hz, 8-10 Hz, and 15-25 Hz.

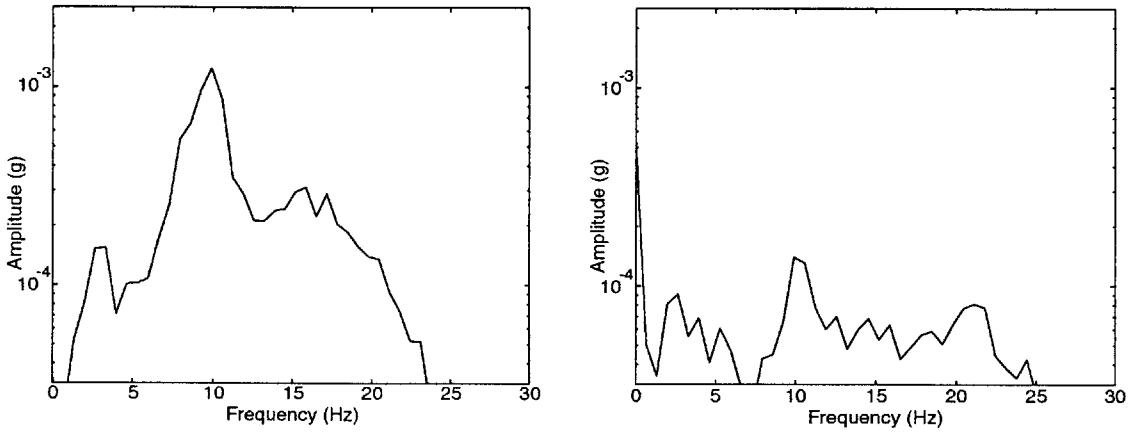

Figure 7-7. Power spectral density of finger jitter.
(a. Left) Parallel to gravity. (b. Right) Perpendicular to gravity.

H. Testing Conclusions

The sensor described in the previous chapters was built and tested to verify its function. A summary of the measured parameters of the system is in Table 7-8.

Table 7-8. Summary of measured sensor specifications.

Parameter	Value
Noise Floor	+/- 2.5 mg
Nonlinearity	>= 7 mg
Cross-sensitivity	<= 3.75%

There were several differences between the designed and measured specifications. The LVDT signal conditioner unexpectedly had a gain of one-half of that designed for, increasing the active range of the sensor but also increasing the noise floor. The higher active range was unutilized because human hand acceleration isn't large enough. Testing the noise floor found it to be about twice as large as the target noise specification of 1 mg. However, the noise floor was considerably less the theoretical level from the actions of the analog and digital filters.

More significant factors affecting the accuracy of measurements are nonlinearity and cross-sensitivity. The nonlinearity cannot be accurately tested because the reference accelerometer for

the testing system has a moderate nonlinearity itself—comparable to the nonlinearity of the sensor. The cross-sensitivity is lower than most commercial accelerometers, but the amplitude is still significant: 3.75% at low accelerations. For example, when measuring tilt with the Earth's gravity, the cross-sensitivity can be as high as 37.5 mg's.

Overall the sensor system developed in this project is effective at measuring human hand acceleration. The data from the sensor identifies the same spectral characteristics seen in published research using one-dimensional accelerometer sensors. However, this new sensor has the added advantage of acquiring three-dimensional data to better characterize complicated hand motion.

Chapter 8. Conclusions

A. Review of the Project

The goal of this project was designing, constructing, and testing a sensor capable of measuring the three-dimensional acceleration of involuntary human hand motion. Reasons for measuring involuntary hand motion include diagnosis of the cause of a tremor, and modeling the control system that regulates hand movement. Based on the goal of measuring involuntary hand motion, ideal specifications for the accelerometer sensor were developed and are repeated in the "Target" column of Table 8-1.

Table 8-1. Accelerometer system parameters.

Parameter	Target	Achieved
Number of Axes	3	3
Frequency Range	0.1 to 25 Hz	0.1 to 25 Hz
Maximum Acceleration Amplitude	+/- 5 g	+/- 10 g
Maximum Acceleration w/o Damage	+/- 20 g	+/- 45 g
Acceleration Resolution:		
Noise floor		+/- 2.5 mg
Nonlinearity		>= 7 mg
Cross-sensitivity		<= 3.75%
Overall (not incl. cross-sensitivity)	+/- 1 mg	+/- 10 mg
Fingertip sensor mass	5 grams	4.88 grams
Fingertip sensor size	(7 mm)^3	(17 mm)^3

The accelerometer sensor was designed to meet the target specifications given the limitations of budget and time. There were several significant technical challenges that needed to be solved during development of the sensor. One challenge was converting the differential capacitance signal from the single-axis accelerometer sensors to a more useful electrical signal, and the solution was using linear variable differential transformer (LVDT) signal conditioners to make an analog voltage proportional to the proof mass position on the die. Another problem was connecting to the accelerometer dies, which was solved by packaging the dies in small chip-scale packages— leadless chip carriers (LCCs)— and connecting the package contacts to the die with gold wire bonds. A third problem was the signals on the fingertip required buffering before being sent to the analog board, which required making a small printed circuit board to put on the fingertip.

After several development cycles the complete sensor was constructed, and the final specifications are repeated in the "Achieved" column of Table 8-1. The frequency range of a particular measurement depends on the digital filters used with the data, but can go as high as the 45 Hz cutoff frequency of the anti-aliasing filter. The maximum acceleration that can be measured is ± 10 g, which is twice as high as designed because the LVDT signal conditioner gain

was one-half that expected. However, the increased range is not useful for measuring involuntary human hand acceleration.

The noise floor of the stationary sensor was measured to be ± 2.5 mg. However, a more significant component to the measurement error is nonlinearity, which is at least 7 mg. Determining a more accurate nonlinearity specification will require a more accurate reference accelerometer for the testing system. A cross-sensitivity of at most 3.75% was experimentally measured, which is better than many commercial accelerometer sensors. The total error was ten times larger than the original specification, not including the effect of cross-sensitivity which is significant. Acceleration data acquired of even a moderate amplitude acceleration signal will have a very large error from cross-sensitivity. For example, when measuring a ± 1 g signal, the cross-sensitivity error on each axis could be as large as ± 37.5 mg depending on the orientation of the axis to the acceleration.

The weight of the fingertip sensor is slightly less than the target specification. However, the size of the fingertip sensor became significantly larger than the original target specification, due to the LCC packages necessary to connect to the dies.

Thus, the final sensor met the target specifications except for the size of the fingertip sensor and the resolution. The precise size of the sensor is not important, as smaller sensors have less hindrance of motion; the original size specification was based on the die size of 5 x 5 mm, and turned out to be unrealistically optimistic. The target resolution specification was not achieved, but the sensor is still able to accurately measure small involuntary hand motion, as demonstrated by the applied testing results presented in Section 7g.

B. Future Work

There are several possible optimizations of the present sensor. Some of the changes are simple while others require significant additional work or redesign of the system.

The construction of the fingertip sensor could be optimized to decrease the mass and the volume of the sensor. The original MTL accelerometer dies have a large area that is unused around the perimeter of the die. Refabricating the accelerometers and cutting the dies smaller could potentially allow the die to be reduced to about 3.5 x 3.5 mm instead of 5 x 5 mm, without changing any of the critical geometry of the MEMS accelerometer. The package containing the die could be smaller than the present package even with the current size die by decreasing the 0.75 mm space between the die and the cavity walls, and the package could be reduced even more if the die size were decreased.

A smaller package would allow the printed circuit board (PCB) to be slightly smaller to match the size of the package. A thinner PCB material would decrease the thickness of a single-axis sensor and the size of the final sensor. A lighter adhesive than hot glue would reduce the weight. Finally, some of the balsa wood cube could be cut out and the thimble made a more integral component of the sensor. The fingertip sensor could be reasonably expected to be decreased to $(10\ mm)^3$ and weigh at most 3 grams.

The printed circuit board designs could be optimized in several ways. Using 0.1% resistors on the fingertip would improve the linearity of the sensor system by 3.4 mg, as discussed in Section 5c. The LVDT signal conditioner could be better applied by decreasing the unused active range of the sensor, which would also decrease the noise floor as well. Using surface mount packages for the LVDT signal conditioners (not available in sufficient quantity at the time of this project) will decrease the size of the analog board to make the board more feasibly positioned on the subject's arm, and improve analog signal quality. On the digital board the connections between the FIFO and the Centronix connector could be flipped, to eliminate the byte-flipping step required in software.

An electrostatic force-feedback circuit would potentially completely eliminate nonlinearity in the accelerometer sensor. Similar to the circuit used in the Analog Devices accelerometer sensor described in Section 3c, the force-feedback system would keep the proof mass in essentially the same place on the die. This would eliminate the 1 mg nonlinearity in the spring over the $\pm$ 5g range. Also, the nonlinearity in the LVDT signal conditioner could potentially be eliminated by using the force-feedback voltage as the output of the circuit, and this voltage would be a more direct indication of the force from acceleration exerted on the proof mass.

The software can be improved in several ways beyond simply using a more sophisticated digital filter and optimizing for speed or running the program on a faster computer to increase the data acquisition rate. One significant change would be compensating for the physical deficiencies of the accelerometer sensors and the three-axis sensor array. For example, the misalignment of the sensors in the array could be corrected for by carefully determining the exact mutual alignment of the three axes. Cross-sensitivity can be characterized and corrected by eliminating the cross-sensitivity component of the measurement from each axis. Nonlinearity can be corrected by characterizing the nonlinearity beforehand and converting the nonlinear measurement to linear data. However, to accurately characterize the cross-sensitivity and nonlinearity of the sensor, a more accurate reference accelerometer than the Brüel & Kjær used for testing in this project needs to be obtained.

C. Recommended Applications of the Sensor

The goal of this project is development of a sensor to measure involuntary human hand acceleration. One of the tests made with the sensor and described in Section 7g is measuring normal hand jitter. In this experiment, the standard deviation of the acceleration signal (equivalent to the signal power) was acquired for the three perpendicular axes of the sensor. Raw data was also acquired, and in post-processing the frequency spectrum of the signal was calculated and compared between different axes.

Most prior work measuring human hand acceleration with accelerometer sensors use one-dimensional sensors to estimate the overall acceleration of the hand. However, involuntary human hand motion can be very complicated and one-dimensional sensors simply make inaccurate measurements. The overall acceleration can be accurately calculated by computing the acceleration magnitude measured from vector addition of the accelerations measured on the three axes of a three-dimensional sensor.

A potential application of the sensor is making measurements of involuntary motion for diagnosing or assessing the severity of tremors. Another application is measuring normal and abnormal (either from disease or in an unusual condition such as microgravity) hand tremor, and using these measurements to model the control system regulating human movement and the physiology of the sensor and effector mechanisms.

A more complete analysis of motion of a non-rigid object such as a human hand or limb could be made using multiple sensors. Multiple sensors allow characterization of the relative phase of acceleration at different places rather than the acceleration of a single point. Complicated movements could be fully characterized, such as positioning a sensor at each finger joint of a hand to measure the acceleration amplitude and phase of the different components of the hand.

Thus the sensor developed in this project offers a new opportunity in clinical and experimental human motion medicine and biomedical engineering to more accurately and more effectively measure involuntary human hand motion.

Appendix A. PCB Copper Plots

Figure A-1. Plots of fingertip printed circuit board copper layers, actual size.

(a. Left) Top copper layer. (b. Right) Bottom copper layer.

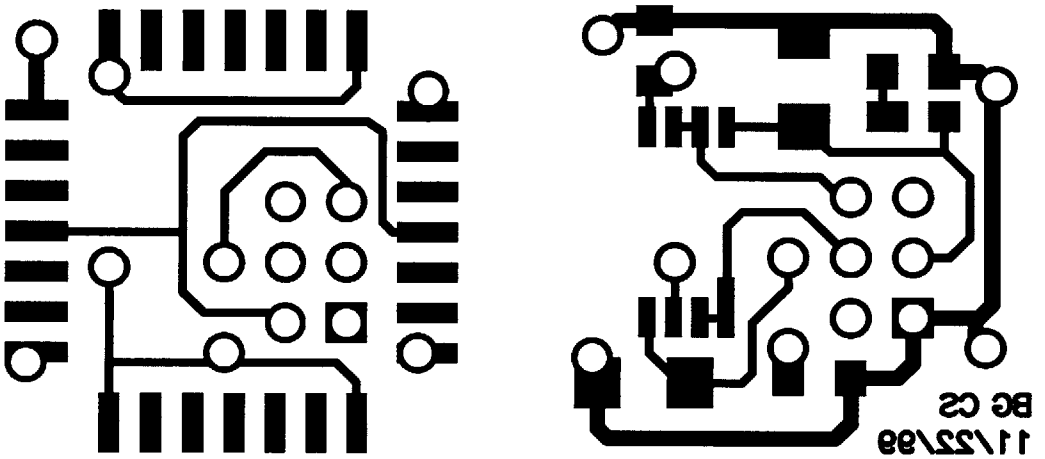

Figure A-2. Plots of fingertip printed circuit board copper layers, enlarged five times.

(a. Left) Top copper layer. (b. Right) Bottom copper layer.

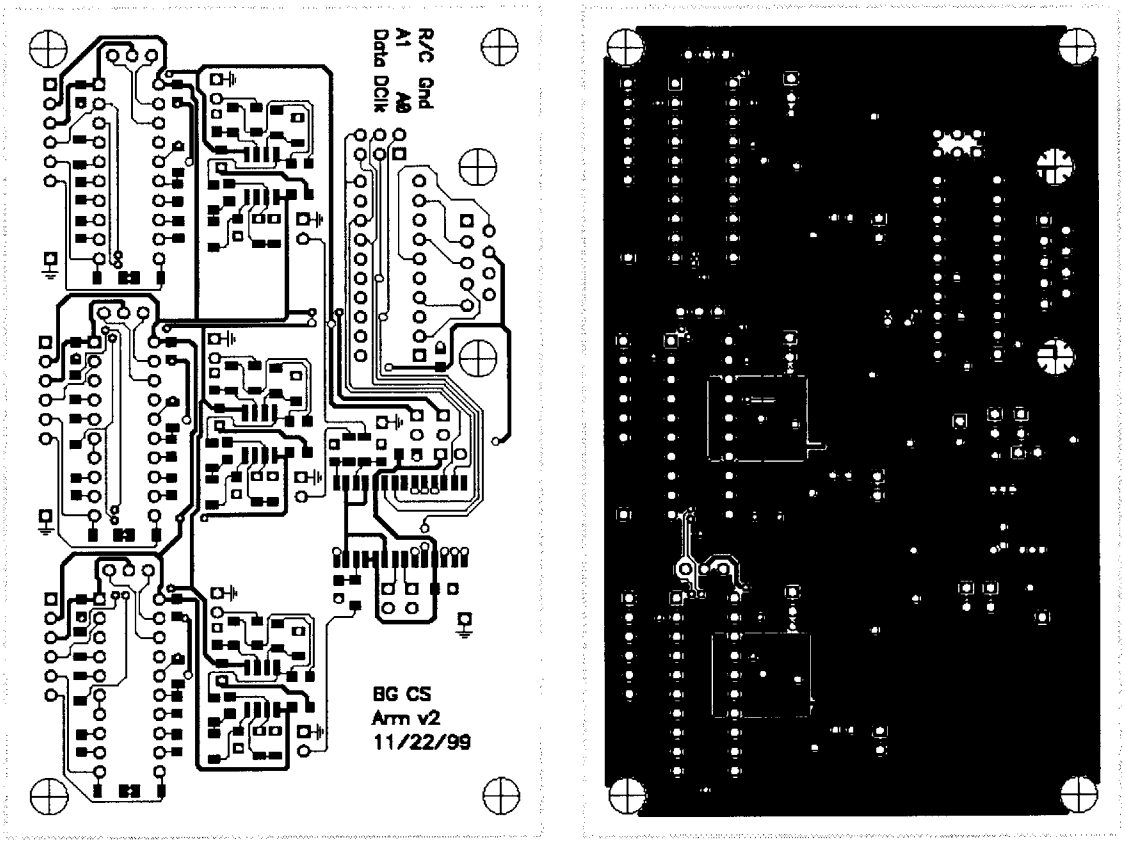

Figure A-3. Plots of analog (arm) printed circuit board copper layers, actual size. (a. Left) Top copper layer. (b. Right) Bottom copper layer.

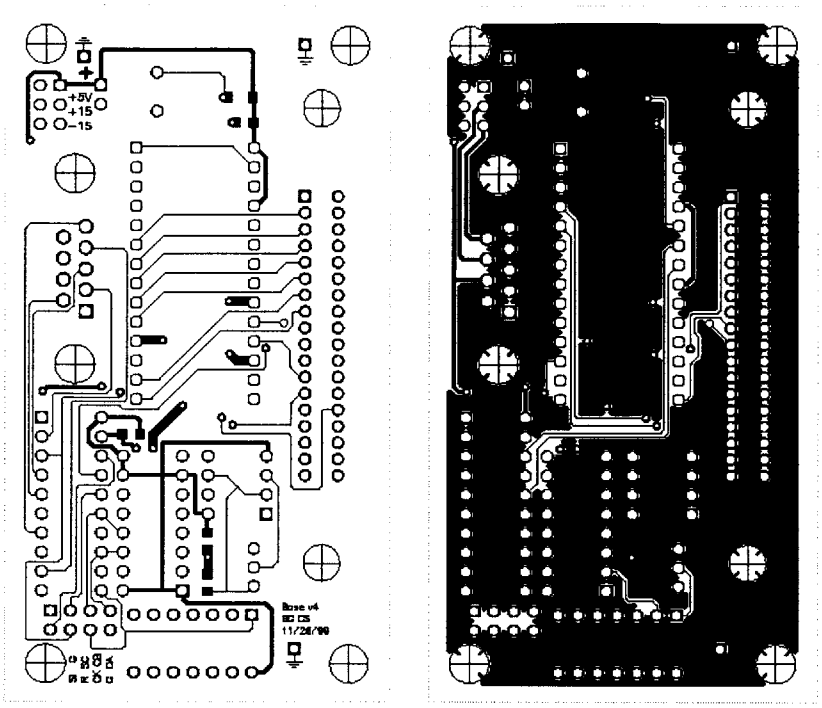

Figure A-4. Plots of digital (base) printed circuit board copper layers, actual size. (a. Left) Top copper layer. (b. Right) Bottom copper layer.

Appendix B. HSPICE Code for the Anti-Aliasing Filter

```
Anti-Aliasing Filter
*April 7, 2000

*Circuit Topology
*First stage
R27 1 2 32k
R28 2 3 32k
C23 2 5 0.1uF
C24 3 0 0.1uF
R15 0 4 125k
R16 4 5 19k
*pos out, neg out, pos in, neg in, gain
E1 5 0 3 4 1meg            *first opamp, U4:A

*Second Stage
R29 5 6 32k
R30 6 7 32k
C25 6 9 0.1uF
C26 7 0 0.1uF
R17 0 8 125k
R18 8 9 156k
E2 9 0 7 8 1meg            *second opamp, U4:B

*Voltage Sources
Vin 1 0 ac 1

*Test Conditions
*.AC DEC ND FSTART FSTOP
.ac dec 50 0.1 100
.ac dec 10 1 1meg
*.plot ac vm(9) vp(9)
.options post

.end
```

Appendix C. Visual Basic Code

```
Const PortAddress = &H378        'the parallel port address
Const config_filename = "C:\Program Files\Microsoft Visual
Studio\VB98\drawing\saved_config5.txt"    'config file name
Const deferral_delay = 3         '# seconds in between deferrals
Dim paused, acq As Boolean       'paused (true); acquiring (true)?
Dim xmax, ymax, xmid, ymid       'variables of the display
Dim channel As Integer           'channel variable
Dim prevbyte As Integer          'variable for getting 16 bit data (msbyte)
Dim prevtime, datacount          'variables for sps calculation, prevtime used
for deferral too
Dim dataset(8) As Double         'data for displaying and writing out, in array
Dim gain                         'variable for the gain of the display.
Const max_filtlength = 100       'maximum possible filter length
Const storelength = 20           'how many pts to display with persistance
Dim filtcount, storecount, stdev_count  'how far along in the filter path
moving through the stored vector
Dim filtx(max_filtlength), filty(max_filtlength), filtz(max_filtlength) 'filter
storage
Dim lastx(storelength), lasty(storelength), lastz(storelength)    'previous
values for x, y, z to display in plot
Dim displaytype                  'is the persistance display of lines or points,
or none?
Dim horizch, horizsign, vertch, vertsign  'channel # and sign of the data
Const v_per_g = 1.875            'number of pixels wide 1 g corresponds to
Dim dispx, dispy, dispz          'filtered values to be displayed
Dim acq_type, stdev_type, filt_type 'select if you filter the data saved or
stdev calculated
Dim xcal, ycal, zcal             'calibration gains for the three channels
Const stdev_length = 5000        'number of stdev points storing
Dim stdevx(stdev_length), stdevy(stdev_length), stdevz(stdev_length)  'standard
deviation data for the axes before printing
Dim filtlength, filt(max_filtlength), filter_divisor 'filter parameters
Dim max_turnover, turnover_count   'how often the filter output goes on to be
displayed

Private Sub acq_button_Click()
    If acq_button.Caption = "Acquire" Then      'if not acquiring yet
        acq_button.Caption = "Start"            'to start acq next click
        savedialog.ShowSave                     'open the save as window
        Open savedialog.FileName For Output As #1   'get the file
        Write #1, Date, Time                    'line 1: the date and time of
acquisition
        Write #1, savedialog.FileName           'line2: the name of the data
file
        Write #1, fileinfo_txt.Text             'line 3: any additional text
description
        Write #1, "sensitivity", xcal, ycal, zcal   'calibrations for
sensitivity
        Write #1, "time", "chA", "chB", "chC"   'line 4: header for column
titles!
    ElseIf acq_button.Caption = "Start" Then    'start the acquisition!
        acq_button.Caption = "Stop Acq."
        acq = True                              'activate acquisition
    Else
        acq_button.Caption = "Acquire"          'otherwise stop the acquisition
        acq = False                             'stop acquisition
        Close #1                                'close the data file
    End If
End Sub

Private Sub save_config()
```

```
    Open config_filename For Output As #2
    Write #2, "sensitivity", xcal, ycal, zcal    'calibration data
    Write #2, "acquisition", acq_type            'type of acquisition
    Write #2, "stdev", stdev_type                'stdev type
    Write #2, "filter", filt_type, filtlength    'filter type and length
    Write #2, "turnover", max_turnover           'number of pts. to turnover
    Write #2, "display", displaytype             'persistance displaying
    Write #2, "magnification", gain              'screen gain
    Write #2, "horiz", horizch, horizsign        'horizontal display
    Write #2, "vert", vertch, vertsign           'vertical display
    Close #2
Debug.Print "updated the configuration!"
End Sub

Private Sub open_config()                        'open up the older
configuration setting
    Open config_filename For Append As #4        'relevent for a new file:
open/create temporarily...
    Close #4                                     'close that new file
    Open config_filename For Input As #3         'open up the file
    If EOF(3) Then                               'if already end then a new
file!
        Close #3                                 'close it
        displaytype = "none"                     'initial display parameters
        horizch = "A"                            'display ch A on horiz
        vertch = "C"                             'display ch C on vert
        filt_type = "hanning"                    'filter type
        acq_filtered_option_Click                'acq type update
        stdev_filtered_option_Click              'stdev type update
        filt_length_scroll.Max = max_filtlength 'filter length
        filt_length_scroll_Change                'update filter length display
        turnover_scroll_Change                   'update the turnover counter
        gainscroll_Change                        'get the default gain values
        horizsign = 1                            'both signs positive
        vertsign = 1
        x_cal_text_Change                        'update calibration displays
        y_cal_text_Change
        z_cal_text_Change
        Debug.Print "new configuration file!"
    Else                                         'the already established
config...
        Input #3, txt, xcal, ycal, zcal          'calibration data
        Input #3, txt, acq_type                  'type of acquisition
        Input #3, txt, stdev_type                'stdev type
        Input #3, txt, filt_type, filtlength     'filter type
        Input #3, txt, max_turnover_temp         'number of pts. to turnover
        Input #3, txt, displaytype               'display type
        Input #3, txt, gain                      'display gain
        Input #3, txt, horizch, horizsign        'horiz display
        Input #3, txt, vertch, vertsign          'vert type
        Close #3                                 'close the config file
        Debug.Print "old configuration file!"
        x_cal_text.Text = xcal                   'update the senstivity
calibration displays...
        y_cal_text.Text = ycal
        z_cal_text.Text = zcal
        Select Case acq_type                     'update the acq type
            Case "filtered"
                acq_filtered_option.Value = True
            Case "raw"
                acq_raw_option.Value = True
            End Select
        Select Case stdev_type                   'update the stdev type
```

```
            Case "filtered"
                stdev_filtered_option.Value = True
            Case "raw"
                stdev_raw_option.Value = True
            Case "none"
                stdev_none_option.Value = True
            Case "intermittent"
                stdev_intermittent_option.Value = True
            End Select
        Select Case filt_type                   'update the filter type
            Case "rectangular"
                filt_rectangular_option.Value = True
            Case "hanning"
                filt_hanning_option.Value = True
            End Select
        filt_length_scroll.Value = filtlength   'update the filter length
        turnover_scroll.Value = max_turnover_temp    'update the turnover
counter
        Select Case displaytype                 'update the display type
            Case "points"
                disp_points_option.Value = True
            Case "lines"
                disp_lines_option.Value = True
            Case "none"
                disp_none_option.Value = True
            End Select
        gainscroll.Value = gain * 10            'update the gain
        Select Case horizch                     'update horiz ch selection
            Case "A"
                horizA_opt.Value = True
            Case "B"
                horizB_opt.Value = True
            Case "C"
                horizC_opt.Value = True
            End Select
        Select Case vertch                      'update the vert ch selection
            Case "A"
                vertA_opt.Value = True
            Case "B"
                vertB_opt.Value = True
            Case "C"
                vertC_opt.Value = True
            End Select
        If horizsign = -1 Then horiz_neg_check.Value = 1    'update pos/neg
selection...
        If vertsign = -1 Then vert_neg_check.Value = 1
    End If
End Sub

Private Sub writedata()                         'record each data point
    If acq Then                                 'if we are recording
        Select Case acq_type                    'what type of data saving?
            Case "filtered"                     'write time, filtered data into
file
                Write #1, Timer, dispx, dispy, dispz
            Case "raw"                          'write raw data (all the time)
                Write #1, Timer, dataset(2), dataset(4), dataset(6)
            End Select
    End If
End Sub

Private Sub disp_points_option_Click()  'persistance display points!
    displaytype = "points"
```

```
    save_config                          'save the new configuration to file
End Sub

Private Sub disp_lines_option_Click()    'persistance display lines!
    displaytype = "lines"
    save_config
End Sub

Private Sub disp_none_option_Click()     'no persistance display!
    displaytype = "none"
    save_config
End Sub

Private Sub acq_filtered_option_Click() 'filtered data acquisition
    acq_type = "filtered"
    save_config
End Sub

Private Sub acq_raw_option_Click()       'raw data acquisition
    acq_type = "raw"
    save_config
End Sub

Private Sub filt_hanning_option_Click() 'filter type: hanning
    filt_type = "hanning"
    update_filter                        'update the filter vector
End Sub

Private Sub filt_length_scroll_Change() 'update filter length
    filtlength = filt_length_scroll.Value
    filt_length_disp.Caption = filtlength
    turnover_scroll.Max = filtlength
    update_filter
End Sub

Private Sub filt_rectangular_option_Click() 'filter type: rectangular
    filt_type = "rectangular"
    update_filter
End Sub

Private Function update_filter()            'make a new filter vector
    Select Case filt_type                   'for convolution...
        Case "rectangular"          'rectangular
            For i = 0 To filtlength - 1 'vector filtlength pts long of 1s
                filt(i) = 1
                Next
            For i = filtlength To max_filtlength    'all the rest are zeros
                filt(i) = 0
                Next
        Case "hanning"              'hanning filter...
            Const pi = 3.14159265
            For i = 0 To filtlength - 1 'make the cos function for the 1st
filtlength pts
                filt(i) = 0.5 - 0.5 * Cos(2 * pi * i / (filtlength + 1))
                Next
            For i = filtlength To max_filtlength        'zeros for the rest of
the points
                filt(i) = 0
                Next
    End Select
    filt_sum = 0                'reset filter integral
    For i = 0 To max_filtlength     'integrate the filter vector
        filt_sum = filt(i) + filt_sum
```

```
        Next
    filter_divisor = filt_sum       'the divisor is the integral of the
vector...
    save_config                     'save new filter configuration
End Function

Private Sub gainscroll_Change() 'selector for the gain control
    gain = gainscroll.Value / 10    'divides by 10; range 0 - 100
    gainlabel.Caption = gain        'update display of the gain...
    save_config
End Sub

Private Sub stdev_filtered_option_Click()       'stdev filtered data
    stdev_type = "filtered"
    save_config
End Sub

Private Sub stdev_none_option_Click()           'no stdev calculation
    stdev_type = "none"
    save_config
End Sub

Private Sub stdev_intermittent_option_Click()   'stdev intermittant data
    stdev_type = "intermittent"
    save_config
End Sub

Private Sub stdev_raw_option_Click()            'stdev of raw data
    stdev_type = "raw"
    save_config
End Sub

Private Sub turnover_scroll_Change()            'the turnover rate of the
filter...
    max_turnover = turnover_scroll.Value        'get the new max turnover value
    turnover_label.Caption = max_turnover       'update the display
    save_config
End Sub

Private Sub horiz_neg_check_Click() 'selector for the sign of horiz display
    If horiz_neg_check.Value Then   'if selected then negative
        horizsign = -1              'set the sign negative
    Else: horizsign = 1             'else positive
    End If
    save_config
End Sub

Private Sub vert_neg_check_Click()  'repeat sign selector for vert display
    If vert_neg_check.Value Then
        vertsign = -1
    Else: vertsign = 1
    End If
    save_config
End Sub

'these are the selectors for the channels to be displayed.
Private Sub horizA_opt_Click()
    horizch = "A"
    save_config
End Sub

Private Sub horizB_opt_Click()
    horizch = "B"
```

```
    save_config
End Sub

Private Sub horizC_opt_Click()
    horizch = "C"
    save_config
End Sub

Private Sub vertA_opt_Click()
    vertch = "A"
    save_config
End Sub

Private Sub vertB_opt_Click()
    vertch = "B"
    save_config
End Sub

Private Sub vertC_opt_Click()
    vertch = "C"
    save_config
End Sub

Private Sub pausebuttn_Click()
    paused = Not (paused)       'flip between paused & not paused
End Sub

Private Sub quitbuttn_Click()
    End                         'ends the program when clicked!
End Sub

Private Sub x_cal_text_Change()     'change the calibration gains
    xcal = x_cal_text.Text          'set the gain to the new value
    If xcal = "" Then xcal = 1      'make sure nonzero just for safety...
    save_config
End Sub

Private Sub y_cal_text_Change()     'calibrate y gain
    ycal = y_cal_text.Text
    If ycal = "" Then ycal = 1
    save_config
End Sub

Private Sub z_cal_text_Change()     'calibrate z gain
    zcal = z_cal_text.Text
    If zcal = "" Then zcal = 1
    save_config
End Sub

Private Sub Form_Load()
    initializeprog                      'initialize the program
    Do                                  'here's the main loop: repeat forever!
        data_avail = check_fifo(False)  'scan the full / empty status
        If data_avail Then
            datacount = datacount + 1   'got another datapt!
            get_output                  'receive data
            End If
        delay                           'delay if appropriate
        Loop
End Sub

Private Function initializeprog()   'initialize program parameters
    open_config                     'open saved configurations
```

```
    fifoadc1.Show                   'show the form
    paused = False                  'starts off running
    datacount = 0                   'start datacount at zero
    delaycounter = 0                'reset delay counter
    prevtime = Timer                'get current time for spspc calcs
    filtcount = 0                   'initialize filter
    turnover_count = 0              'initialize filter turnover
    storecount = 0                  'initialize data stored length
    xmax = ch1plot.Width            'get the parameters for the window
    ymax = ch1plot.Height
    xmid = xmax / 2
    ymid = ymax / 2
    For i = 0 To storelength        'reset the display persistance for the
display middle...
        lastx(i) = xmid
        lasty(i) = ymid
        lastz(i) = xmid
        Next
    initialize_stdev                'initialize stdev calculations...
End Function

Private Function delay()
    If (Timer - prevtime) > deferral_delay Then
        garbage = check_fifo(True)  'check the fifo and display flags, don't
use output
        display_stats               'spspc and stdev statistics
        DoEvents                    'defer to delay
        pause                       'pause if necessary
        End If
End Function

Private Function display_stats()
    spspc_calc                      'run spspc calculation
    x_stdev_disp.Caption = Format(stdev_calc(stdevx), "###0.0")  'display stdev
calcs
    y_stdev_disp.Caption = Format(stdev_calc(stdevy), "###0.0")  'x, y, and z
axes
    z_stdev_disp.Caption = Format(stdev_calc(stdevz), "###0.0")
    initialize_stdev                'initialize the stdev calculations again
End Function

Function initialize_stdev()
    stdev_count = 0             'set the stdev count back to zero
End Function

Function stdev_calc(input_vector) As Single     'outputs stdev for a set of
data scaled to mg's (1000 times!)
    If stdev_count = 0 Then stdev_count = 1     'avoid dividing by zero farther
down
    Select Case stdev_type
        Case "filtered"                         'filtered data: need stdev
calculation!
            mean = 0
            stdev_sum = 0
            For i = 0 To stdev_count - 1        'first calculate the mean value
                mean = input_vector(i) + mean
                Next
            i_count = stdev_count               'total number of pts = stdev
count
            mean = mean / i_count               'mean = sum / count
            For i = 0 To stdev_count - 1        'do the stdev calc. for each pt
                stdev_sum = stdev_sum + ((input_vector(i) - mean) ^ 2)
                Next
```

```
            stdev_calc = gscale((stdev_sum / i_count) ^ 0.5)     'final stdev
calculation
        Case "intermittent"                         'intermittent data: need to
average it out!
            mean = 0
            For i = 0 To stdev_count - 1            'first calculate the mean value
                mean = input_vector(i) + mean
                Next
            i_count = stdev_count                   'total number of pts = stdev
count
            mean = mean / i_count                   'mean = sum / count
            stdev_calc = gscale(mean)               'final stdev calculation
        Case "raw"                                  'case for raw data: calculate
stdevs
            mean = 0
            stdev_sum = 0
            For i = 0 To stdev_count - 1            'first calculate the mean
                mean = input_vector(i) + mean
                Next
            i_count = stdev_count                   'the total count = stdev count
            mean = mean / i_count                   'finish mean calculation
            For i = 0 To stdev_count - 1            'calculate the stdev for each
point
                stdev_sum = stdev_sum + ((input_vector(i) - mean) ^ 2)
                Next
            stdev_calc = gscale((stdev_sum / i_count) ^ 0.5)     'the final
stdev calculation
        End Select
End Function

Function gscale(datain) As Single   'input: g's
    gscale = datain * 1000          'output: mg's
End Function

Private Function spspc_calc()
    deltatime = Timer - prevtime            'calculate time elapsed
    prevtime = Timer                        'reset the previous time
    If deltatime = 0 Then deltatime = -1    'avoid divide by 0 errors
    spspc = datacount / (deltatime * 8)     '8 bytes per cycle...
    spspc_output_label.Caption = Format(spspc, "###")   'display spspc
    cutoff_freq spspc                       'display cutoff_freq
    datacount = 0                           'reset the datacounter
End Function

Private Function cutoff_freq(F)     'calculate the cutoff frequency
    Select Case filt_type           'calculation dependent on the filter type
        Case "rectangular"
            multiplier = 1
        Case "hanning"
            multiplier = 2
        End Select
    deltaF = (multiplier / filtlength) * F      'the cutoff freq calculation
    filt_cutoff_freq.Caption = Format(deltaF, "###")        'display the result
End Function

Private Function pause()
    Do While paused                 'if paused
        garbage = check_fifo(True)  'check and display the fifo while paused,
don't use output
        prevtime = Timer            'correct time for spspc calculation
        DoEvents                    'pass the buck endlessly
        Loop
End Function
```

```
Function check_fifo(display_flags As Boolean) As Boolean
    Dim fifo_status As Integer
    '0: empty, 1: almost empty, 2: less than half, 3: more than half, 4: almost
full, 5: full
    Flags = StatusPortRead(PortAddress) 'get the current flags from the fifo
    f3 = (Flags And &H8) <> 0           'extract the 4 flags (only f3-f6 are
needed...)
    f4 = (Flags And &H10) <> 0          'flag3: aef; flag4: ff; flag5: hf;
flag6: ef
    f5 = (Flags And &H20) <> 0
    f6 = (Flags And &H40) <> 0
    fifo_status = 9
    If (f4 And Not (f3) And f5 And Not (f6)) Then   'figure out what the fifo
status is
        fifo_status = 0 'empty!
        ElseIf (f4 And Not (f3) And f5 And f6) Then fifo_status = 1
        ElseIf (f4 And f3 And f5 And f6) Then fifo_status = 2
        ElseIf (f4 And f3 And Not (f5) And f6) Then fifo_status = 3
        ElseIf (f4 And Not (f3) And Not (f5) And f6) Then fifo_status = 4
        ElseIf (Not (f4) And Not (f3) And Not (f5) And f6) Then fifo_status = 5
        End If
    If display_flags Then flag_operation fifo_status      'display the fifo
status...
    If fifo_status = 0 Then     'if not empty, then indicate data available
        check_fifo = False      'it's empty-- don't get data
        Else
        check_fifo = True       'it's not empty-- get the data
        End If
    If fifo_status = 9 Then Debug.Print "flag error: invalid fifo flags!"
End Function

Private Function flag_operation(flag As Integer)
    Select Case flag                'depending on the state of the fifo
        Case 0                      'indicate which flag is correct
            fifo_empty_option.Value = True
            DoEvents                'might as well delay if empty...
        Case 1
            fifo_almostempty_option.Value = True
        Case 2
            fifo_lessthanhalf_option.Value = True
        Case 3
            fifo_morethanhalf_option.Value = True
        Case 4
            fifo_almostfull_option.Value = True
        Case 5
            fifo_full_option.Value = True
        End Select
End Function

Function get_output()   'need to make sure the port is input here! &H20
    Dim converted As Integer
    Dim validch As Boolean
    ControlPortWrite PortAddress, &H23      'hit the read line
    ControlPortWrite PortAddress, &H22      'set it low again
    fifobyte = DataPortRead(PortAddress)    'recover the data
    converted = byteswap(fifobyte)          'swap msb to lsb in each byte
    validch = channelprog(converted)        'get channel info on data
    If validch Then process (converted)     'work with good data
    prevbyte = converted                    'save the new previous byte
End Function

Function byteswap(c) As Integer
```

```
'swaps the msbit for the lsb for all bits in a byte
    Dim b(8) As Boolean  'bits in
    Dim e As Integer     'final result out
    b(0) = (c And &H1) <> 0     'determine which bits are going in
    b(1) = (c And &H2) <> 0
    b(2) = (c And &H4) <> 0
    b(3) = (c And &H8) <> 0
    b(4) = (c And &H10) <> 0
    b(5) = (c And &H20) <> 0
    b(6) = (c And &H40) <> 0
    b(7) = (c And &H80) <> 0
    e = b(7) * &H1          'swap the bits & reconstruct the output
    e = e + b(6) * &H2
    e = e + b(5) * &H4
    e = e + b(4) * &H8
    e = e + b(3) * &H10
    e = e + b(2) * &H20
    e = e + b(1) * &H40
    e = e + b(0) * &H80
    byteswap = -1 * e       'multiply by negative 1 for some reason...?
End Function

Private Function channelprog(newdata) As Boolean
'channels of interest:  channel 0: always high (parsing channel)
'                       channel 2: channel A
'                       channel 4: channel B
'                       channel 6: channel C
    Dim validchannel As Boolean
    validchannel = False
    If ((newdata = 255) And (prevbyte = 255)) Then 'if both high,
        channel = 0                                 'it must be channel 0!
        validchannel = True
    ElseIf channel > 7 Then                 'don't let go beyond channel 8
        channel = 8
    Else
        channel = channel + 1               'otherwise just increment channel #
by 1
        If ((channel Mod 2) = 0) Then validchannel = True   'if an even channel
then ready to combine bytes
    End If
    channelprog = validchannel      'return true if the channel is complete
End Function

Function process(newdata As Integer)        'general data processing subroutine
    fulldata = combined(newdata)            'get the msb + lsb calculation
    completeset = fullset(fulldata)         'the prog to organize into arrays
    If completeset Then                     'if all three channels present
        displayit = filter                  'filter the data, see if ready to
display
        If acq_type = "raw" Then writedata  'save data if raw acq. data
        If displayit Then                   'if ready to display...
            If acq_type = "filtered" Then writedata 'write the data if
necessary
            threedplot                      'display the data
            End If
        End If
End Function

Function combined(converted As Integer) As Double   'recover the 16 total bits;
output range 0 to 256
    present = converted / 256       'divide the lsb by 256
    past = prevbyte                 'get the msb: previous byte
    combined = present + past       'the total data: msb + lsb
```

```
End Function

Function fullset(datain) As Boolean              'datain range: 0 to 256
    temp = ((datain - 128) / 256)                'range to +/- 0.5
    dataset(channel) = 2 * temp * 20 / v_per_g 'scale to +/- 5g output range
    If channel = 6 Then                          'if channel C is completed,
then...
        fullset = True                           'ready to display!
    Else                                         'not ready yet so...
        fullset = False                          'don't display
    End If
End Function

Private Function filter() As Boolean
    filtx(filtcount) = dataset(2) * xcal         'store the newest data points
    filty(filtcount) = dataset(4) * ycal         'in the vectors for all three
channels
    filtz(filtcount) = dataset(6) * zcal
    filtcount = filtcount + 1                    'increase filter count by 1
    turnover_count = turnover_count + 1          'increase turnover count by 1
    If filtcount > filtlength - 1 Then filtcount = 0    'if the filter is full,
ready to start over
    If turnover_count > max_turnover - 1 Then           'if time to filter the
data...
        turnover_count = 0                       'reset the turnover counter
        sumx = 0                                 'initialize the summations
        sumy = 0
        sumz = 0
        For i = 0 To filtlength - 1              'do the convolution w/ each
dataset
            sumx = filtx((filtlength + filtcount - 1 - i) Mod filtlength) *
filt(i) + sumx
            sumy = filty((filtlength + filtcount - 1 - i) Mod filtlength) *
filt(i) + sumy
            sumz = filtz((filtlength + filtcount - 1 - i) Mod filtlength) *
filt(i) + sumz
            Next
        dispx = sumx / filter_divisor            'divide by the integral of each
filter to avoid scaling
        dispy = sumy / filter_divisor
        dispz = sumz / filter_divisor
        filter = True                            'ready to keep going with
display
    Else: filter = False                         'need to repeat for more data
    End If
    Select Case stdev_type                       'do the standard deviation
calculations
        Case "intermittent"     'average of many stdevs for each filter length
            If filter Then
                stdevx(stdev_count) = stdev_inst(filtx, dispx)  'get the stdev
for this
                stdevy(stdev_count) = stdev_inst(filty, dispy)  'point given
the dataset and
                stdevz(stdev_count) = stdev_inst(filtz, dispz)  'the mean
already calculated
                stdev_count = stdev_count + 1                   'go on to next
stdev point
                End If
        Case "filtered"         'get just the most recent filter output
            If filter Then
                stdevx(stdev_count) = dispx                     'take the
filtered data
```

```
                stdevy(stdev_count) = dispy                         'for each of
the channels
                stdevz(stdev_count) = dispz
                stdev_count = stdev_count + 1                       'go on to next
stdev point
                End If
        Case "raw"              'get the newest raw data
            For i = 0 To max_turnover - 1
                stdevx(stdev_count) = filtx((filtlength + filtcount - 1 - i)
Mod filtlength)         'take the raw data
                stdevy(stdev_count) = filty((filtlength + filtcount - 1 - i)
Mod filtlength)         'for all three chs
                stdevz(stdev_count) = filtz((filtlength + filtcount - 1 - i)
Mod filtlength)         'of that just obtained
                stdev_count = stdev_count + 1                       'go on to next
stdev point
                Next
        End Select
End Function

Function stdev_inst(vector, mean)           'brief stdev calculation given data
and mean
    For i = 0 To filtlength - 1             'for all of the points from the
data...
        stdev_inst = ((vector(i) - mean) ^ 2) + stdev_sum   'calculate the
stdev
        Next
    stdev_inst = (stdev_inst / filtlength) ^ 0.5  'sqrt of (sum / length)
End Function

Private Function threedplot()
    ch1plot.Cls                         'clear the screen
    lastx(storecount) = scaler(dispx)  'get the next data to be displayed
    lasty(storecount) = scaler(dispy)
    lastz(storecount) = scaler(dispz)
    Select Case horizch     'select the data for horiz display
        Case "A"
            horizdata = lastx
        Case "B"
            horizdata = lasty
        Case "C"
            horizdata = lastz
        End Select
    Select Case vertch      'select the data for vertical display
        Case "A"
            vertdata = lastx
        Case "B"
            vertdata = lasty
        Case "C"
            vertdata = lastz
        End Select
    If horizsign = -1 Then  'if want to negate, negate them!
        For i = 0 To storelength
            horizdata(i) = ymax - horizdata(i)
            Next
        End If
    If vertsign = -1 Then
        For i = 0 To storelength
            vertdata(i) = ymax - vertdata(i)
            Next
        End If
    If displaytype = "lines" Then               'if lines to be displayed,
display the lines
```

```
        For i = 0 To storelength
            coloration = 255 * 0.75 * (((storelength + storecount - i) Mod
storelength) / storelength) 'gets darker as i goes to storelength!
            ch1plot.Line (xmid, ymid)-(horizdata(i), vertdata(i)),
RGB(coloration, coloration, coloration)  'display the lines
            Next
    ElseIf displaytype = "points" Then
        For i = 0 To storelength - 1    'display points up until the line...
            coloration = 255 * 0.75 * (((storelength + storecount - i) Mod
storelength) / storelength) 'gets darker as i goes to storelength!
            ch1plot.PSet (horizdata(i), vertdata(i)), RGB(coloration,
coloration, coloration)  'display the points
            Next
        ch1plot.Line (xmid, ymid)-(horizdata(storecount),
vertdata(storecount)), RGB(0, 0, 0)    'the line
    Else    'case where no persistance display
        ch1plot.Line (xmid, ymid)-(horizdata(storecount),
vertdata(storecount)), RGB(0, 0, 0)    'the line
    End If
    ch1plot.Circle (xmid, ymid), gain * ymax * v_per_g / 20, RGB(200, 200, 200)
    storecount = storecount + 1     'update counter to next storage element
    If storecount > storelength Then storecount = 0 'if exceed max amount,
reset counter!
End Function

Function scaler(datain) As Double  'datain ranges from +/- 5g
    convert_to_screen = datain * v_per_g / 20         'range to +/-.5
    scaler = (gain * (ymax) * convert_to_screen) + (ymax / 2)   'range ymax/2
+/- ymax*gain/2
End Function
```

References

[1] Lee JD, Lee H, et.al; A monolithic thermal inkjet printhead utilizing electrochemical etching and two-step electroplating techniques; 1995 IEEE Electron Devices Meeting: 601-4

[2] Clark SK, Wise KD; Pressure sensitivity in anisotropically etched thin-diaphragm pressure sensors; IEEE Trans Electron Devices 1979;ED-26(12):1887-96

[3] Lemkin MA, Boser BE, Auslander D, Smith JH; A 3-axis force balanced accelerometer using a single proof-mass; IEEE Transducers '97, June 1997 Chicago

[4] Brosnihan TJ, Pisano AP, Howe RT; Surface micromachined angular accelerometer with force feedback; Digest ASME Int Conf and Exp, Nov 1995

[5] Shajii J, Ng K, Schmidt MA; A microfabricated floating-element shear stress sensor using wafer-bonding technology; J Microelectromech Syst 1992;1(2):89-94

[6] Vig JR, Filler RL, Kim Y; Chemical sensor based on quartz microresonators; J Microelectromech Syst 1996;5(2):138-40

[7] Gretillat F, Gretillat M, de Rooij NF; Improved design of a silicon micromachined gyroscope with piezoresistive detection and electromagnetic excitation; IEEE J Microelectromech Syst 1999;8(3):243-50

[8] Goodenough F; Airbags boom when IC accelerometer see 50 g; Electronic Design Aug 8, 1991:45-56,

[9] Two mass-produced MEMS accelerometers are the ADI ADXL105, and the Motorola MMA2200.

[10] One inertial guidance unit is the Honeywell Miniature Inertial Measurement Unit (MIMU), datasheet at http://content.honeywell.com/space/Productsheets/mimu.pdf (also Ash [11,12])

[11] Nishizawa, M, et.al; Development of silicon capacitive accelerometer for subsurface microseismic measurement; Geophysical Exploration; 1998;51(2):174-5

[12] Martin R., Pike W., Silicon micromachined accelerometer/seismometer, NASA TechBriefs, Nov 98 http://www.nasatech.com/Briefs//Nov98/NPO19875.html

[13] Lemaire, C. Direct and Indirect Out-of-Balance Detection for Future Generation Washing Machines, presented at 1999 Appliance Manufacturer Conference & Expo, Sept 27-29. http://www.analog.com/publications/whitepapers/products/dir_indir/

[14] Stiles RN, Randall JE; Mechanical factors in human tremor frequency; J Appl Physiol 1967;23(3):324-30

[15] International Tremor Foundation website; http://www.essentialtremor.org/

[16] Boose A; http://www.uni-tuebingen.de/uni/kha/tremor/tremor.htm

[17] Website specifically concerning pediatric tremors: http://www.icondata.com/health/pedbase/files/ESSENTIA.HTM

[18] Gross TS, Nelson RC; The shock attenuation role of the ankle during landing from a vertical jump; Med Sci Sports Exerc 1988;20(5):506-14

[19] Randall JE, Stiles RN; Power spectral analysis of finger acceleration tremor; J Appl Physiol 1964;19:357-60

[20] Wade P, Gresty MA, Findley LJ; A normative study of postural tremor of the hand; Arch Neurol 1982;39:358-62

[21] International Tremor Foundation website; http://www.essentialtremor.org/

[22] Worldwide Education and Awareness for Movement Disorders website on Parkinsons Disease: http://www.wemove.org/par_faq.html

[23] Worldwide Education and Awareness for Movement Disorders website on Essential Tremor: http://www.wemove.org/et_he.html

[24] Viby-Mogensen J, Jensen E, Werner M, Nielsen HK; Measurement of acceleration: a new method of monitoring neuromuscular function; Acta Anaesthesiol Scand 1988;32(1):45-8

[25] Lippold OC, Williams EJ, Wilson CG; Finger tremor and cigarette smoking; Br J Clin Pharmacol 1980; 10(1):83-6

[26] Warrad HJ, et.al.; The influence of fasting and of caffeine intake on finger tremor; Eur J Clin Pharmacol 1985;29(1):37-43

[27] Koller W, Cone S, Herbster G; Caffeine and tremor; Neurology 1987;37(1):169-72

[28] Humayun MU, et.al; Quantitative measurement of the effects of caffeine and propranolol on surgeon hand tremor; Arch Ophthalmol 1997;115(3):371-4

[29] Bauer, LO; Motoric signs of CNS dysfunction associated with alcohol and cocaine withdrawal; Psychiatry Res 1993; 47(1):69-77

[30] Lotvall J, Lunde H, Svedmyr N; Onset of bronchodilation and finger tremor induced by salmeterol and salbutamol in asthmatic patients; Can Respir J 1998;5(3):191-4
[31] Koller WC; Propranolol therapy for essential tremor of the head; Neurology 1984;34(8):1077-9
[32] Koller WC, Royse VL; Time course of a single oral dose of propranolol in essential tremor; Neurology 1985;35(10):1494-8
[33] Pozos RS, Iaizzo PA; Effects of topical anesthesia on essential tremor; Electromyogr Clin Neurophysiol 1992;32(7-8):369-72
[34] Itsy website: http://www.research.digital.com/wrl/projects/Itsy/index.html. Direct technical access with my personal url: http://crl.research.compaq.com/downloads/download.cgi/bbgraham@mit.edu/Itsy/
[35] ADXL202 datasheet available at: http://products.analog.com/products/info.asp?product=ADXL202
[36] Method is called "Rock 'n' Scroll"; the website is: http://www.research.digital.com/wrl/projects/RocknScroll/RocknScrollOverview.htm
[37] SmartQuill webpage: http://www.bt.com/innovation/exhibition/smartquill/index.htm
[38] ADI accelerometer application note: http://www.analog.com/iMEMS/markets/consumer/Joymfsto.html
[39] Brosnihan TJ, Pisano AP, Howe RT; Surface micromachined angular accelerometer with force feedback; Digest ASME Int Conf and Exp, Nov 1995
[40] Endevco Piezoelectric Accelerometer Instruction Manual; 1979
[41] Figure redrawn from http://www-ccrma.stanford.edu/CCRMA/Courses/252/sensors/img4.gif
[42] Weinberg MS; Working equations for piezoelectric actuators and sensors; J Microelectromech Syst; 1999;8(4):529-533
[43] Kourepenis A; Petrovich A; Meinberg M; Development of a monolithic quartz resonator accelerometer; Proc 14th Biennial Guidance Test Symp, Hollman AFB, NM, Oct 2-4, 1989
[44] Figure from http://www-ccrma.stanford.edu/CCRMA/Courses/252/sensors/img8.gif
[45] PCB Piezotronics 352C67 datasheet available at http://www.pcb.com/products/svs/svs352c67.html
[46] Endevco 7265A-HS datasheet available at http://www.endevco.com/pdf_originals/section1_123/7265a_hs.pdf
[47] ADXL105 datasheet available at http://products.analog.com/products/info.asp?product=ADXL105
[48] Figure redrawn from: Introduction to Piezoelectric Accelerometers, PCB Piezotronics tech support; http://www.pcb.com/tech_accel.html
[49] Figure redrawn from: Link B, Suminto J, Young M; A rugged, high performance piezoresistive accelerometer; Sensors 1991;8(11)
[50] Figure redrawn from: Doscher J; Accelerometer design and applications; http://www.analog.com/industry/iMEMS/library/Sensor971.pdf
[51] Analog Devices iMEMS website: http://www.analog.com/industry/iMEMS/
[52] Figure from: Lemaire C; New generation of micromachined accelerometers and DSP offer low cost alternative to machine condition monitoring; http://www.analog.com/industry/iMEMS/markets/industrial/machine_condition.html
[53] Figure from: Doscher J; Using iMEMS accelerometers in instrumentation applications; http://www.analog.com/industry/iMEMS/library/imems_accl.html
[54] Lemkin M, Boser BE; A three-axis micromachined accelerometer with a CMOS position-sense interface and digital offset-trim electronics; IEEE J Solid-State Circuits 1999;34(4):456-68
[55] Lemkin MA, Boser BE, Auslander D, Smith JH; A 3-axis force balanced accelerometer using a single proof-mass; IEEE Transducers '97, June 1997 Chicago
[56] Figure from: Lemaire, C. Direct and indirect out-of-balance detection for future generation washing machines; presented at 1999 Appliance Manufacturer Conference & Expo, Sept 27-29. http://www.analog.com/publications/whitepapers/products/dir_indir/
[57] Figure from: http://www-mtl.mit.edu/mtlhome/6Res/src99/003-Fig2.gif
[58] Photo on left from: Yung C; A process technology for realizing integrated inertial sensors using deep reactive ion etching (DRIE) and aligned wafer bonding; MS Thesis, MIT EECS; June 1999
[59] Photo on right from: http://www-mtl.mit.edu/mtlhome/6Res/src99/003-Fig2.gif
[60] Figure from: Yung C; A process technology for realizing integrated inertial sensors using deep reactive ion etching (DRIE) and aligned wafer bonding; MS Thesis, MIT EECS; June 1999
[61] Senturia S; MIT course notes from 6.971: Microelectromechanical Systems. Lecture notes 10/8/97, pg4

[62] For a detailed description of the fabrication process, refer to Chapter 2 of Yung C; A process technology for realizing integrated inertial sensors using deep reactive ion etching (DRIE) and aligned wafer bonding; MS Thesis, MIT EECS; June 1999

[63] Courtesy of C Yung.

[64] Yung C; A process technology for realizing integrated inertial sensors using deep reactive ion etching (DRIE) and aligned wafer bonding; MS Thesis, MIT EECS; June 1999, p15-6

[65] A VHS video was recorded showing the process of testing at the probe station and several examples of what was seen during testing. This video was submitted with the thesis, and is entitled: Supplemental Video: Quality Control Testing.

[66] Ishihara K, Yung C, Ayon A, Schmidt M; Inertial sensor technology using DRIE and wafer bonding with Interconnecting Capability; J Microelectromech Syst; 1999;8(4):403-8.

[67] Epoxy Technology webpage: http://www.epotek.com/

[68] Kulicke and Soffa Industries, Inc. website: http://www.kns.com/

[69] American fine wire (334-875-4040, http://www.knsafw.com/), AW8 alloy: gold with 20 ppm silver, 5-8 ppm beryllium, 1-5 ppm calcium. Tensile strength: 9 grams minimum; Elongation 3-5%. 0.001" dia.

[70] Harman GG; Wire bonding-towards 6- sigma yield and fine pitch; IEEE Trans Comp, Hybrids, Manuf Technol; 1992;15(6):1005-12

[71] Khoury SL, Burkhard DJ, et.al; A comparison of copper and gold wire bonding on integrated circuit devices; proc Electronic Components and Technology Conference; 1990;1:768-76

[72] Magill PA, Baggs JW; CSP present and future; Proc Intl Symp Advanced Packaging Materials: Processes, Properties and Interfaces; 1999:218-20

[73] Photo from: http://www-mtl.mit.edu/CAFE/pic/wirebonder_icl.jpg

[74] The units for the settings on the gold ball bonding machine are relative: no documentation on the actual bonding parameters is included in the manual.

[75] Maximum integral linearity error (MILE) is the maximum deviation in g's at any acceleration between ± 5 g from a straight line drawn between the LVDT signal conditioner outputs at ± 5 g. Also discussed in Section 3e.

[76] OPA2137 datasheet available at http://www.burr-brown.com/WebObjects/BurrBrown/download/DataSheets/OPA137.pdf

[77] AD598 datasheet available at http://www.analog.com/pdf/ad598.pdf

[78] Lancaster D; Lancaster's active filter cookbook; Butterworth-Heinemann publisher (2nd edition—1996--currently available)

[79] LF353M datasheet available at http://www.national.com/pf/LF/LF353.html

[80] AD974 datasheet available at http://www.analog.com/pdf/AD974_a.pdf

[81] 74LS244 datasheet available at: http://www.fairchildsemi.com/pf/DM/DM74LS244.html

[82] IDT72142L50P datasheet available at: http://www.idt.com/products/pages/FIFO-72142.html

[83] LM555 datasheet available at: http://www.national.com/pf/LM/LM555.html

[84] 74LS161 datasheet available at: http://www.fairchildsemi.com/pf/DM/DM74LS161A.html

[85] 74HC04 datasheet available at: http://www.fairchildsemi.com/pf/MM/MM74HC04.html

[86] More information on Visual Basic is available at: http://msdn.microsoft.com/vbasic/

[87] Alberta Printed Circuits' webpage: http://www.apcircuits.com/

[88] Specifications of the Keithley 2000 DMM are available at: http://www.keithley.com/products/prod_pages/inst_lvl3_pages/summary_pgs/2000_dmm_summary.html

[89] Ling Dynamic Systems website: http://www.lds-usa.com/

[90] Brüel & Kjær website: http://www.bkhome.com/
B&K piezoelectric (including 4383) website: http://www.bk.dk/5000/piezoacc/piezoacc.htm

[91] Gallasch E, Rafolt D, Moser M, et.al; Instrumentation for assessment of tremor, skin vibrations, and cardiovascular variables in MIR space missions; IEEE Trans Biomed Eng; 1996;43(3):328-33

[92] Stiles RN; Frequency and displacement amplitude relations for normal hand tremor; J Appl Physiol 1976;40(1):44-54